ADDIS ABABA UNIVERSITY

ADDIS ABABA INSTITUTE OF TECHNOLOGY

SCHOOL OF MECHANICAL AND INDUSTRIAL ENGINEERING

Numerical modelling of low velocity impact in GFRP-woven and GMT composites

By: YARED GETAHUN

2018

ADDIS ABABA, ETHIOPIA

ADDIS ABABA UNIVERSITY

ADDIS ABABA INSTITUTE OF TECHNOLOGY

SCHOOL OF MECHANICAL AND INDUSTRIAL ENGINEERING

Numerical Modelling of Low Velocity Impact in GFRP-Woven and GMT Composites

By:

YARED GETAHUN

Main -Adviser: Ermias G. Koricho (PhD)

Co-Adviser: Mulugeta H. (PhD. Candidate)

A Thesis submitted at Addis Ababa Institute of Technology in partial

fulfillment of the requirements for the Degree of Master of Science in

Mechanical Engineering

2018

Addis Ababa

The undersigned have examined the thesis entitled '**Numerical modelling of low velocity impact in GFRP-Woven and GMT composites** presented by YARED GETAHUN, a candidate for the degree of Master of Science and hereby certify that it is worthy of acceptance.

_____________	_____________	_________
Advisor	Signature	Date
_____________	_____________	_________
External Examiner	Signature	Date
_____________	_____________	_________
Internal Examiner	Signature	Date
_____________	_____________	_________
Chairman	Signature	Date

Declaration

I certify that the research work titled "**Numerical Modelling of Low Velocity Impact in GFRP-Woven and GMT Composites** " is my own work. The work has not

been presented elsewhere for assessment. Where material has been used from other sources,

it has been properly acknowledged /referred.

Name: YARED GETAHUN

signature: _____________

Main -Adviser: Ermias G. Koricho (PhD)

signature: ______________

Co-Adviser: Mulugeta H. (PhD. Candidate)

signature: _____________

Acknowledgments

First, I want to thank Ermias Gebrekidan (Ph.D.), Assistant Professor Mechanical Engineering Georgia Southern University, for his continuous and unlimited support in supervising, teaching every detail and spent his time for detail assessment of my work.

Secondly, my thank goes to Mulugeta Habte Mariyam (Ph.D. Candidate Addis Ababa university school of mechanical and industrial engineering) for his continues supervision, providing material data and showing the way for the problems that I face.

Thirdly I want to acknowledge Hadi Mehdipour (Ph.D.), Politecnico di Torino, Italy who help me in solving problem-related to ABAQUS VUMAT code.

The last thanks are to my friends and staffs of a school of mechanical and industrial engineering Addis Ababa Institute of technology.

Table of Contents

List of tables iv

List of abbreviations v

LIST OF FIGURES vi

Abstract x

Chapter 1 2

1 introduction 2

Plain 4

Twill 5

Satin 5

1.1 Background of study 6

Statement of the problem 7

1.2 Objectives 8

General objective 8

Specific objectives 8

1.3 Organization of the paper 10

1.4 Scope of the research 9

1.5 Limitation of the research 9

1.7 Significance of the research 9

Chapter 2 11

2 Literature review 11

2.1Failure criterion 15

2.2 Modeling damage and failure of composite 16

2.3 Modeling composites with Abaqus 18

2.4 Intralaminar damage models 19

Chapter 3 21

3 Mathematical modeling or formulation 21

3.1 Stress computation of woven composites 21

3.2 stress computation for Glass mat reinforced composites 25

3.3 Mathematical modeling of impact and damage formation 27

Chapter 4 33

4 Material and method 33

4.1 Material Description 33

4.1Material properties 34

4.2 Method and methodology 35

Chapter 5 37

5 Numerical Modeling and analysis 37

5.1 Finite element modeling for GMT 38

5.2 Finite element for GFRP-woven composites 39

Chapter 6 41

6 Result and discussion 41

6.1 Result and Discussion For GMT 41

6.2 Result and Discussion For GFRP-Woven composites for 28 J 44

Chapter 7 67

7 Conclusions, Recommendations and Future work 67

7.1 Conclusion 67

7.2 Recommendation 68

7.3 Future work 68

References 69

Appendix 73

List of tables

Table 1 Damage initiation criteria 29

Table 2 Failure evolution laws... 30

Table 3 GFRP – material and contents..33

Table 3 mesh convergence...38

List of abbreviations

Xt, tensile strength

3D, 3 dimensional

F, force

σ, stress

Xc, compressive strength

Cij, stiffness matrix

E, young’s modulus

ε , strain

ѵ = Poisson’s ratio

RF3, reaction force in Z direction

J, joule

LIST OF FIGURES

Figure 1.1 Intralaminar and interlaminar damage mode in a composite laminate and their interaction (de Jong et al., 2001; Suiker and Fleck, 2006).(Wang et al. 2017)..............................3
Figure 1.2 Plain weave (Grishanov, Meshkov, and Omelchenko 2009) 4
Figure 1.3 Twill structure reconstructed by directly accumulating CT images (dotted line indicates the portion for which the CT image of Fig is used)(Shinohara and Takayama 2005) 5
Figure 1.4 Satin wave 6
Figure 2.1 Traction-separation law for the cohesive material. (Riccio et al. 2017) 19
Figure 3.1 (Abrate n.d.) Stiffness and compliance matrices of a triclinic material 21
Figure 3.2 (Abrate n.d.) stiffness and compliance matrices of a monoclinic material (z = 0) 22
Figure 3.3 (Park n.d.) stiffness and compliance matrices of an orthotropic material 23
Figure 3.4: (Park n.d.) stiffness matrix of an isotropic material. all shear components are related to normal components 25
Figure 5.1 Specimen and fixture (Wang et al.)2017...37
Figure 5.2 FE model used for numerical simulation in case of impactor velocity 4m/sec.......... 38
Figure 5.3 Mesh convergence for GMT composite...38
Figure 5.4 Configuration of GFRP -woven composite 39
Figure 5.5 Top view of meshed area..40
Figure 6.1 Stress distribution in GMT Material 41
Figure 6.2 Logarisimc strain of GMT 42
Figure 6.3 Tsi hill failure measure at integration point 42
Figure 6.4 RF3 vs time of GMT material 43
Figure 6.5 RF3 vs displacement of GMT 43
Figure 6.6 Impact energy of GMT with 293.75 43
Figure 6.7 Von mises stress of 0% nano clay..44

Figure 6.8 Stress concentration of 0% nano modified in laminate form......................................44

Figure 6.9 Logarisimc strain of 0% nano clay 44

Figure 6.10 Von mises stress of 0.5% nano clay..45

Figure 6.11 Stress concentration of 0.5% nano clay modified in laminate form..........................45

Figure 6.12 Logarisimc strain of 0.5% nano clay 45

Figure 6.13 Von mises stress of 1% nano clay 46

Figure 6.14 Stress concentration of 1% nano modified in laminate form 46

Figure 6.15 Logarisimc strain of 1% nano clay 46

Figure 6.16 Von mises stress of 2% nano clay...47

Figure 6.17 Stress concentration for 2% nano clay in laminate form...47

Figure 6.18 Logarisimc strain of 2% nano clay 47

Figure 6.19 RF3 vs displacement profile of 0% 28.8J..48

Figure 6.20 Energy time profile 0 % nano clay 28.8J 48

Figure 6.21 RF3 vs displacement profile of 0.5% 28.8 J 48

Figure 6.22 Energy time profile nano clay of 28.8J 48

Figure 6.23 RF3 vs displacement profile 1% nano clay..49

Figure 6.24 Energy vs time profile of 1% nano clay 49

Figure 6.25 RF3 vs displacement profile for 2% nano clay 49

Figure 6.26 Energy vs time profile for 2% nano clay 49

Figure 6.27 Comparison of pristine and 0.5% nano clay 50

Figure 6.28 Comparison of pristine and 1% nano clay 50

Figure 6.29 Comparison of pristine and 2% nano clay..50

Figure 6.30 Comparation of pristine,0.5%,1% and 2% nano clay 50

Figure 6.31 RF3 vs displacement profile of pristine at 39.2 J 51

Figure 6.32 Energy time profile of pristine at 39.2 J.. 51

Figure 6.33 RF3 vs displacement profile of 0.5% at 39.2 J..51

Figure 6.34 Energy vs time profile of 0.5% at 39.2 J 51

Figure 6.35 RF3 vs displacement profile of 1% nano clay at 39.2 J..52

Figure 6.36 Energy vs time profile for 1% at 39.2 J 52

Figure 6.37 RF3 vs displacement of 2% nano clay at 39.2 J..52

Figure 6.38 Energy vs time of 2% nano clay at 39.2 J 52

Figure 6.39 Comparation of pristine and 0.5% nano clay at 39.2 J 53

Figure 6.40 Comparation of pristine and 1% nano clay 39.2 J 53

Figure 6.41 Comparison of pristine and 2% nano clay at 39.2 J 53

Figure 6.42 Comparation of 0%, 1% and 2% nano clay at 39.2 J 53

Figure 6.43 Comparison of pristine, 0.5% nano clay, 1% nano clay and 2% nano clay at 39.2 J54

Figure 6.44 RF3 vs displacement of pristine at 57.8 J..55

Figure 6.45 Energy vs time profile of pristine at 57.8 J 55

Figure 6.46 RF3 vs displacement 0.5% nano clay at 57.8 J..55

Figure 6.47 Energy vs time graph, of 0.5% nano clay at 57.8 J 55

Figure 6.48 RF3 vs displacement of 1% nano clay at 57.8 J...56

Figure 6.49 Energy vs time of 1% nano clay at 57.8 J 56

Figure 6.50 RF3 vs displacement of 2% nano clay at 57.8 J 56

Figure 6.51 Energy vs time of 2% nano clay at 57.8 J 56

Figure 6.52 Comparison of 0% and 0.5% nano clay at 57.8 J 57

Figure 6.53 Comparation of 0% and 1% nano clay at 57.8 J 57

Figure 6.54 Comparison of 0% and 2% nano clay at 57.8 J..57

Figure 6.55 Comparation of 0%, 1%, and 2% at 57.8 J... 59
Figure 6.56 Comparation of 0%, 0.5% 1% and 2% nano clay at 57.8 J 59
Figure 6.57 RF3 vs displacement of 0% nano clay at 72.2J...59
Figure 6.58 Energy vs time of 0% nano clay at 72.2J 59
Figure 6.59 RF3 vs displacement of 0.5% nano clay at 72.2J..59
Figure 6.60 Energy vs time of 0.5% nano clay at 72.2J 59
Figure 6.61 RF3 vs displacement graph of 1% nano clay at 72.2J...60
Figure 6.62 Energy vs time of 1% nano clay at 72.2J 60
Figure 6.63 RF vs displacement of 2% nano clay at 72.2J 60
Figure 6.64 Energy time of 2% nano clay, at 72.2J... 60
Figure 6.65 Comparation of 0% and 0.5% nano c lay at 72.2J 61
Figure 6.66 Comparation of 0% and 1% nano clay 72.2J 61
figure 6.67 Comparation of 0% and 2% nano clay at 72.2J...61
Figure 6.68 Comparation of 0%, 1%, and 2% nano clay... 61
Figure 6.69 Comparation of 0%, 0.5%, 1% and 2% nano clay 62
Figure 6.70 RF3 vs time of 0%, 0.5%,1% and 2% nano clay, ... 62
Figure 6.71 Mat lab reaction force vs time result 63
Figure 6.72 Comparation of RF3 vs displacement for subroutine and without subroutine...........63
Figure 6.73 Energy vs time 28.8J 63
Figure 6.74 Energy vs time graph in 39.2J..63
Figure 6.75 Energy vs time graph for 57.8 J..64
Figure 6.76 Energy vs time graph for 72.2J... 65
Figure 6.77 Variation of peak deflection with impact energy 65

Abstract

Due to their draping, stiffness, improved ductility, and damage tolerance properties woven and mat composites are being increasingly used for the construction of crash-relevant structural parts like in the automotive industry.

Composite materials are susceptible to low-velocity impact and the induced damage substantially reduces the residual mechanical performance and safe-service life. Due to this low-velocity impact, failure of structures, properties injuries and death are the main problem. Finding novel material and study the energy absorption capacity is the solution expect from material researchers.

Finite element simulation of GMT and GFRP is based on ASTM – Designation D7136M-15. The constitutive models for intralaminar modes were incorporated into the ABAQUS/Explicit FE code by user-defined VUMAT material subroutines.

The impact and stiffness behavior of Glass Mat Thermoplastic (GMT) and Glass fiber reinforced plastics (GFRP) are studied. GFRP has the different label of Cloisite® 20B nano clay, i.e., pristine, 0.5%, 1%, and 2% nano clay were investigated. The result shows the addition of nano-clay with 0.5% and 1% nano clay increase the stiffness while adding of nan clay with 2% decrease the stiffness of GFRP.

Based on the stress concentration, damage in adding of nano-clay with 0.5 % shows poor tolerance as it has high-stress penetration. While adding nano-clay with 2% shows good resistance. Adding 1% nano clay has high stress concentration area and leads to high damage area. The energy absorption of 0.5% nano-clay is greater than 1% and 2% nano-clay while energy absorption of 2 % and 1% nano-clay is lower than the energy absorption capacity of pristine. From all observations of results, the best performance of material obtained in energy absorption is by loading Glass fiber reinforced polymer with 0.5% Cloisite® 20B nano-clay. The comparison of GMT and GFRP – woven composites, based on reaction force vs time graph the GMT composites fail firstly than GFRP woven composites of all clay label. Comparison of reaction force and displacement for Vumat and without Vumat done for pristine material.

Keywords: Glass fiber reinforced plastics (GFRP) Glass mat thermoplastic (GMT), Cloisite® 20B, nano-clay.

Chapter 1

1 Introduction

A composite is a structural material that consists of two or more combined constituents that are combined at a macroscopic level and are not soluble in each other. One constituent is called the reinforcing phase and the one in which it is embedded is called the matrix. The reinforcing phase material may be in the form of fibers, particles, or flake. Monolithic metals and their alloys cannot always meet the demands of today's advanced technologies. Only by combining several materials can one meet the performance requirements. In many cases, using composites is more efficient. In the highly competitive airline and automotive market, the company continuously looking for ways to lower the overall mass of those vehicles without decreasing the stiffness and strength of its components.

There are around four fiber factors that contribute to the mechanical performance of a composite; the first factor is length; the fibers can be long or short. Long, continuous fibers are easy to orient and process, but short fibers cannot be controlled fully for proper orientation. Long fibers provide many benefits over short fibers. These include impact resistance, low shrinkage, improved surface finish, and dimensional stability, the second is Orientation: Fibers oriented in one direction give very high stiffness and strength in that direction. If the fibers are oriented in more than one direction, such as in a mat and woven, there will be high stiffness and strength in the directions of the fiber orientations.

The third factor is Shape: The most common shape of fibers is circular because handling and manufacturing them is easy.

The material is the fourth and the material of the fiber directly influences the mechanical performance of a composite. Fibers are generally expected to have high elastic moduli and strengths. This expectation and cost have been key factors in the graphite, aramids, and glass dominating the fiber market for composites. (Kaw and Group 2006)

when considering the use of perforated GFRP in structural applications that will experience harsh environments (such as in oil wells), the influence of the environment on the composite should be carefully considered to ensure that the structure would perform satisfactorily during the anticipated service life.(Eslami and Taheri 2013)

Composites are classified by the geometry of the reinforcement particulate, flake, and fibers or by the type of matrix polymer, metal, ceramic, and carbon.

Particulate composites consist of particles immersed in matrices such as alloys and ceramics. They are usually isotropic because the particles are added randomly. Particulate composites have advantages such as improved strength, increased operating temperature, and oxidation resistance

Flake composites consist of flat reinforcements of matrices. Fiber composites consist of matrices reinforced by short (discontinuous) or long (continuous) fibers, Nanocomposites consist of materials that are of the scale of nanometers (10–mm).

Fracture and failure are one of the challenging issues in solid mechanics, especially in composite materials. Under high levels of mechanical loads, the fracture can occur in different materials ranging from metals, ceramics to polymers and composites. Depending on the microstructure of the materials, a fracture can originate from voids, microcracks, movement of dislocations, de-bonding and even structural effects such as buckling. Besides the multiscale nature of the response of the structure, the failure behavior of composites is often a combination of multiple damage mechanisms. Intralaminar damage, such as fiber breakage and matrix cracking, can cause interlaminar damage mechanisms (delamination), and vice versa. (Version 2014)

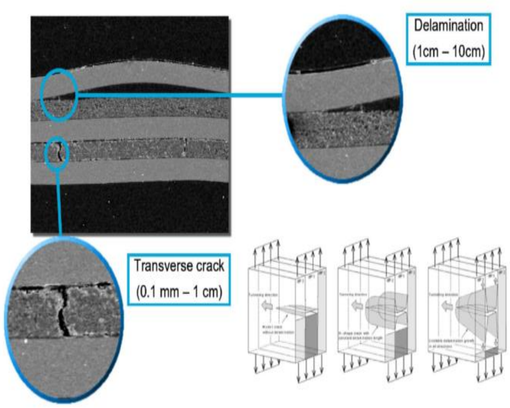

Figure 1.1 Intralaminar and interlaminar damage mode in a composite laminate and their interaction (de Jong et al., 2001; Suiker and Fleck, 2006).(Wang et al. 2017)[i]

Numerical simulation plays an irreplaceable role in reducing time and cost for the development of aerospace and automotive structures, such as composite fan cases, car roof, and body panels etc.

For applications where more than one fiber orientation is required, a fabric combining 0° and 90° fiber orientations is useful.

Woven fabrics are produced by the interlacing of warp (0°) fibers and weft (90°) fibers in a regular pattern or weave style. The fabric's integrity is maintained by the mechanical interlocking of the fibers. Drape (the ability of a fabric to conform to a complex surface), surface smoothness and stability of a fabric are controlled primarily by the weave style. The following is a description of some of the more commonly found weave styles.

Plain

Each warp fiber passes alternately under and over each weft fiber. The fabric is symmetrical, with good stability and reasonable porosity. However, it is the most difficult of the weaves to drape, and the high level of fiber crimp imparts relatively low mechanical properties compared with the other weave styles. With large fibers (high tex) this weaving style gives excessive crimp and therefore it tends not to be used for very heavy fabrics.

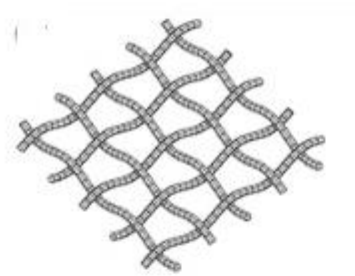

Figure 1.2 Plain weave (Grishanov, Meshkov, and Omelchenko 2009)

Twill

One or more warp fibers alternately weave over and under two or more weft fibers in a regular repeated manner. This produces the visual effect of a straight or broken diagonal 'rib' to the fabric. Superior wet out and drape are seen in the twill weave over the plain weave with only a small reduction in stability. With reduced crimp, the fabric also has a smoother surface and slightly higher mechanical properties.

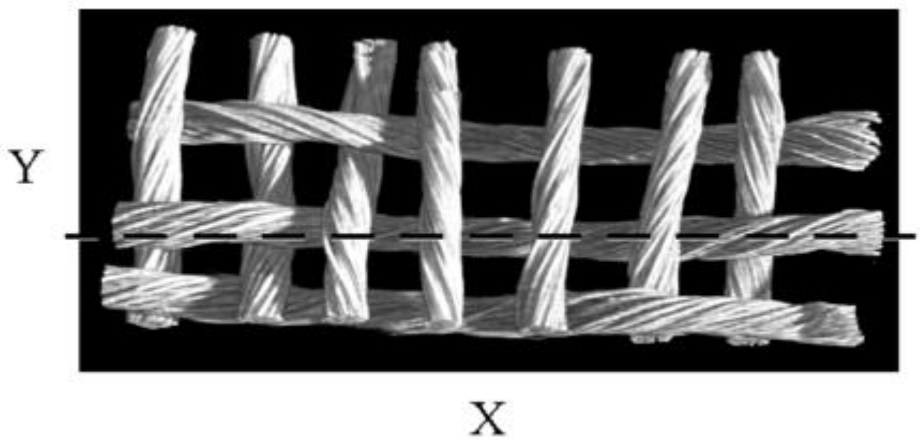

Figure 1.3 Twill structure reconstructed by directly accumulating CT images (dotted line indicates the portion for which the CT image of Fig is used)(Shinohara and Takayama 2005)

Satin

Satin weaves are fundamentally twill weaves modified to produce fewer intersections of warp and weft. The ‘harness’ number used in the designation (typically 4, 5 and 8) is the total number of fibers crossed and passed under before the fiber repeats the pattern. A ‘crows’ foot’ weave is a form of satin weave with a different stagger in the repeat pattern. Satin weaves are very flat, have good wet out and a high degree of drape. The low crimp gives good mechanical properties. Satin weaves allow fibers to be woven in the closest proximity and can produce fabrics with a close ‘tight’ weave. However, the style’s low stability and asymmetry need to be considered. The asymmetry causes one face of the fabric to have fiber running predominantly in the warp direction while the other face has fibers running predominantly in the weft direction. Care must be taken in assembling multiple layers of these fabrics to ensure that stresses are not built into the component through this asymmetric effect.

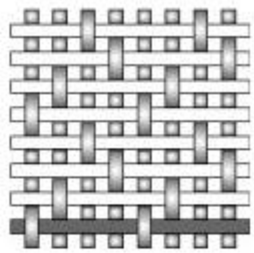

Figure 1.4 Satin wave

1.1 Background of the study

Low-velocity impact (LVI) events on a composite laminate, usually, cause concurring failure mechanisms such as matrix cracks, fiber failure, and delamination. Generally, matrix cracking is the first occurring failure mechanisms induced by LVIs and, even if not able to considerably reduce the laminate material properties, it acts as a delamination initiation trigger. Delamination occurs at the interface between differently oriented layers driven by interlaminar shear stresses, stiffness variation between the adjacent plies, and structural deflection. Consequently, the key point for a correct impact phenomenon prediction is the accurate simulation of the interaction between intralaminar damage (matrix cracks and fiber failure) and interlaminar damage (delamination). Modeling has been implemented in Fe code Abaqus/Explicit using Vumat subroutine.

Statement of the problem

In today's world crashing of vehicles, loss of property and injury is the main problem. Crashing is caused by the different phenomenon. Among these causes are a drop of unexpected mass with certain velocity, crashing with other vehicles. The high rate of crash accidents facilities urged the car manufacturing companies to improve the safety of vehicles.

Glass fiber reinforced composite laminates have advantages in impact resistance can cause extensive sub-surface damage that may not be visible on the laminate surfaces that is why need to do this research on GFRF (glass fiber reinforced plastic) woven composites on impact and damage analysis.

Number of literature are done on low-velocity impact using different materials even using GFRP experimentally and numerically. For this proposed material, literature are tried to do experiments using Nano and micro fillers as well as different surface treatments. Developing Numerical modeling of this material is as a gap and also helps the researcher to study laminate weakness and treat the week which influences the damage energy absorption label.

From all observation there is a research gap in Cloisite® 20B (Southern Clay Products, Inc., TX) 0%, 0.5% 1% and 2% clay volume energy analysis which is newly extracted. There for this research try to address the energy absorption capacity and stiffness of these four materials and identify the best material in these regards.

1.2 Objectives

General objective

The general objective of this thesis is Numerical modeling of low velocity impact behavior in glass fiber reinforced plastic – woven using Abaqus subroutine VUMAT and GMT composites using Abaqus explicit for vehicle application.

Specific objectives

This research is done to achieve the following specific objectives.

- To calculate material properties of GFRP –Woven composites in a different direction obtained from literature and some properties like shear modulus for each clay label of clay
- To find optimum value of clay content by different clay combination by developing Abaqus subroutine and analyze obtained data for identification of best material with different regards.
- To do stress distribution and energy absorption

1.3 The scope of the research

The research covers numerical modeling of GFRP- woven and GMT composites and compare the impact resistance of nanomodified GFRP- woven composite numerically. For GFRP-woven composites VUMAT is introduced for better prediction of damage which is code written in Fortran language.

Using these results, the research tried to address the comparison of impact damage resistance of nanomodified composites.

1.4 Limitation of the research

As a limitation the work is focused only on the numerical model and did not include an experimental comparison for pristine nano modified GFRP-woven material and GMT, to remodel the materials by looking at different variables. The second limitation deletion damaged elements are not included due to programming capability due to this reason, how damage expand and evolution is not visible.

1.5 Significance of the research

The significance of this research is to characterize the impact behavior of GFRP and GMT composites numerically, using finite element method.

Finite Element Method (FEM) are needed for an efficient and detailed assessment of the characteristics of laminated fabric composites subjected to impact loads especially using subroutines to upgrade the failure prediction of ABAQUS for that material.

Secondly, this research is done to identify the proper nano clay content for better impact resistance among four clay contents, i.e. pristine (0%), 0.5%,1% and 2% nano modified GFRP- woven

Composites.

1.6 Organization of the paper

The first chapter of this paper is an introduction, in this chapter, the paper presents the general terms and concept of the material and event that proposed in the research. This chapter also includes the background of the study, statement of the problem, specific and general objectives, scope and limitation of the research.

In the second chapter, literature is reviewed which is related to the work. In this chapter failure criteria, modeling of composite damage and failure, intralaminar and interlaminar damage is discussed, modeling with Abaqus are discussed which followed by the conclusion

In the third chapter Mathematical modeling or formulation of the material and impact of foreign particles are discussed, here the research tries to discuss how the material behaves and impact energy calculations using formulas.

The fourth chapter also addressed the material and method that proposed in the research, here some material data are obtained and some are also calculated for real simulation. The method and methodology also included here.

In the fifth chapter numerical modeling of materials are discussed which include the boundary condition that is desirable for impact

In chapter six and seven results with discussion and conclusion are made for this work.

Chapter 2

2 Literature review

This chapter presents a literature review of the relevant research done on the topics proposed in this study. The overview is intended to give a background regarding some of the methods currently in use, and present comparisons and extensions for the applicability of this research. Primarily in this review, the numerical methods and techniques of finite element analysis modeling and some applicable results for the woven and mat composites will be presented.

In the last decade, the increased use of laminated composites in advanced structural applications has required the development of a wide variety of modeling strategies for the description of composite materials and structures. The validation of the predictive capabilities of such models for damage becomes a real challenge, which needs to be addressed if these strategies are to be introduced in industrial practice. (Sun, Wisnom, and Hallett 2016)

Damage plays an important role in many fibrous composite materials with non-ductile matrices. Their elastic-brittle behavior is characterized by the formation and evolution of micro-cracks (surface discontinuities) and cavities (volume discontinuities). Before the constitutive equations are developed, the mechanical behavior of a broad range of laminated fiber- reinforced composite, is outlined briefly. Glass- or carbon-fiber reinforced vinyl ester or epoxy resins typically fall into this class of materials. Their mechanical response to deformations casted into a mathematical model. Special emphasis is given to the interaction between fiber damage due to fiber stress and matrix damage due to transverse and shear stress on the elastic response and the ability to transmit various states of stresses. A given set of microcracks and cavities has a different influence on the effective elastic properties of the material under tension or compression.(Anon 1993),(Kim et al. 2017)

The different failure mechanisms due to tension or compression are reported in (Matzenmiller, Lubliner, and Taylor 1995) (Kim and Sham 2000) and discussed below: those caused by normal stress in fiber direction and those caused by normal stress transverse to the fibers as well as by shear stresses.

The first mode is mode 1 which is Fiber rupture is primarily caused by tensile stresses 0-11 in the fiber direction. Failure is initiated by a number of fiber breaks in the vicinity of one another. The ruptured fibers deboned from the matrix material and cavities are formed between the broken fiber ends. In a homogenized continuum model, the strains between the deboned ends of the fiber rapidly grow, whereas outside of this region the strains decrease and unloading takes place. The strength parameter Xt, associated with critical loading, is governed by the tensile strength of the fibers and the fiber-matrix volume ratio. Its value is assumed to be given for the lamina. The matrix strength contributes little to Xt because the failure strains of resin matrices are usually higher than the ones of the fibers. However, uniaxial off-axis tests show a pronounced sensitivity of the failure load with respect to the shear strength of the resin or the fiber-matrix bond strength, if the loading direction slightly deviates from the fiber direction.

The second mode is mode 2 which is Buckling and kinking of fibers, accompanied by matrix fragmentation, is observed in uniaxial compression tests with loading in the fiber direction. It results from transverse tensile stresses due to Poisson's ratio differences between the matrix and the fibers and the weakness of the fiber-matrix interface. The compressive strength of the lamina Xc is not only influenced by the compressive strength of its constituents, but also by the elastic stiffness and by the shear strength of the matrix. Micro buckling of fibers starts with the buckling of a single fiber and progressively involves additional fibers as the damage propagates in the kink-band. The buckled fibers reduce the load carrying part of the cross-section. Stress-strain curves from compression tests of composites with a stiff matrix show little nonlinearity prior to failure. However, a nonlinear pre-failure response is typical for composites with a soft matrix reinforced by fibers, which fail at high strain.

Mode III: Matrix cracking under transverse tension and shearing Microcrack growth in a graphite- or glass-epoxy lamina under transverse tension is unstable under load control and sudden failure is initiated by a few macro cracks along the fiber-matrix interface.

Mode IV: Matrix crushing under transverse compression and shearing Microcracking of the resin is observed in graphite- or glass-epoxy laminae under in-plane shear and transverse compression. Local tensile stresses in the resin are due to the differences of Poisson's ratio between the fibers and the matrix and the splitting effect of a fiber pressed against the neighboring fibers close to the lamina surface. With increasing shear strains, the direction of crack growth is turned parallel to the fibers at the fiber-matrix interface.

Delamination of individual layers or separation of stacks of layers is typically encountered in composite structures. It is a failure form of the laminate and not of the lamina. Debonding of fibers from the surrounding matrix or fiber pullout are consequences of interfacial failure.

In order to study the delamination of thick composite laminates under low-energy impact, damage prediction and analysis were presented in (Version 2014) The simulation results showed a good correlation to the experimental observations. The delamination location was limited by the impact zone and the fiber distribution. And the numerical method is based on Tsai–Wu failure criterion.

As per (Williams and Vaziri 2001) using continuum damage mechanics based model show improvement in prediction of damage growth.

Low-velocity impact test was done in carbon fiber/epoxy composite laminates reinforced by short fiber and other material to investigated in (Sohn et al. 2000) and the result shows that composite material experience varies fracture, delamination, intra ply cracking, matrix cracking, fiber breakage, and damage depending on the interlayer material.

Two non-crimp 3D woven carbon fiber composites (through thickness angle interlock) of binder volume fraction 3% and 6% were characterized (Gerlach et al. 2012) for their response to applied deformation. Experiments were performed at quasi-static, medium and high strain rates under a large variety of load cases (tension in warp/ weft direction, interlaminar/intralaminar shear, through-thickness tension/compression, 3-point bending and plate bending). During the study, novel experimental methods were developed in order to address several challenges specific to 3D composite materials. The results show that, while the different binder volume fractions of 3% and 6% have only a small effect on the in-plane stiffness (warp and weft direction), its effect on the delamination resistance in plate bending experiments is considerable.

Delamination resistance of glass fiber reinforced polymers (GFRP) and its influence on GFRP's resistance to transverse, point impact is concentrated (Kuboki, Jar, and Forest 2003). The study used two GFRP, one with polyurethane matrix and the other isophthalic polyester. The two GFRPs show distinctly different mode I delamination resistance. Under the same impact condition, at speeds from

1.5 to 5 m/s, the polyurethane-based GFRP developed a smaller damage size than the isophthalic polyester-based counterpart, suggesting that the former has higher impact toughness. However, the two GFRPs showed little difference in the total energy absorbed during the impact, which is another measure commonly used for impact toughness evaluation. And concluded that a consistent trend exists between the delamination resistance in mode I and the critical force for the incipient impact damage. The difference of the impact resistance between the two GFRPs is mainly on the impact damage size developed. The total energy absorbed during the impact remains the same, which is independent of mode I delamination resistance of the GFRP.

The behavior of pristine and nano-/micro-modified GFRP composites under quasi-static indentation and low-velocity impact tests were studied (Koricho et al. 2015). These nanofillers are glass bubble (GB) and nano clay (NC). The impact tests were performed at varying impact energy levels to study the damage tolerance of composite laminates. The stacking sequence of the laminates and impact test procedures were adopted according to the ASTM standard D7136. The experimental test results found from quasi-static indentation and low-velocity impact tests were evaluated using reaction force–time, energy– time histories, and extent of the damage. Additionally, the perforation energy, bending stiffness, and geometry parameters were also considered to evaluate the performance of the developed composite laminates. Impact behavior of GFRP composite for Pristine, GB modified, NC modified, and Hybrid were investigated and found that Nano clay-modified laminate showed the highest absorbed energy and minimum peak reaction force without penetration.

Addition of nano-clay as a filler has attracted a lot of attention as it enhances mechanical and barrier properties of polymer composites studied in (Rafiq et al. 2017). The effect of nano-clay addition in Glass Fiber Reinforced Epoxy (GFRE) composites on impact response was studied. GFRE samples with nano clay exhibited better impact resistance as compared to neat GFRE samples. Samples with 1.5 wt.% nano clay loading showed an increase in peak load of about 23% while the improvement for samples with 3.0 wt.% clay was around 14%. Hybrid composites absorbed less energy as compared to GFRE which led to less physical damage. Impact energy of 35 J was found to be the threshold energy beyond which samples gave in and had complete failure. Samples with clay loading of 1.5 wt.% showed the lowest absorbed energy which was related to the uniform dispersion of nano-clay. Deflection at peak load was found to be lowest for samples with nano clay which suggested that nano clay addition increased the stiffness, by up to 11%.

The numerical model of woven composites is based on the prediction of the linear elastic behavior of an orthotropic material (Cousigné et al. 2014), and these formulation is derived from generalized hooks law.

2.1 Failure criterion

According to (Tsai and Wu 2009) tsi wu failure criteria is the generalized failure theory for anisotropic material. This is the most general form of failure criterion. It is assumed that the failure surface in stress space can be represented by a tensor polynomial function in the following scalar form

$Fij\sigma i\sigma j + Fi\sigma i = 1$ $\quad i,j \quad 1,2,3$ $\quad$ *equation 2.1*

According to (Hashin and Rotem 1973) If a laminate which is symmetric with respect to its middle plane is subjected to membrane forces and to no bending moments the laminae are in a state of plane stress except at the edges where interlaminar shear and normal stresses occur. The most basic problem is, therefore, that of a uniaxial lamina in plane stress. The form of the criterion has been suggested by two distinct experimentally observed failure modes: the fiber failure mode in which fiber fail progressively and the matrix failure mode in which a crack runs through the matrix, parallel to the fibers which can extend in four sub failure criteria as below.

Fiber tensile failure ,fiber compressive failure ,matrix tensile Failure and matrix compressive failure.

Again (Puck and Deuschle 2002) report another failure criteria called puck, The Puck fracture criteria for unidirectional and woven fibre/polymer composites are widely accepted for physically based prediction of failure and post-failure degradation behavior. The core of the theory, the inter-fibre fracture criteria, are criteria of the Coulomb/Mohr type. Accordingly, the inclination of the fibre-parallel fracture plane – in other words: the fracture angle – has to be determined in the first analysis step. Afterwards the fracture stresses acting on the predicted fracture plane can be determined. Since the theory has first been introduced continuous efforts have been taken to reduce the computational cost of such two-step approach

It divides into two sub criteria

The first is Inter fiber fracture IFF (matrix- fracture or fiber- matrix decohesion, it is TSI -WU failure criteria in modified form where Xt, Xc Replaced by $E1\varepsilon_{1t}$, $E1\varepsilon_{1c}$ where ε_{1c} ε_{1t} tensile and compressive failure strain of the pure matrix material.

Stress-based criteria may be divided into three categories: non-interactive like the maximum stress and strain criteria; partially interactive like the Tsai-Hill and Hashin-Rotem criteria; and fully interactive such as the Tsai-Wu criterion with the Hoffman criterion as a special case. Generally speaking, the predictions from the first type of criterion are the poorest while those from the last type of criterion are the best. This shows that the interaction between stress components is important in delamination. Although the physical basis of the interaction may not be correct, reasonable results can still be obtained because all the interactive criteria are essentially curved fitting in nature. The more parameters that are left to be specified, the more accurate the predictions will be. These criteria were developed for predicting in-plane failure but have been found to be equally applicable to interlaminar failure.

There is a large amount of scattering in the location of delamination. The Tsai-Wu quadratic criterion predicts the delamination location reasonably well, although there is a tendency for failure to occur closer to the thin section than expected (Cui, Wisnom, and Jones 1992)

2.2 Modeling damage and failure of composite

As one of the principal aspects of the current research, a comprehensive review of the approaches currently available for predicting damage in composites is given in this section. Incorporation of failure and damage modeling into composite constitutive models is one of the advanced issues and most challenging areas in nowadays' research. Remarkable advances have been reported in recent years toward a better understanding of the failure mechanism in composite mechanics and dynamics.

Contrary to the traditional metallic materials, failure mechanism of the composite material is considered to be composed of a series of cracking or fracture at different scales and characteristics

Current approaches for predicting damage in advanced composites subject to severe static loads or impulsive loadings remain either simplistic or highly complex with many parameters to be determined. Up to the low and medium velocity regime, these can be divided broadly into four areas (Iannucci 2006):

Roughly, the damage modeling approaches are divided into following four areas: 1) failure criteria approach, 2) damage mechanics approach, 3) fracture mechanics-based approach and 4) plasticity approach.

In general failure criteria approaches to modeling composite failure have been developed in and restricted to the static regime. Either they can be broadly divided into specific failure criteria for the various damage mechanisms, or polynomial-based criteria Well-developed failure criteria on lamina level fall short in predicting failure of textile composites, due to the severe anisotropy in the individual ply of this type of composites. Only textile composites with minimal fiber undulations and low 3D reinforcement density may be approximated by failure criteria built on lamina levels such as Puck and Tsai-Wu theory.

Researches like (Mines, Roach, and Jones 1999) shows local energy absorption is, in proportion, the largest for the 6 ply case, and that the delamination energy absorption dominates for the 12 ply and 24 ply cases. It is assumed in these calculations that the local perforation is dominated by shear effects. The predicted energy absorption shows considerable scatter compared with the corresponding measured values

2.3 Modeling composites with ABAQUS

Experts in Aerospace, Automotive, Shipbuilding, Defense, and Energy are using Abaqus to model and study the linear and nonlinear behavior of composites to improve their understanding of composite behavior and their designs. Both Abaqus/Explicit as well as Abaqus/standard solvers have variety of functionalities and leading technology for basic and advanced modeling and analyzing composite materials and structures. Additionally, Abaqus provides a comprehensive pre and post-processing tool called Abaqus/CAE, to offer a Complete Abaqus Environment, which is especially efficient and powerful for modeling and visualizing the analysis result for composites, say, defining and viewing the composite layup and the varying orientations. Depending on the purpose of the analysis, different modeling techniques equipped in Abaqus for composites can be used as outlined below:

1) Microscopic modeling: The matrix and reinforcement material are both modeled separately as deformable continua.

2) Macroscopic modeling: The composite is modeled as a single orthotropic material or a single fully anisotropic material.

3) Mixed modeling: The composite is modeled by a number of discrete, macroscopically modeled reinforced layers.

4) Discrete reinforcement modeling: Reinforcement modeled with discrete elements or other modeling tools (e.g., rebar).

5) Sub modeling: Useful for studying stress concentrations around the tips of reinforcing fibers for both static and dynamic analysis.

In addition to the modeling of matrix and reinforcement, progressive damage and failure of the materials and their interfaces can be modeled as well. The capability for modeling progressive damage and failure, that is, the prediction of failure modes for both fiber and matrix materials includes:

1) Hashin Failure Criteria limited to plane-stress formula, so it is not available for 3D solid elements;

2) user material subroutine UMAT (Abaqus/Standard) and VUMAT (Abaqus/Explicit) to give the users the opportunity to incorporate material models into Abaqus that are not available as standard embedded function;

3) Delamination—Separation of adhesively bonded sections of laminated composites;

4) Virtual Crack Closure Technique (VCCT);

5) Cohesive Elements and Cohesive Contact to define the bonding and debonding between lamina.

6) CZone, an Add-on capability to Abaqus/Explicit that allows a user to include material crush behavior in FEA simulations of composite structures subjected to impact

Interlaminar damage model

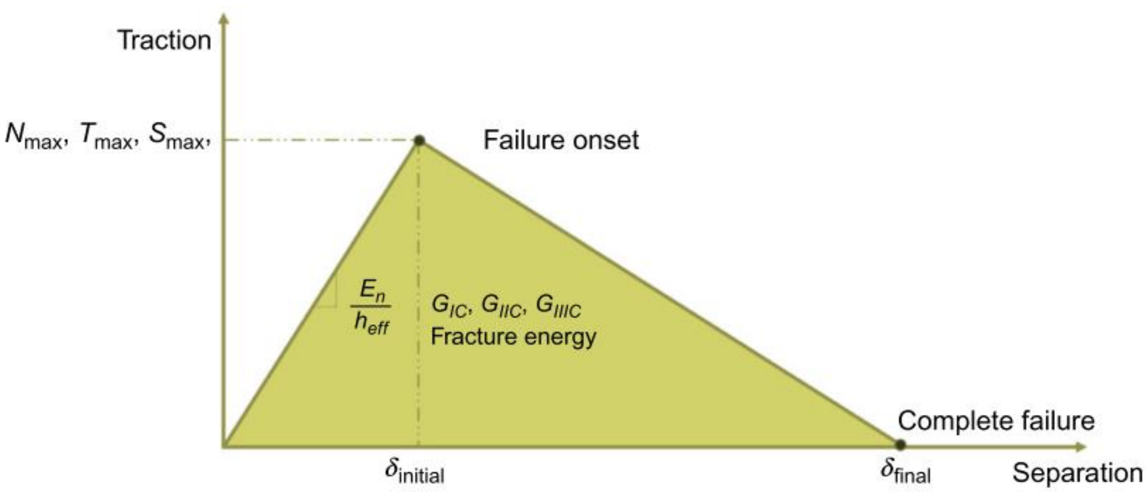

Figure 2.1 Traction-separation law for the cohesive material. (Riccio et al. 2017)

2.4 Intralaminar damage models

Two numerical models for the simulation of the intralaminar damage onset and evolution have been adopted in this paper. the ABAQUS standard approach has been implemented in GMT material, and with a newly developed procedure implemented in ABAQUS by the user subroutine feature for GFRP- woven composites.

ABAQUS standard approach for intralaminar damage prediction. The ABAQUS considers, as standard formulation for the simulation of intralaminar damage onset and propagation, criteria associated to composite failure modes (Hashin’s criteria formulation)

According to these criteria, it is possible to distinguish among different failure modes such as matrix tensile and compression cracking and fiber tensile and compression breakages discussed above.

Many researchers have shown that the enhancement of the fracture toughness of the polymer matrix may be achieved by particles' inclusion from the addition of several micro- and nanoparticles, highlighting the different effects due to the soft or rigid nature of the particles, and to the molecular structure of the polymer (crystalline, semi crystalline, and amorphous). In addition, size, concentration of particles has been pointed out as important aspects that influence the matrix toughness and thus the fracture failure modes of the overall composite material. As a fracture criterion Hashin criteria is simple but in 3D form to experimental result. But tsi -wu failure or puck criterion is much converge to experimental result.

From observation of literatures thre is a gap in combining tsi wu failure criteria and 3D approach for woven material and even introducing four material in one composite by adding nano clay and energy absorption capacity by introducing different clay volume. There for this research is try to introduce these two-approach using Abaqus subroutine and identify the best energy absorption capacity and stiffness for GFRP – woven composition clay volume perspective.

Chapter 3

3 Mathematical modeling or formulation

3.1 Stress computation of woven composites

The generalized Hooke's law is the linear stress-strain relation for an anisotropic material. It is derived from the existence of an elastic energy in the theory of elasticity. Several commonly encountered symmetries described in.(Park n.d.)

Triclinic Symmetry

There are 36 components or constants which completely describe this material. It has no material symmetry. This stiffness matrix, however, is symmetric from the energy consideration. Only 21 of the 36 constants are independent. Similarly, the compliance matrix of a triclinic material has 36 components, of which 21 are independent, and in compliance form.

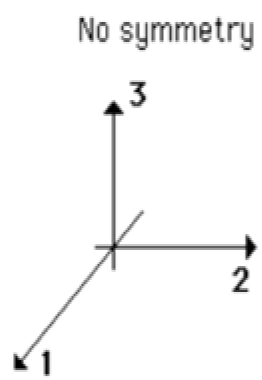

$$\begin{pmatrix} C_{11} & C_{12} & C_{13} & C_{14} & C_{15} & C_{16} \\ C_{21} & C_{22} & C_{23} & C_{24} & C_{25} & C_{26} \\ C_{31} & C_{32} & C_{33} & C_{34} & C_{35} & C_{36} \\ C_{41} & C_{42} & C_{43} & C_{44} & C_{45} & C_{46} \\ C_{51} & C_{52} & C_{53} & C_{54} & C_{55} & C_{56} \\ C_{61} & C_{62} & C_{63} & C_{64} & C_{65} & C_{66} \end{pmatrix} \quad \begin{pmatrix} S_{11} & S_{12} & S_{13} & S_{14} & S_{15} & S_{16} \\ S_{21} & S_{22} & S_{23} & S_{24} & S_{25} & S_{26} \\ S_{31} & S_{32} & S_{33} & S_{34} & S_{35} & S_{36} \\ S_{41} & S_{42} & S_{43} & S_{44} & S_{45} & S_{46} \\ S_{51} & S_{52} & S_{53} & S_{54} & S_{55} & S_{56} \\ S_{61} & S_{62} & S_{63} & S_{64} & S_{65} & S_{66} \end{pmatrix}$$

Figure 3.1 (Abrate n.d.) stiffness and compliance matrices of a triclinic material

Monoclinic Symmetry

If any material symmetry exists, the number of constants will reduce. For example, if the plane of 1-2, 3 = 0, or z = 0 is a plane of symmetry, this is a monoclinic material. All constants associated with the positive 3- or z-axis must be the same as those with the negative 3- or z-axis. The Hooke's law in Figure 3.2 can be simplified for a material having a plane of symmetry; i.e., a monoclinic material. If the symmetry plane lies in the plane of 1-2, 3 = 0, or z = 0, the components in Figure above will be reduced to those in Figure below.

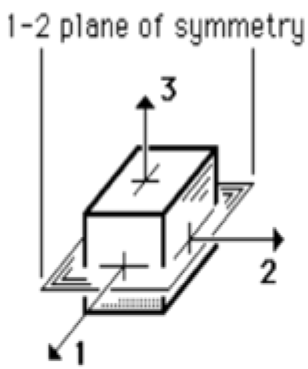

$$\begin{pmatrix} C_{11} & C_{12} & C_{13} & 0 & 0 & C_{16} \\ C_{21} & C_{22} & C_{23} & 0 & 0 & C_{26} \\ C_{31} & C_{32} & C_{33} & 0 & 0 & C_{36} \\ 0 & 0 & 0 & C_{44} & C_{45} & 0 \\ 0 & 0 & 0 & C_{54} & C_{55} & 0 \\ C_{61} & C_{62} & C_{63} & 0 & 0 & C_{66} \end{pmatrix} \begin{pmatrix} S_{11} & S_{12} & S_{13} & 0 & 0 & S_{16} \\ S_{21} & S_{22} & S_{23} & 0 & 0 & S_{26} \\ S_{31} & S_{32} & S_{33} & 0 & 0 & S_{36} \\ 0 & 0 & 0 & S_{44} & S_{45} & 0 \\ 0 & 0 & 0 & S_{54} & S_{55} & 0 \\ S_{61} & S_{62} & S_{63} & 0 & 0 & S_{66} \end{pmatrix}$$

Figure 3.2 (Abrate n.d.) *stiffness and compliance matrices of a monoclinic material (z = 0)*

Orthotropic Symmetry

As the level of material symmetry increases, the number of independent constants continues to reduce. If we have symmetry in three orthogonal planes we have an orthotropic material. The number of independent constants is now 9.

If the planes of symmetry coincide with the reference coordinate system; the nonzero components are 12; this is shown in Figure below. If the symmetry planes are not coincident with the reference coordinates, the nonzero components can be those shown in Figure 3.1. If one of the symmetry planes coincide with the 3- or z-coordinate axis, the nonzero components will be those shown in Figure 3.2. The number of independent constants remains 9 for orthotropic materials irrespective of the orientation of the symmetry planes.

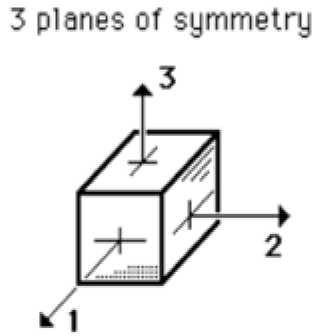

$$\begin{pmatrix} C_{11} & C_{12} & C_{13} & 0 & 0 & 0 \\ C_{21} & C_{22} & C_{23} & 0 & 0 & 0 \\ C_{31} & C_{32} & C_{33} & 0 & 0 & 0 \\ 0 & 0 & 0 & C_{44} & 0 & 0 \\ 0 & 0 & 0 & 0 & C_{55} & 0 \\ 0 & 0 & 0 & 0 & 0 & C_{66} \end{pmatrix} \quad \begin{pmatrix} S_{11} & S_{12} & S_{13} & 0 & 0 & 0 \\ S_{21} & S_{22} & S_{23} & 0 & 0 & 0 \\ S_{31} & S_{32} & S_{33} & 0 & 0 & 0 \\ 0 & 0 & 0 & S_{44} & 0 & 0 \\ 0 & 0 & 0 & 0 & S_{55} & 0 \\ 0 & 0 & 0 & 0 & 0 & S_{66} \end{pmatrix}$$

Figure 3.3(Park n.d.) *stiffness and compliance matrices of an orthotropic material*

The governing equation is based on compliance and let us change to stress strain equation, It relies on the calculation of each term of the stiffness matrix Cij (i,j = 1,...,6) and on an incremental implementation.

$$\begin{bmatrix} \sigma_1 \\ \sigma_2 \\ \sigma_3 \\ \sigma_4 \\ \sigma_5 \\ \sigma_6 \end{bmatrix} = \begin{bmatrix} C_{11} & C_{12} & C_{13} & 0 & 0 & 0 \\ C_{12} & C_{22} & C_{23} & 0 & 0 & 0 \\ C_{13} & C_{23} & C_{33} & 0 & 0 & 0 \\ 0 & 0 & 0 & C_{44} & 0 & 0 \\ 0 & 0 & 0 & 0 & C_{55} & 0 \\ 0 & 0 & 0 & 0 & 0 & C_{66} \end{bmatrix} \begin{bmatrix} \varepsilon_1 \\ \varepsilon_2 \\ \varepsilon_3 \\ \varepsilon_4 \\ \varepsilon_5 \\ \varepsilon_6 \end{bmatrix}$$ -------*Equation 3.1*

where the different components of the stiffness matrix are expressed by:

$$C_{11} = \frac{(1 - v23 * v23) * E1}{S}$$ ....*Equation 3. 2 (a)*

$$C_{12} = \frac{(v21 + v31 * v23) * E1}{S}$$ ....*Equation 3.2 (b)*

$$C_{13} = \frac{(v31 + v21 * v32) * E1}{S}$$ ....*Equation 3.2(c)*

$$C_{22} = \frac{(1 - v31 * v13) * E2}{S}$$ ....*Equation 3.2(d)*

$$C_{23} = \frac{(v32+v31 * v12) * E2)}{S}$$ ....*Equation 3.2 (e)*

$$C_{33} = \frac{(1- v12 * v21) * E3)}{S}$$ ....*Equation 3.2(f)*

$$C_{44} = G_{12}$$

$$C_{55} = G_{23}$$

$$C_{66} = G_{31}$$

and the parameter S is defined by

$$S = 1 - v12 * v21 - v23 * v32 - v13 * v31 - 2v21 * v32 * v13$$ .... *Equation 3.3*

In the previous equations, E1 is the longitudinal Young's modulus, E2 is the transverse Young's modulus and E3 is the through- the-thickness Young's modulus. G12 is the in-plane shear module and G23 and G31 are the transverse shear modules. The different Poisson's ratios are expressed by vij (i≠j i,j = 1,.......,6)The stresses in each direction are then determined from the current strain state

Considering the governing equation of orthotropic material which is in eq. (1) the current stress state σ_i^{tn} (i = i, ...,6) is expressed in the function of the stress at last time step σ_i^{tn-1} (i = i, ...,6) of the strain increment dεi (i=1....6) and the stiffness matrix C_{ij} (i,j = 1,......6):

$$\sigma_1^{tn} = \sigma_1^{tn-1} + C11 d\varepsilon_1 + C12 d\varepsilon_2 + C13 d\varepsilon_3$$ ....*Equation 3.4(a)*

$$\sigma_2^{tn} = \sigma_2^{tn-1} + C12 d\varepsilon_1 + C22 d\varepsilon_2 + C23 d\varepsilon_3$$ ....*Equation 3.4(b)*

$$\sigma_3^{tn} = \sigma_3^{tn-1} + C13 d\varepsilon_1 + C23 d\varepsilon_2 + C33 d\varepsilon_3$$ ....*Equation 3.4(c)*

$$\sigma_4^{tn} = \sigma_4^{tn-1} + C44 d\varepsilon_4$$ ....*Equation 3.4(d)*

$$\sigma_5^{tn} = \sigma_5^{tn-1} + C55 d\varepsilon_5$$ ....*Equation 3.4(e)*

$$\sigma_6^{tn} = \sigma_6^{tn-1} + C44 d\varepsilon_6$$ ....*Equation 3.4(f)*

3.2 Stress Computation for Glass Mat Reinforced Composites

The GMT material presented in (Li et al. 2004) is a kind of 30% glass fiber mat reinforced polypropylene (GRPP), it is isotropic in the in-plane direction, therefore the stress computation is based on these isotropic property of the material.

If a material is fully isotropic, the number of independent constants reduces from 5 to 2 This is shown in Figure below. This is apparently the minimum number of nonzero constants regardless of material symmetry. All three shear components are expressed in terms of the normal components.

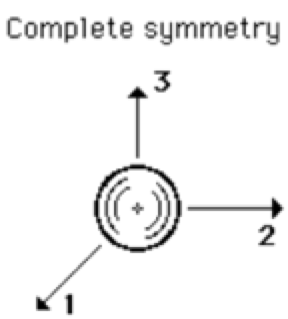

$$\begin{bmatrix} C_{11} & C_{12} & C_{12} & 0 & 0 & 0 \\ C_{21} & C_{11} & C_{12} & 0 & 0 & 0 \\ C_{21} & C_{21} & C_{11} & 0 & 0 & 0 \\ 0 & 0 & 0 & (C_{11}-C_{22})/2 & 0 & 0 \\ 0 & 0 & 0 & 0 & (C_{11}-C_{22})/2 & 0 \\ 0 & 0 & 0 & 0 & 0 & (C_{11}-C_{22})/2 \end{bmatrix} \begin{bmatrix} S_{11} & S_{12} & S_{12} & 0 & 0 & 0 \\ S_{21} & S_{11} & S_{12} & 0 & 0 & 0 \\ S_{12} & S_{12} & S_{11} & 0 & 0 & 0 \\ 0 & 0 & 0 & (S_{11}-S_{22})2 & 0 & 0 \\ 0 & 0 & 0 & 0 & (S_{11}-S_{22})/2 & 0 \\ 0 & 0 & 0 & 0 & 0 & (S_{11}-S_{22})/2 \end{bmatrix}$$

Figure 3.4: (Park n.d.) *Stiffness Matrix Of An Isotropic Material. All Shear Components Are Related to Hormal Components*

For transversely isotropic material the equation (6) the mathematical relation further modified to

$$C_{11} = \frac{(1 - v23 * v23) * E1)}{S} \quad \text{.............................Equation 3.5(a)}$$

$$C_{22} = C_{33} = \frac{(1 - v21 * v12) * E2)}{S} \quad \text{..................Equation 3.5 (b)}$$

$$C_{12} = C_{13} = \frac{v12(1 + v23) * E1)}{S} = \frac{v21(1 + v23) * E2)}{S} \quad \text{.... Equation 3.5 (c)}$$

$$C_{23} = \frac{(v23 + v21 * v12) * E2)}{S} \quad \text{..Equation 3.5 (d)}$$

$$C_{44} = \frac{(1 - v23 - 2v21 * v12) * E2)}{2S} \quad \text{..Equation 3.5(e)}$$

$$C_{55} = C_{66} = G_{12} = E_6 \quad \text{...Equation 3.5(f)}$$

$Where\ S = (1 + v23)(1 - v23 - 2v21 * v12)$ ....*Equation 3.5(g)*

For an isotropic material the abve Equation can be further simplified

$$C_{11} = C_{22} = C_{33} = (\frac{(1- v) * E)}{S} \text{ ....} \textit{Equation 3.6 (a)}$$

$$C_{23} = C_{31} = C_{12} = \frac{(v) * E}{S} \text{ ....} \textit{Equation 3.6(b)}$$

$$C_{44} = C_{55} = C_{66} = G = \frac{(1+v) * E}{2S} \text{ ....} \textit{Equation 3.6(c)}$$

$$Where\ S = (1 + v)(1 - 2v) \text{ ....} \textit{Equation 3.7(d)}$$

3.3 Mathematical Modeling of Impact and Damage Formation

Mathematical modeling used for analysis of impact between foreign body and composite structure is currently classified in four categories.(Abrate 2001) Those are spring mass model, energy - balance model, complete model and impact on infinite model.

Impact energy

The maximum energy E_o in the hummer or in instrument tup assembly prior to impact of specimen is given by

$$E_o = ½(mv_o^2) \ldots\ldots\ldots\ldots\ldots\ldots \text{Equation 3.7}$$

where v_o = is the the velocity of impactor and m mass of the impactor.

Hashin damage formulation 2D

Fiber tensile failure

$$\left(\frac{\sigma 1}{Xt}\right)^2 + \left(\frac{\tau 12}{s}\right)^2 = 1 \quad for\ \sigma 1 > 0 \ldots \text{Equation 3.8(a)}$$

Fiber compressive failure

$$\sigma 1 = -X_c \qquad for\ \sigma 1 < 0 \ldots \text{Equation 3.8(b)}$$

matrix tensile Failure

$$\left(\frac{\sigma 2}{Yt}\right)^2 + \left(\frac{\tau 12}{s}\right)^2 = 1 \qquad for\ \sigma 2 > 0 \ldots\ldots\ldots\ldots\ldots\ldots\ldots\ldots\ldots\ldots \text{Equation 3.8(c)}$$

Matrix compressive failure

$$\left(\frac{\sigma 2}{2S}\right)^2 + \left(\frac{\tau 12}{s}\right)^2 + \left(\frac{\sigma 2}{Yc}\right)^2 + \left[\left(\frac{Yc}{2s}\right)^2 - 1\right] = 1 \quad for\ \sigma 2 > 0 \ldots\ldots\ldots\ldots \text{Equation 3.8(d)}$$

Where $\sigma 1, \sigma 2$ $\tau 12$ pure tensile, compressive and shear stresses. whereas Xt, Xc, and S are strength of the material with respect to tensile compressive and shear direction.

Hashin failure formulation 3D

1. Tensile fibre failure for $\sigma_{11} \geq 0$

$$\left(\frac{\sigma_{11}}{X_T}\right)^2 + \frac{\sigma_{12}^2 + \sigma_{13}^2}{S_{12}^2} = \begin{cases} \geq 1 & \text{failure} \\ < 1 & \text{no failure} \end{cases}$$ ....*Equation 3.9(a)*

2. Compressive fibre failure for $\sigma_{11} < 0$

$$\left(\frac{\sigma_{11}}{X_C}\right)^2 = \begin{cases} \geq 1 & \text{failure} \\ < 1 & \text{no failure} \end{cases}$$ ....*Equation 3.9(b)*

3. Tensile matrix failure for $\sigma_{22} + \sigma_{33} > 0$

$$\frac{(\sigma_{22} + \sigma_{33})^2}{Y_T^2} + \frac{\sigma_{23}^2 - \sigma_{22}\sigma_{33}}{S_{23}^2} + \frac{\sigma_{12}^2 + \sigma_{13}^2}{S_{12}^2} = \begin{cases} \geq 1 & \text{failure} \\ < 1 & \text{no failure} \end{cases}$$ ....*Equation 3.9(c)*

4. Compressive matrix failure for $\sigma_{22} + \sigma_{33} < 0$

$$\left[\left(\frac{Y_C}{2S_{23}}\right)^2 - 1\right]\left(\frac{\sigma_{22} + \sigma_{33}}{Y_C}\right) + \frac{(\sigma_{22} + \sigma_{33})^2}{4S_{23}^2} + \frac{\sigma_{23}^2 - \sigma_{22}\sigma_{33}}{S_{23}^2} + \frac{\sigma_{12}^2 + \sigma_{13}^2}{S_{12}^2} = \begin{cases} \geq 1 & \text{failure} \\ < 1 & \text{no failure} \end{cases}$$ *Equation 3.9(d)*

(Tsai and Wu 2009) tsi wu failure criteria

And the failure equation will be

$$\left(\frac{\sigma 1^2}{XtXc}\right) - \left(\frac{\sigma 1.\sigma 2}{\sqrt{Xt}.Xc.Yt.Yc}\right)^2 + \frac{\sigma 2^2}{YtYc}\Big) + \left(\frac{\tau 12^2}{s^2}\right) + \sigma 1\left(\frac{1}{Xt} - \frac{1}{Xc}\right)$$

$$+\sigma 2\left(\frac{1}{Yt}\frac{1}{Yc}\right) = 1$$ ....*Equation 3.10*

(Puck and Deuschle 2002)

And the second sub criteria are fiber fracture FF (fracture for tensile loading, fiber buckling for compressive loading)

$$(\frac{\sigma 1^{\wedge}2}{xt^{\wedge}2}) = 1 \quad \text{for } \sigma_1 > 0 \text{............Equation 3.11(a)}$$

$$((\sigma_1^2)/(x_c^2))^2 = 1 \quad \text{for} \quad \sigma_1 > 0 \text{..................................Equation 3.11(b)}$$

Interaction of laminates have been used to simulate the interlaminar damage formation and propagation. The interaction in constitutive response is based on two different phases, the initial damage phase (representative of the damage onset) and the evolution damage phase (representative of the propagation of the damage up to the complete failure of the element) (Riccio et al. 2017). with the chance to remove the fully damaged elements.

Abaqus FE code allows to define two different stress-based initiation criteria for the traction-separation law, maximum nominal stress criterion (MAXS), and quadratic nominal stress criterion (QUADS). The MAXS criterion does not assume any relation between the different stress directions while the QUADS criterion considers concurring quadratic ratios between nominal stress and allowable stress acting in different directions.

MAXS	MAX $\left\{\frac{\sigma n}{Nmax}, \frac{\sigma t}{Tmax}, \frac{\sigma s}{Smax},\right\} = 1$
QUADS	$\left(\frac{\sigma n}{Nmax}\right)^2 \left(\frac{\sigma t}{Tmax}\right)^2 + \left(\frac{\sigma s}{Smax}\right)^2 = 1$

Table 1 Damage initiation criteria

Abaqus FE code allows to define different failure evolution laws for cohesive element, the “Power law PW,” the “Benzeggagh-Kenane BK”

Power law	$\left(\frac{GI}{GIc}\right)^{a} + \left(\frac{GII}{GIIc}\right)^{a} + \left(\frac{GIII}{GIIIc}\right)^{a} = 1$
Benzeggagn – Kenane(BK)	$GIc + (GIIc - GIc)\left(\frac{GSHEAR}{GT}\right)^{\eta} = G_{TC}$

Table 2 Failure evolution laws

G_j is the Energy Release Rate associated to the fracture mode j, G_{jc} is the critical Energy Release Rate associated to the fracture mode j (with G_{Ic} Normal mode fracture energy; G_{IIc} Shear mode fracture energy first direction; G_{IIIc} Shear mode fracture energy second direction). For isotropic fractures $G_{Ic} = G_{IIc}$ the material response is independent by η value. Besides $G_{SHEAR} = G_{II}+G_{III};$ $G_T = G_I+G_{SHEAR}$. α and η are empiric values, usually ranging between 1 and 1.6, defined by means of ad hoc experimental tests**.**

Calculate Poisson’s ratio by Equation below.

$$v = -\frac{\Delta\varepsilon t}{\Delta\varepsilon l}$$ --*Equation 4*

v = Poisson’s ratio

Δεt = difference in lateral strain between the longitudinal strain

Δεl =difference between the two longitudinal strain points

From above equation Δεt = v* Δεl, which implies the slop two strain graphs is Poisson’s ratio

Calculating shear modules for pristine GFRP – woven

For calculation the material data obtained from literature in progress and will describe in chapter 4.

From material isometry

$$G = \frac{(1+v) * E}{2S} \quad \text{Where } S = (1+\ v)(1-2\ v)$$

$$G_{11} = \frac{(1+v11) * E11}{2S} \quad \text{Where } S = (1+\ v11)(1-2\ v11)$$

$$G_{11} = \frac{(1+0.1214) * 25008.0}{2(1+0.1214)(1-2*0.1214)} = 28043.9712/1.69824816 = 16513.47047$$

$$G_{22} = \frac{(1+v22) * E22}{2S} \quad \text{Where } S = (1+\ v22)(1-2\ v22)$$

$$G_{22} = \frac{(1+0.1196) * 23249.0}{2(1+0.1196)(1-2*0.1196)} = 26029.5804/1.70358336 = 15279.3113$$

FOR 0.5 % NANO clay modified GFRP – woven

$$G_{11} = \frac{(1+v11) * E11}{2S} \quad \text{Where } S = (1+\ v11)(1-2\ v11)$$

$$G_{11} = \frac{(1+0.1238) * 23110.7}{2(1+0.1238)(1-2*0.1238)} = 25971.8047/1.69109424 = 15357.9878$$

$$G_{22} = \frac{(1+v22) * E22}{2S} \quad \text{Where } S = (1+\ v22)(1-2\ v22)$$

$$G_{22} = \frac{(1+0.1534) * 26541.8}{2(1+0.1534)(1-2*0.1534)} = 30613.3121/1.59907376 = 19144.4028$$

FOR 1 % NANO clay modified GFRP – woven

$$G11 = \frac{(1+v11) * E11}{2S} \quad \text{Where } S = (1+\ v11)(1-2\ v11)$$

$$G11 = \frac{(1+0.0888)*23480}{2(1+0.0888)(1-2*0.0888)}$$ = 25565.024/1.79085224 = 14275.3397

$$G22 = \frac{(1+v22)*E22}{2S}$$ Where $S = (1+\ v22)(1-2\,v22)$

$$G22 = \frac{(1+0.0890)*24393.7}{2(1+0.0890)(1-2*0.0890)}$$ = 26564.7393/1.790316 = 14838.017

FOR 2 % NANO clay modified GFRP – woven

$$G11 = \frac{(1+v11)*E11}{2S}$$ Where $S = (1+\ v11)(1-2\,v11)$

$$G11 = \frac{(1+0.0816)*20632.8}{2(1+0.0816)(1-2*0.0816)}$$ = 22316.4365/1.81016576 = 12328.3939

$$G22 = \frac{(1+v22)*E22}{2S}$$ Where $S = (1+\ v22)(1-2\,v22)$

$$G22 = \frac{(1+0.0720)*20656.0}{2(1+0.0720)(1-2*0.0720)}$$ = 22143.232/1.835264 = 12065.2941

Chapter 4

4 Material and method

4.1 Material Description

As a material, this research will be expected to use GFRP (glass fiber reinforced plastic) woven and glass mat thermoplastics (GMT) composite materials for automotive crashworthiness analysis.

The material data are obtained from (Mulugeta et. in progress). and described as follows. The GFRP – plain weave composites are four types the first is a pristine material which is free of Nano clay. The second is 0.5 % per volume 20B Nano clay modified, the third is 1% per volume 20B Nano clay modified, and the forth 2% is per volume 20B Nano clay modified. In this work, S2-glass plain weave fabric Owens Corning Shield Strand S with areal weight of 818 g/m^2 was used as the primary reinforcement. The resin used was two-part toughened epoxy, namely SC-15 (Applied Poleramic, CA). The micro- and nano-additives used is Nano clay, Cloisite® 20B (Southern Clay Products, Inc., TX)

Number	Name used in this research	Percent in nano clay
1,	pristine	0 percent Nano clay, Cloisite® 20B nano clay
2	0.5% nano clay	0.5 percent Nano clay, Cloisite® 20B nano clay
3	1% nano clay	1 percent Nano clay, Cloisite® 20B nano clay
4	2% nano clay	2 percent Nano clay, Cloisite® 20B nano clay

Table 3 GFRP – material and contents

The mechanical property of the material is calculated based on (Method 2002). This test method is designed to produce tensile property data for material specifications, research and development, quality assurance, and structural design and analysis. Factors that influence the tensile response and should, therefore, be reported include the following: material, methods of material preparation and lay-up, specimen stacking sequence, specimen preparation, specimen conditioning, environment of testing, specimen alignment and gripping, speed of testing, time at temperature, void content, and volume percent reinforcement. Properties, in the test direction, which may be obtained from this test method include the following: Ultimate tensile strength, Ultimate tensile strain, Tensile chord modulus of elasticity, Poisson's ratio, and Transition strain.

In this thesis, few material data are taken from another work and Poisson's ratio are calculated based on standards. According to this standard if bonded resistance strain gages are being used, the error produced by the transverse sensitivity effect on the transverse gage will generally be much larger for composites than for metals. An accurate measurement of Poisson's ratio requires correction for this effect.

Poisson's Ratio by Chord Method—. Determine (by plotting or otherwise) the transverse strain (measured perpendicular to the applied load), $\varepsilon_{t,}$ at each of the two longitudinal strains (measured parallel to the applied load), $\varepsilon_{l,}$ strain range endpoints. If data is not available at the exact strain range endpoints (as often occurs with digital data), use the closest available data point.

Regarding to Glass mat thermoplastics, GMTs are produced on huge laminators, using a thermoplastic resin and one or more forms of reinforcement. The process yields a lightweight, partially consolidated, semi-finished composite in sheet form. GMT makes possible the production of large parts (up to 27.7 ft^2/2.58 m^2, with current press technology) with low tooling costs and fast cycle times via compression molding [Mulugeta et. el. In progress]. The potential for parts consolidation presents the opportunity to further reduce weight and cost.

4.1 Material properties

The material properties are referred from (Mulugeta et. el. In progress) and using this referred data few material properties are calculated.

4.2 Method and methodology

The research is done using a numerical method and FE solver ABAQUS software. All the simulation will produce and analyses using this software.

ABAQUS /CAE, or ‘’Complete ABAQUS Environment ‘’ is a software application used for both the modeling and analysis of mechanical components and assemblies (pre-processing) and visualizing the finite element analysis result. Product simulation is often performed today by engineering group using niche simulation tools from different vendors to simulate various design attributes.

ABAQUS/Explicit VUMAT: User subroutine to define material behavior is achieved by linking three software. FORTRAN linking and user subroutines working in Abaqus 2017. These instructions have been tested with the following software combination (Microsoft community Visual Studio 2013 + ABAQUS 2017 + Intel Parallel Studio XE 2016 update 4). These instructions may work with other versions but it needs to check that Intel Parallel Studio can be integrated to MS Visual Studio and that Intel Parallel Studio does not override MS MPI version coming with Abaqus installation.(Tanska 2017).

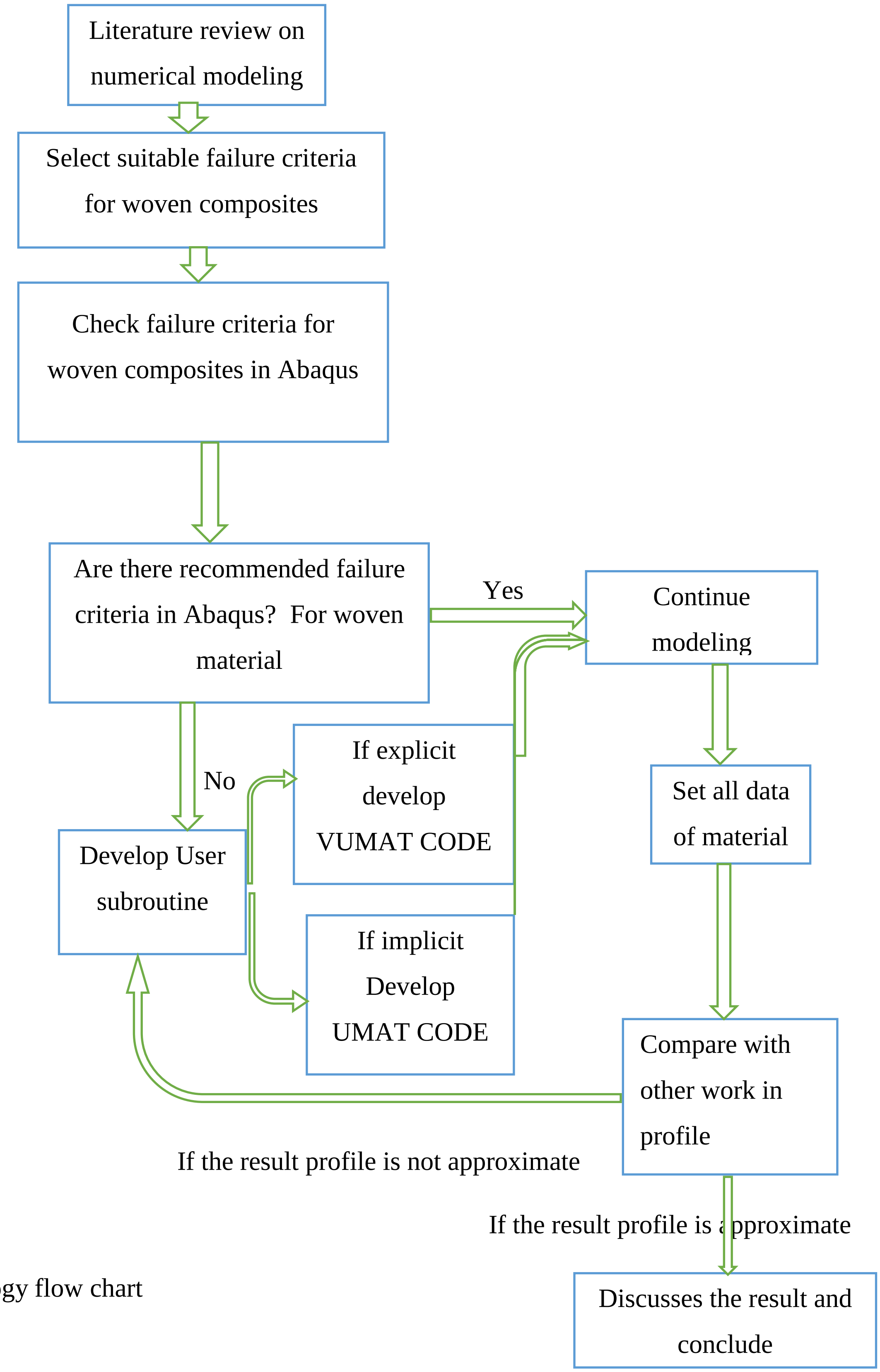

Methodology flow chart

Chapter 5

5 Numerical Modeling and analysis

In (Koricho et al. 2015) The drop-weight tests were carried out according to ASTM D7136 using Instron 9250 HV Dynatup, which is equipped with an 88.96 kN load cell impactor, a velocity detector, and a pneumatic brake to avoid multiple strikes. The specimen was clamped by pneumatically assisted grips. The exposed diameter of composite plate for impact loading was 76.2 mm, according to ASTM standard. A 12.7 mm diameter hemisphere head impactor was used throughout the quasi- static indentation and impact tests. The impacting mass was measured externally using a portable digital scale to verify the accuracy of mass measured by the transducer of the drop-weight testing machine. The total impacting mass was found to be 23.55 kg. Considering the desired impact energy, the impact velocity was adopted within a range of Research Council for Automobile Repair (RCAR) protocol for low velocity impact test (5-20 km/h). Additional impact velocity, 17 km/h, was also considered to investigate the strain rate effect on the performance of the composite materials. The extent of damage on the specimen was then investigated using dye penetration technique.

Finite element simulation of GMT and GFRP is Based on ASTM – Designation D7136M-15 and the fixture are shown below.

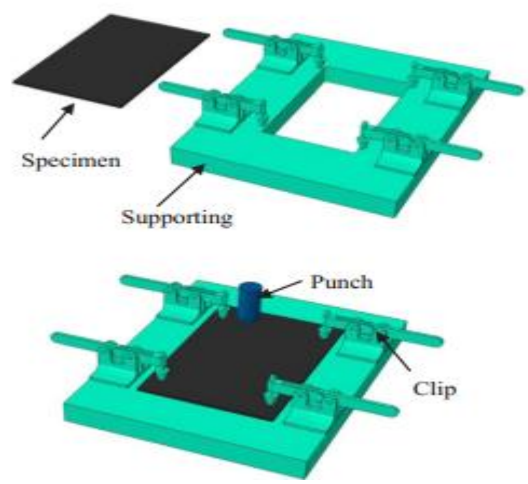

Figure 5.1 Specimen and fixture(Wang et al. 2017)

5.1 Finite element modeling for GMT

Based on ASTM standards, dimension of GMT is 62.5 x 37.5 mm with one lamina., impactor diameter is 16 mm and initial velocity 5 m/sec, impactor mass 23.45 kg with Contact between impactor and plate is simulated using the penalty contact elements with the coefficient of friction of 0.3. Quarter symmetry is used at symmetric faces whereas other boundary faces are kept fixed.

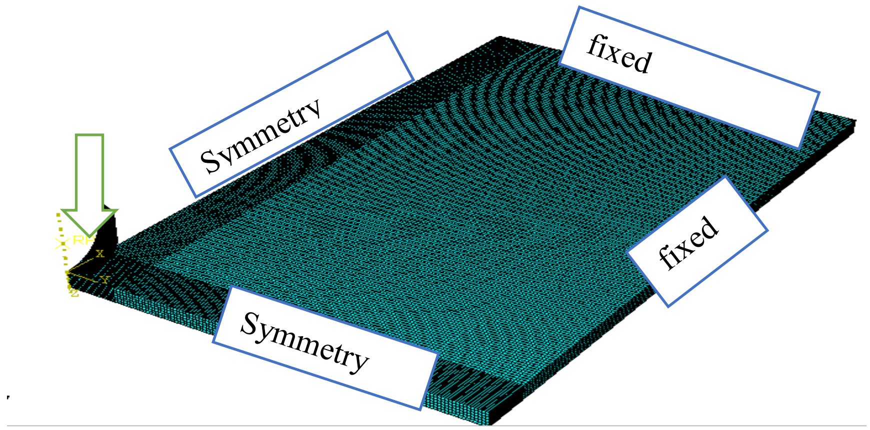

Figure 5.2 FE model used for numerical simulation in case of impactor velocity of 4 m/s

Mesh convergence is done using internal energy versus time graph and the results are nearly the same for 633150 elements and 8721000 elements and 633150 elements are selected for analysis.

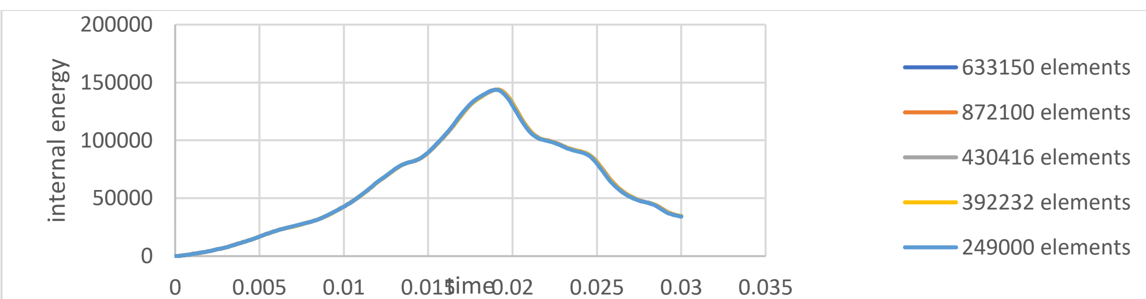

Figure 5.3 Mesh convergence for GMT composite

Maximum energy value(KJ)	Number of elements	different from next mesh
144.0067	872100 elements	
143.9909	633150 elements	0.015.1
143.9169	430416 elements	0.074
143.8059	392232 elements	0.111
143.6933	249000 elements	0.112.6

Table 3 mesh convergence

5.2 Finite element for GFRP-woven composites

Finite element simulation of all nano clay modification GFRP-WOVEN composites is based on ASTM – Designation D7136 M-15 with dimension 62.5 x 37.5 x 5.4 mm with 8 laminas. Each lamina is 0.675 mm thickness. Impactor diameter is 16 mm with mass 40 and 49 kg, respectively, with the velocity of impactor 1.2 m/sec, 1.7 m/sec 1.9 m/sec

For simulation purpose, for reducing simulation tim, quarter of specimen of GFRP and impactor are used as shown below.

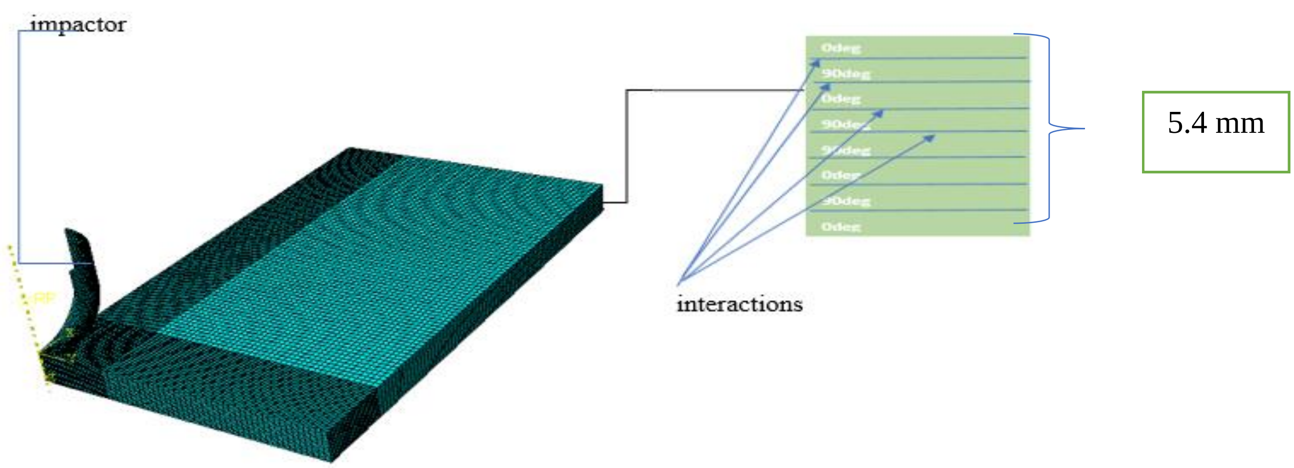

Figure 5.4 Configuration of quarter GFRP -woven composite

The contact between ply to impactor is interaction and contact between the layer to layer is interaction 2 and the properties for this interaction are described below. Quarter symmetry is used at symmetric faces whereas other boundary faces are kept fixed. Based on many works of literature recommendation for this work as failure initiation criterion QUADS approach and for failure evolution laws for interaction element, the “Benzeggagh-Kenane BK” has been adopted, in addition, for the woven material model for analysis using Abaqus subroutine VUMAT.

There are three interaction properties used in modeling of eight layer the first one is to trick Abaqus. The second is between 0/90 degree, which named as intprp-1, and the third is between 90/90 degree at symmetry and named as int prop -2

5.2.1 Meshing

Even though the so-far reported mesoscale methods by Abaqus use continuum shell (SC8R) to mesh the fiber tows unexceptionally, the current study suggested using the solid element (C3D8R) to model all fiber tows. This is because, when simulating the dynamic event, the deformation may go very severe, the thickness may change very significantly, causing the analysis to fail prematurely if the continuum shell were used. causing the analysis to fail prematurely if the continuum shell were used. Even in a simple tensile test, the specimen may undergo a thickness change of greater than 10% of its original thickness. A robust algorithm should be able to consider this. An inherent limitation and disadvantage exist with continuum shell are that the thickness change on the SC8R elements should not be significantly larger than 10%. Even though the SC8R elements do provide a larger stable time increment than the same dimensional C3D8R favorably enough for an explicit simulation, the solid elements are essentially needed for modeling the impact response of the materials like braided composites.

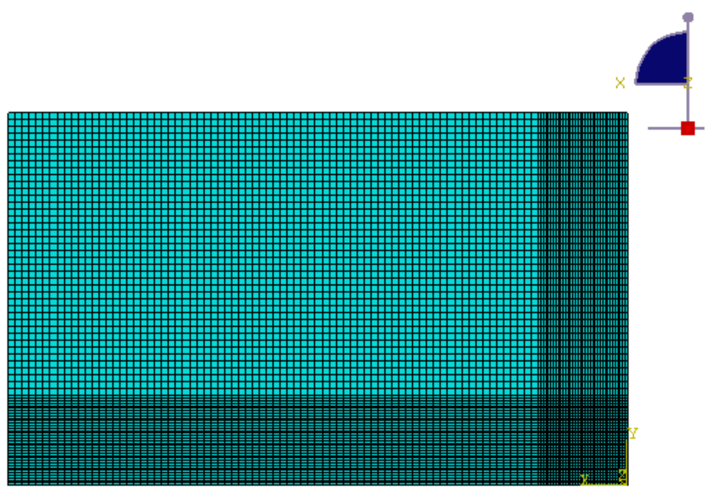

Figure 5.5 Top view of meshed area

The reason using solid element than continuum shell elements in meshing of GFRP is in VUMAT program there is a way to do using stress and select 3D stress element type.

In this simulation For GFRP – woven composites the research uses the same element number for all specimen and used for identifying the best material and mesh convergence is not that much essential.

Chapter 6

6 Result and discussion

In this chapter, results of GMT and GFRP are discussed and interpreted in different perspective.

6.1 Result and Discussion For GMT

According to (Cousigné et al. 2014) longitudinal shear overall and plastic strains are also used to analyze damage. Here also in this result logarisimc strain and von mises stress are in the same area, and has high failure measure.

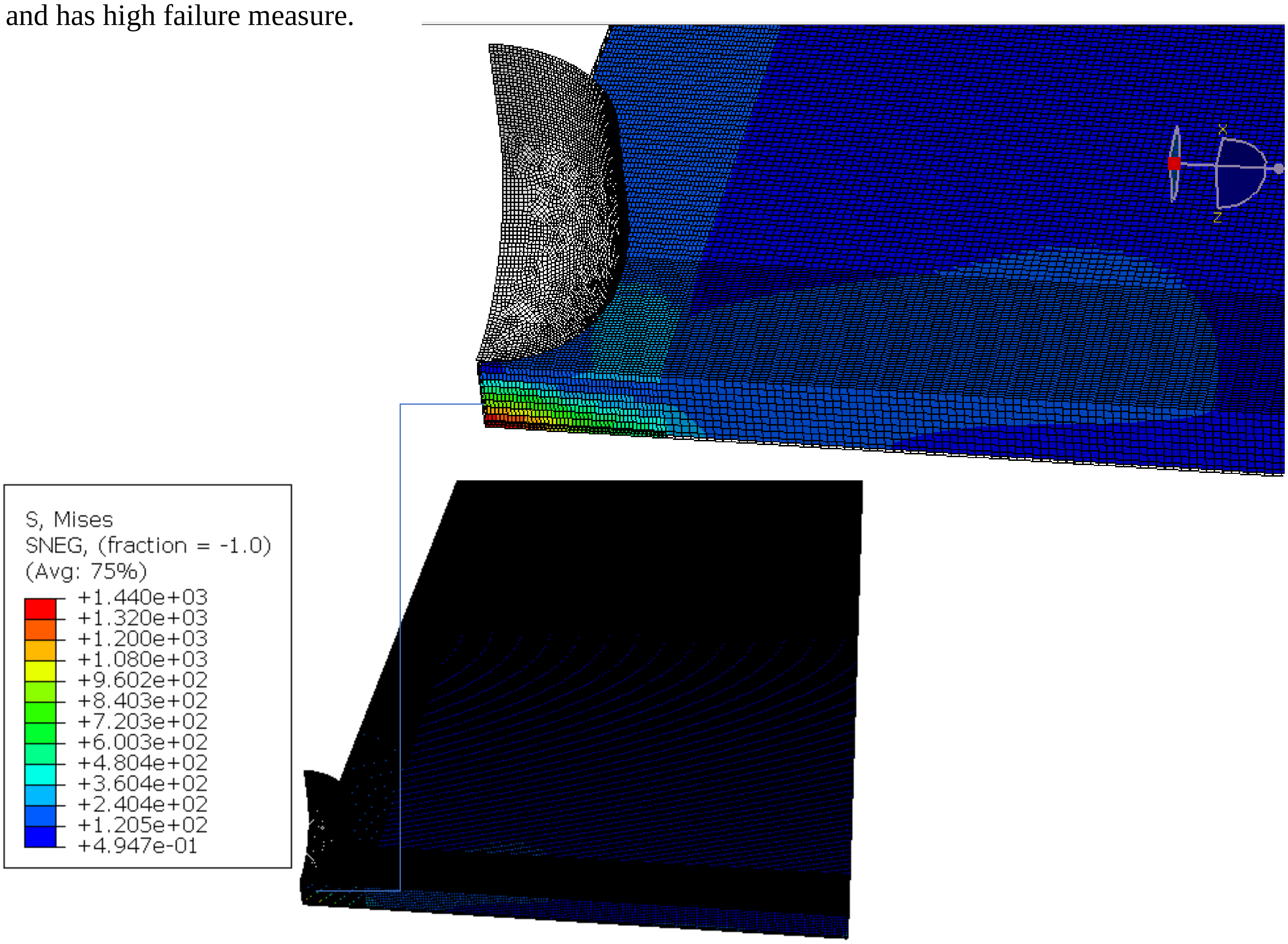

Figure 6.1 Stress distribution in GMT Material

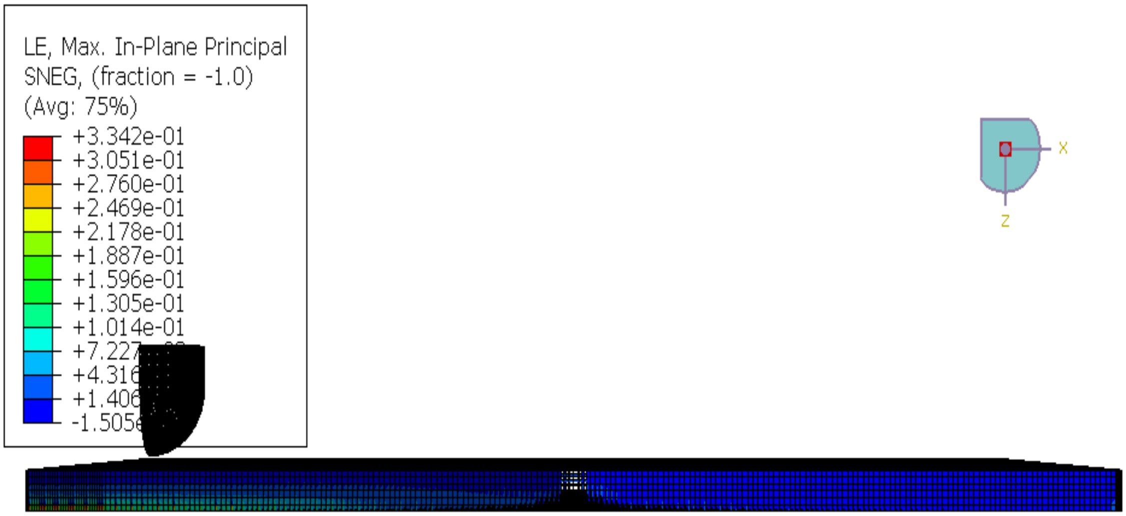

Figure 6.2 Logarisimic strain of GMT

In figure 6.1,6.2 and 6.3 the result shows that the high stress concentration area is in high damage count. In addition, there is also stress concentration in surface around impactor as shown and the shape of damage is as shown zoom of figure 6.1.

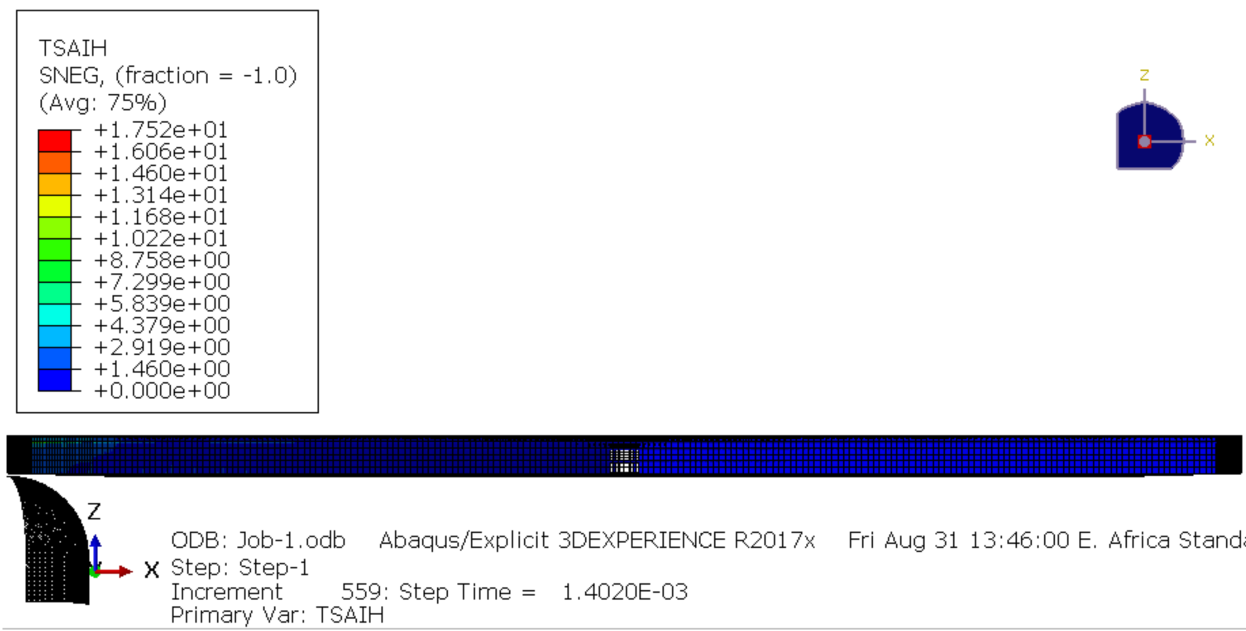

Figure 6.3 Failure measure at integration point

The profile of these three graphs I.e. figure 6.4, figure 6.5, and figure 6.6 are the same of (Belingardi et al. 2015) and shows GMT material absorbs less energy based on . Figure 6.6. around 131 J energy is absorbed from 293 J of impact energy. The reaction force is collected at the node which down ward velocity is applied.

For configuration like figure 6.6 impact energy is the heist energy and the final tip energy is absorption energy.

RF3 is reaction force in Z – direction as Z axis is visible in figure 6.2.

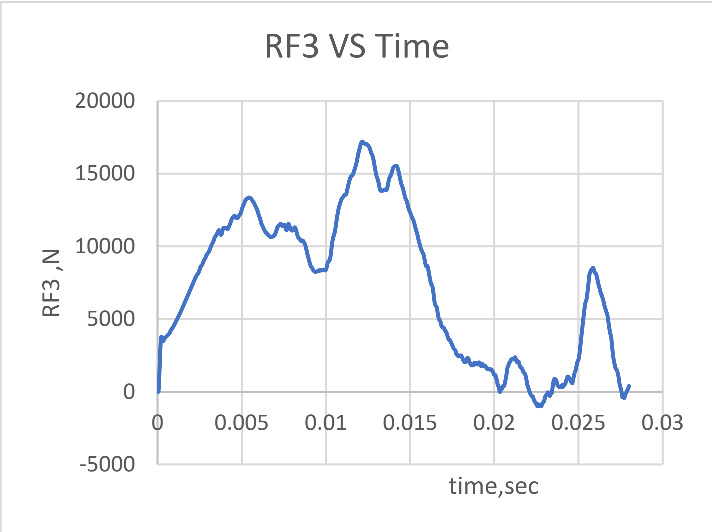

Figure 6.4 RF3 vs time of GMT

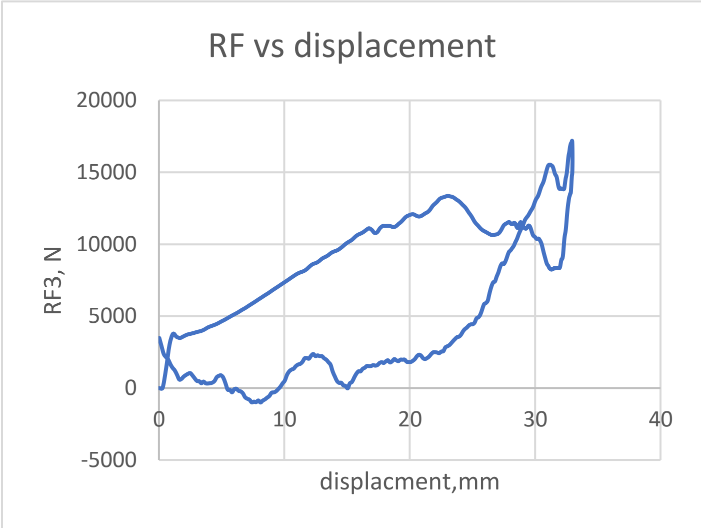

Figure 6.5 RF3 vs displacement of GMT

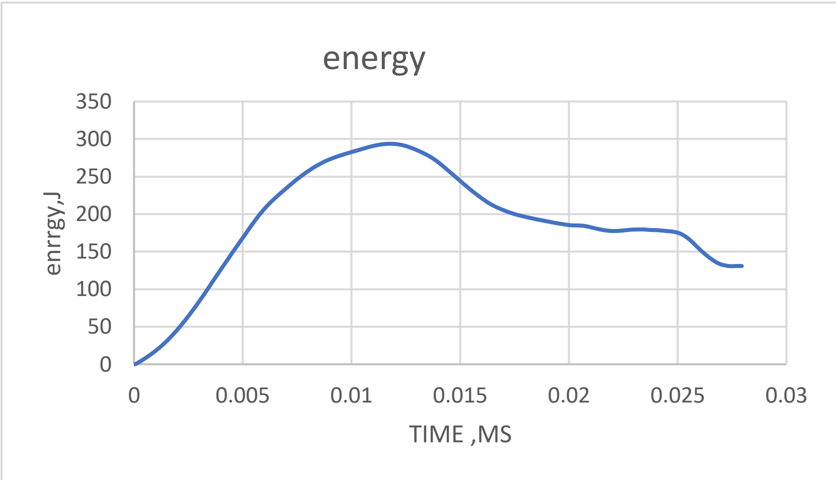

Figure 6.6 Impact energy of GMT with 293.75

6.2 Result and Discussion For GFRP-Woven composites for 28 J

Result for pristine GFRP – Woven composites

(Hyer n.d.) With a compressive stress in the fiber direction, contemporary polymer-matrix composites fail by fiber kinking, or micro buckling. And as per 6.9 Logarithmic Strain (LE) and stress penetration in the layer was also used for analysis of delamination and damage. All samples in 28.8J show high strain and stress penetration is in the fourth and fifth layer and show there is a delamination occurs in this area which is 90/90 degree. The second strain elongation is in the first and second layer which shows the second delamination has occurred in this area. In surface below there is edge stress concentration and distribute in zoom quarter cross shape as shown in figure 6.7

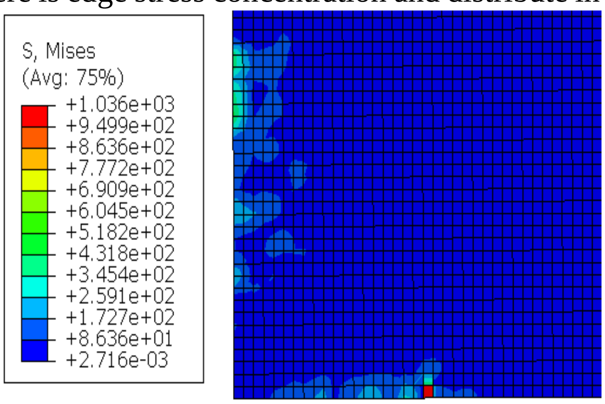

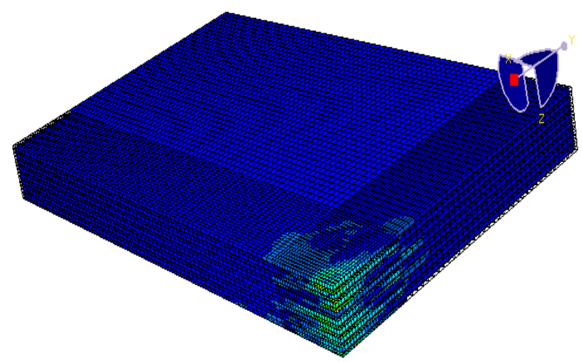

and 6.8 for pristine material.

Figure 6.7 Von mises stress of 0% nano clay

Figure 6.8 Stress concentration of 0% nano modified laminate

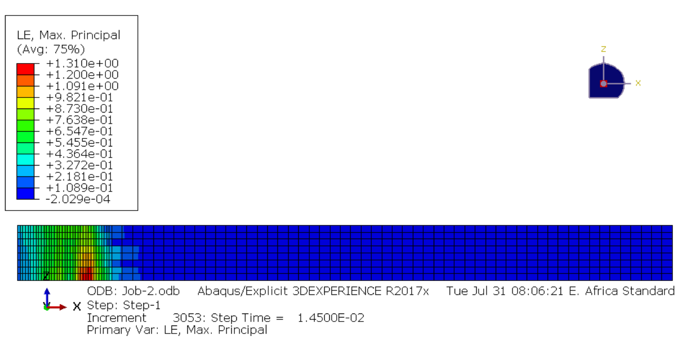

Figure .6.9 Logarisimic strain of 0% nano clay

Result for 0.5 % nano modified GFRP – woven composite

As per figure 6.10 and figure 6.11 Logarithmic Strain (LE) and stress penetration in the layer was also used for analysis of delamination and damage. All samples in 28.8J show high strain and stress penetration is in the fourth and fifth layer and show there is a delamination occurs in this area which is 90/90 degree. The second strain elongation is in the first and second layer which shows the second delamination has occurred in this area. In the surface below there is high stress concentration and concentrated especially in edges for 0.5% nano clay loading.

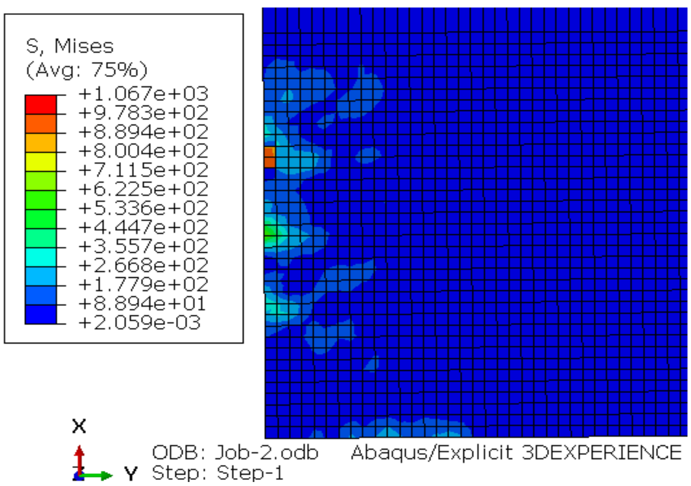

Figure 6.10 Von mises stress of 0.5% nano clay

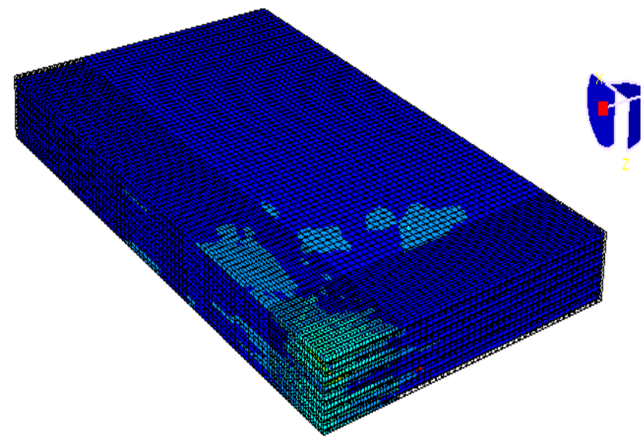

Figure 6.11 Stress concentration of 0% nano modified laminate

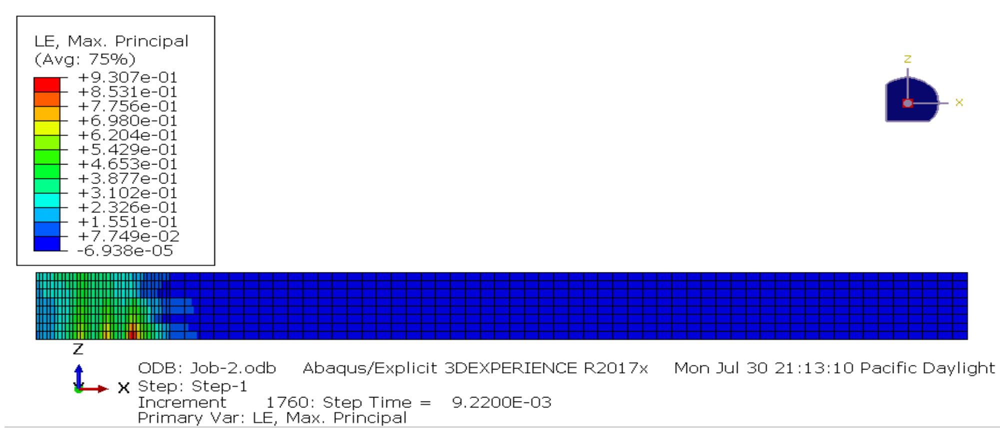

Figure 6.12 Logarisimc strain of 0.5% nano clay

Result 1 % Nano clay nano modified

As per figure 6.13 and figure 6.14 Logarithmic Strain (LE) and stress penetration in the layer was also used for analysis of delamination. All samples in 28.8 J show high strain and stress penetration is in the fourth and fifth layer and show there is a delamination occurs in this area which is 90/90 degree. The second strain elongation is in the first and second layer which shows the second delamination has occurred in this area. In the above surface there is small stress concentration and concentrated especially in edges for 2 % nano clay loading. In figure 6.13 we can see that high penetration of stress in fourth layer.

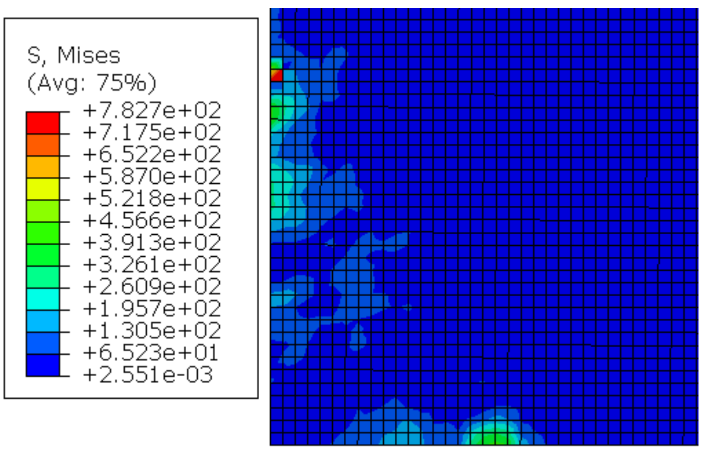

Figure 6.13 Von mises stress of 1% nano clay

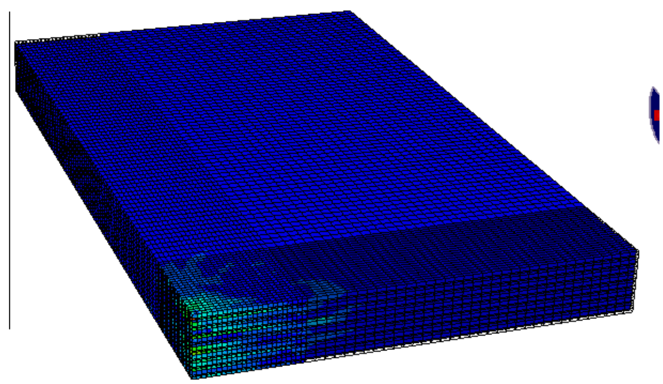

Figure 6.14 Stress concentration of 1% nano modified laminate

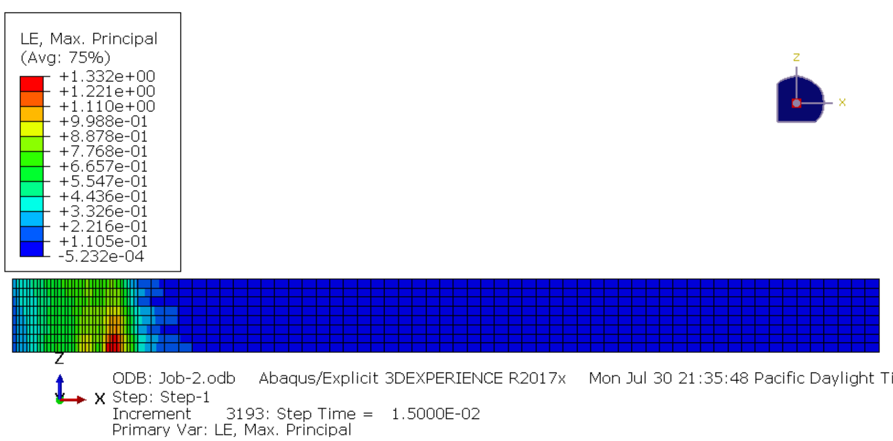

Figure 6.15 Logarisimc strain of 1% nano clay

Result for 2% nano clay modified

As per figure 6.17 and figure 6.18 Logarithmic Strain (LE) and stress penetration in the layer was also used for analysis of delamination. All samples in 28.8J show high strain and stress penetration is in the fourth and fifth layer and show there is a delamination occurs in this area which is 90/90 degree. The second strain elongation is in the first and second layer which shows the second delamination has occurred in this area. In the above surface there is small stress concentration and concentrated especially in edges for 2 % nano clay loading. As per figure 6.16 there is higher stress concentration area and shows higher damage area.

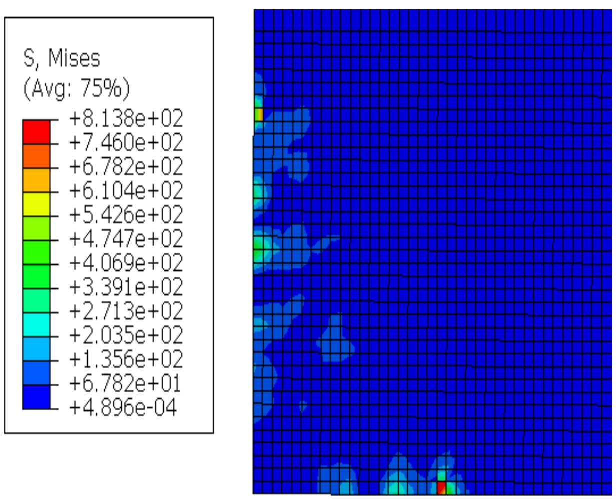

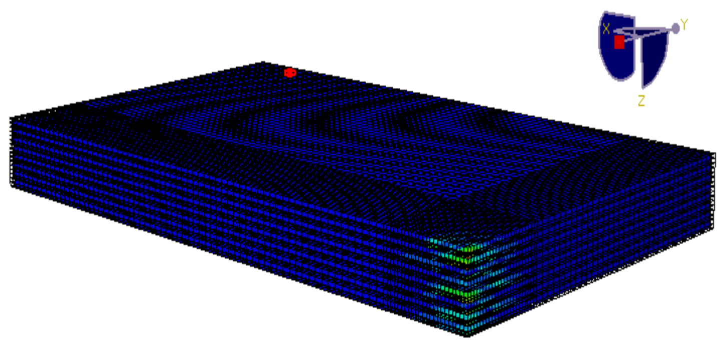

Figure 6.16 Von mises stress of 2% nano clay

Figure 6.17 Stress concentration for 2% nano clay in laminate.

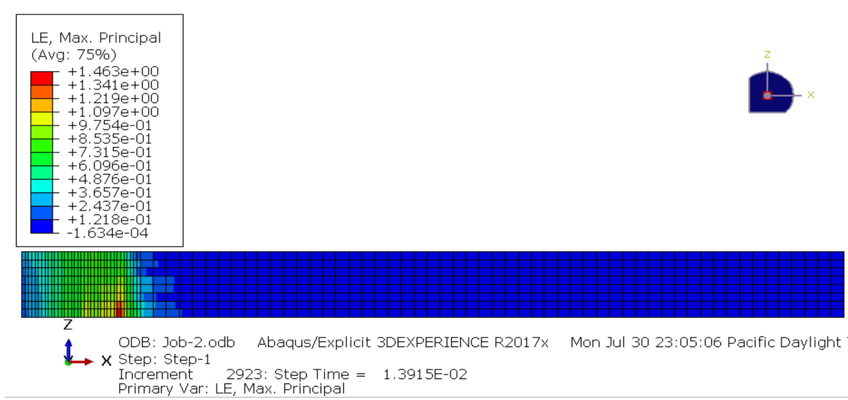

Figure 6.18 Logarisimc strain of 2% nano clay

pristine

A) 28.8 Joule (m=40 kg, v=1.2 m/sec)

The peak force in the curve represents the load that a laminate can withstand before undergoing critical damage few fluctuations in the curve represent the propagation of cracks, which also results in the stiffness degradation.(Bandaru et al. 2016). Thus, from observations for this impact energy 0.5% nano clay withstand 10.2% higher load before going critical damage.

Regarding to fluctuation of graph for it can be used for analysis also as per(Zhang, Duodu, and Gu 2017) Figure 6.20 shows the energy absorption as the aim of this research is to identify the best material that absorb energy. With impact energy write below the figures.

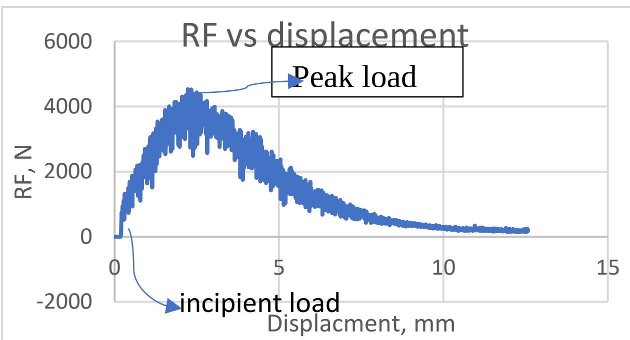

Figure 6.19 RF3 vs displacement profile of 0%

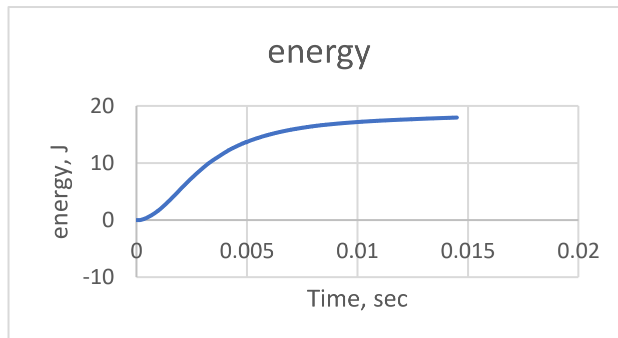

Figure 6.20 energy time profile 0 % nano clay 28.8 J

0.5% nano clay

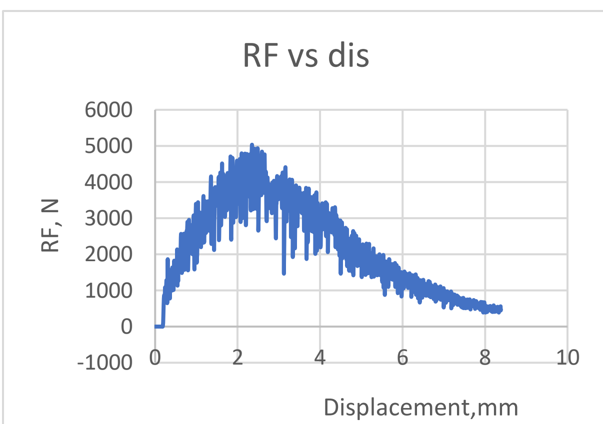

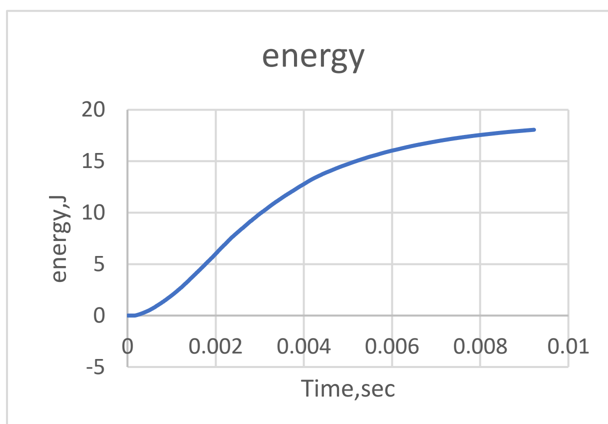

Figure 6. 21 RF3 vs displacement profile of 0.5% 28.8 J.

Figure 6.22 Energy time profile 0.5% nano clay at 28.8 J

From figure below Adding 2% Cloisite® 20B nano clay in GFRP -woven composites has low load resistance before going to critical failure as compared to three GFRP composites.

1% nano clay modified

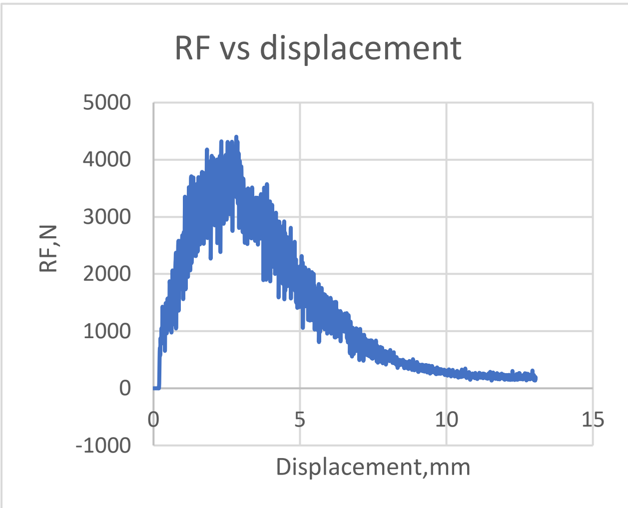

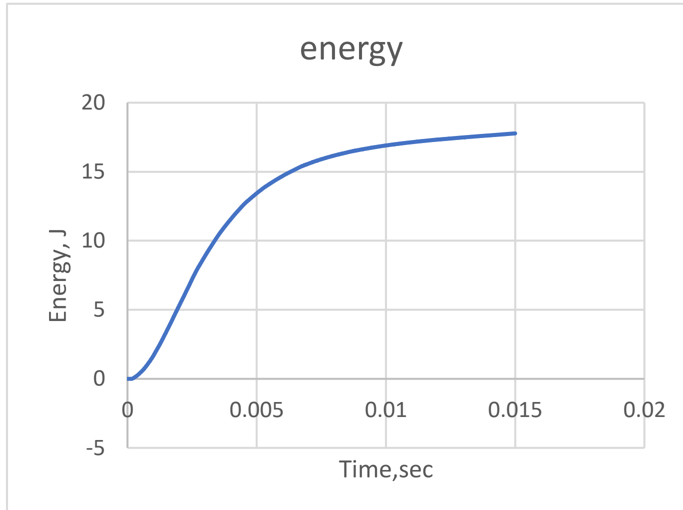

Figure 6.23 RF3 vs displacement profile 1% nano clay

Figure 6.24 Energy vs time profile of 1% nano clay

2% nano clay

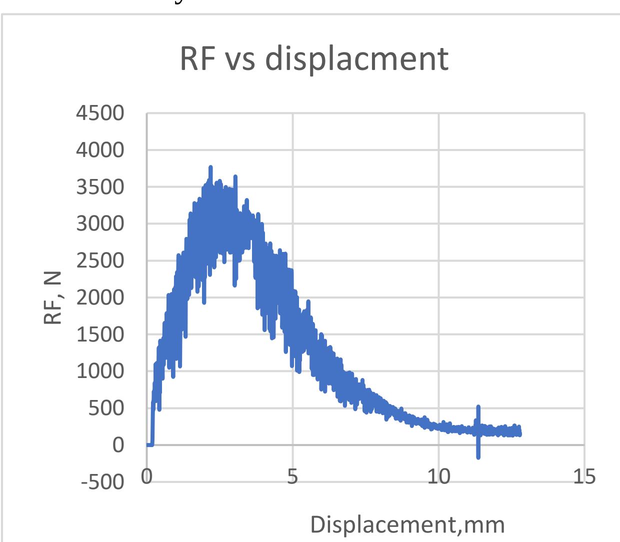

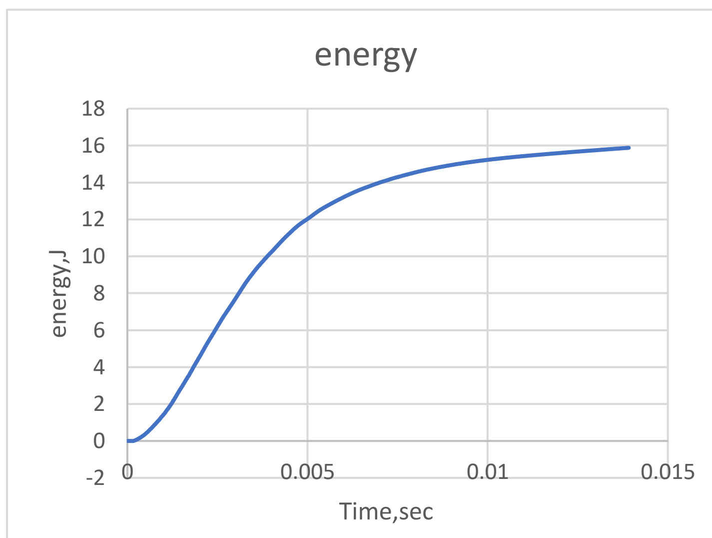

Figure 6.25 RF3 vs displacement profile for 2% nano clay.

Figure 6.26 Energy vs time profile for 2% nano clay

Comparisons

In figure 6.27 shows the comparison of reaction force for pristine and o.5% nano clay, and shows 0.5% nano clay loading shows higher reaction force than pristine material. In figure 6.35 shows the comparation of pristine, 0.5% nano clay, 1% nano clay and 2% nano clay and shows 0.5% nano clay is the highest, followed by pristine,1% and 2% nano clay. 2% nano clay loading reaches its maximum reaction force first, followed by pristine. Reaction force of 0.5 % nano clay loading reaches last of all GFRP – woven composites.

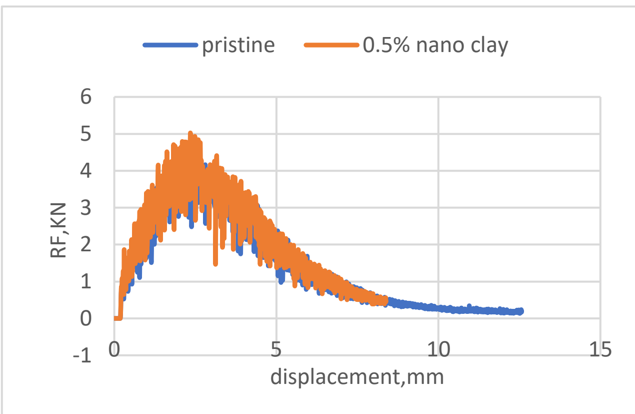

Figure 6.27 Comparison of pristine and 0.5% nano clay

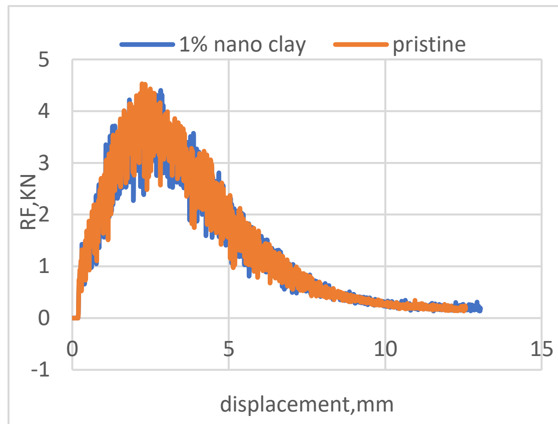

Figure 628 Comparison of pristine and 1% nano clay

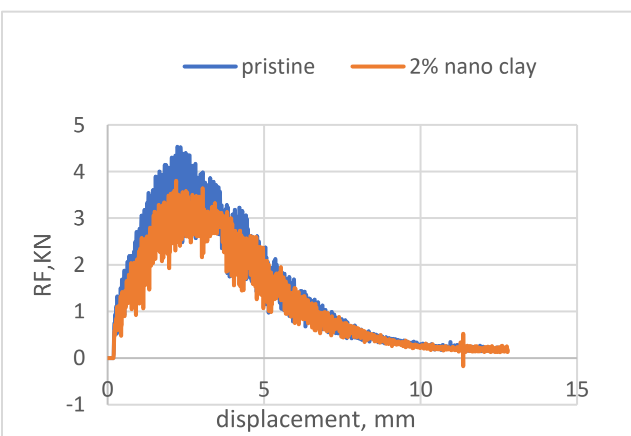

Figure 6.29 Comparison pristine and 2% nano clay.

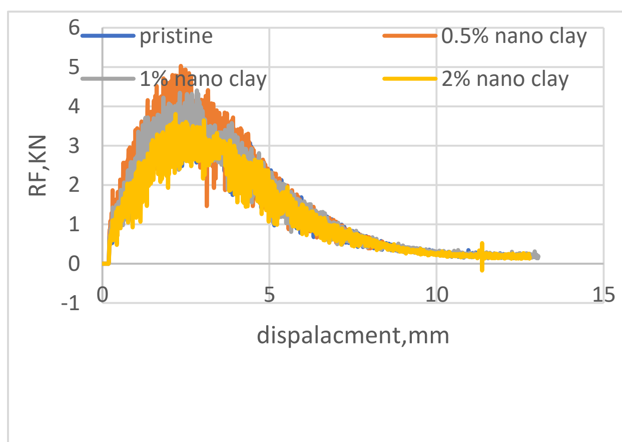

Figure 6.30 Comparation pristine, 0.5%,1% and 2% nano clay

For 32.2 J in Figure 6.31, 6.32, 6.33 and 6.34 impact energy also show adding nano clay with 0.5% loading can with stand high load before reaching critical failure.

B) Force and energy graph, 39.2 J (m=40 kg, 1.4 m/sec)

Pristine

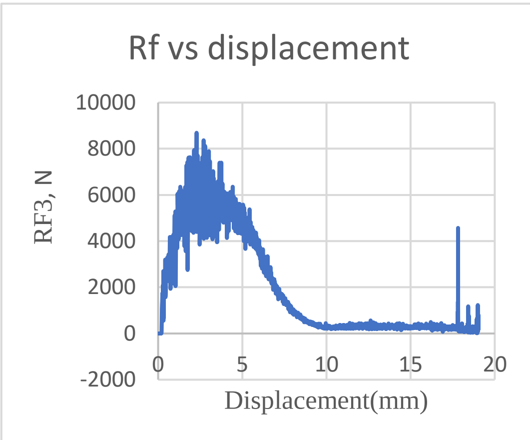

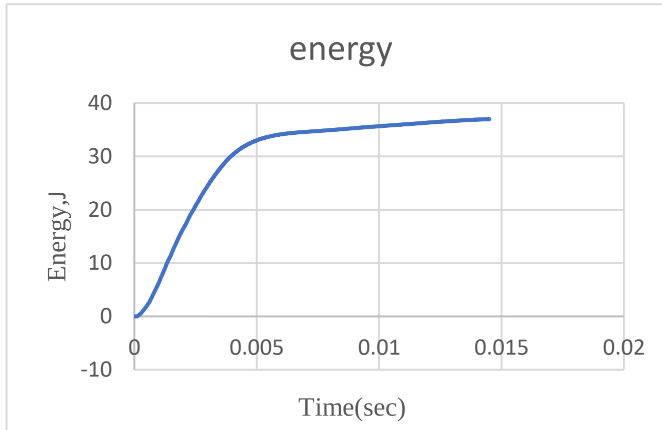

Figure 6.31 RF3 vs displacement profile of pristine. Figure 6.32 Energy time profile of pristine at 39.2 J

0.5 % nano clay

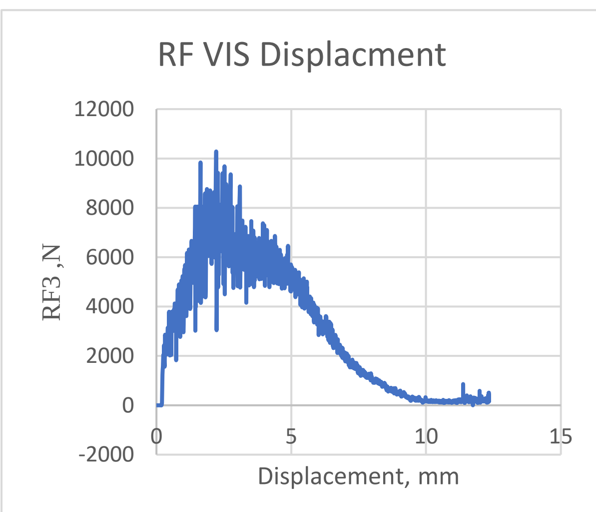

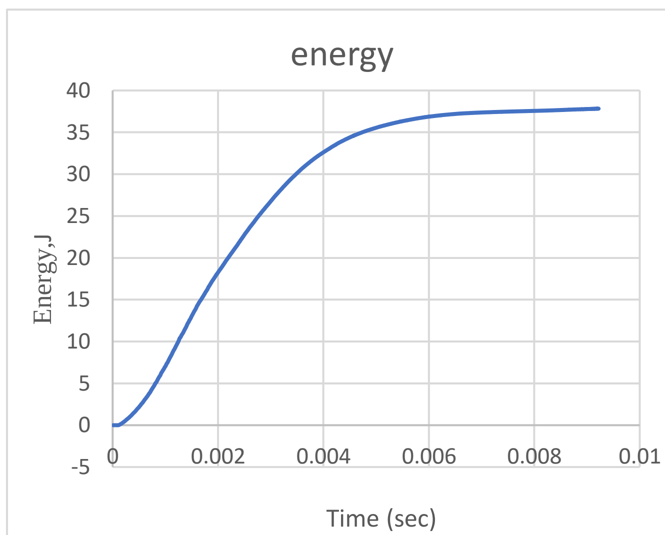

Figure 6.33 RF3 vs displacement profile of 0.5% nano clay Figure 6.34 Energy vs time profile of 0.5% at 39.2 J

1% nano modified

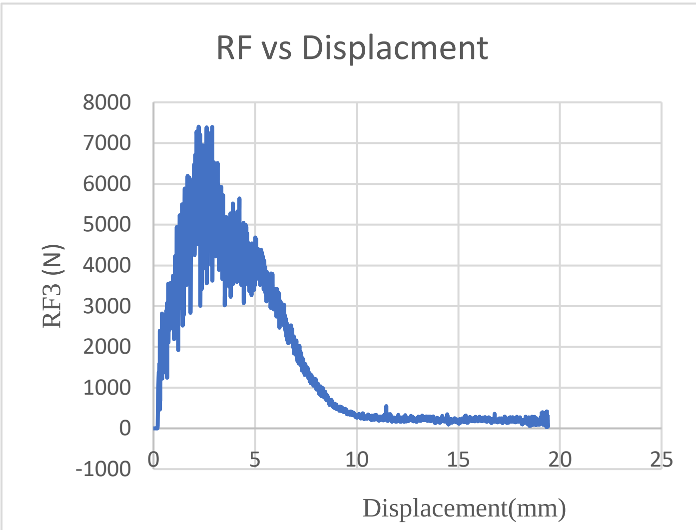

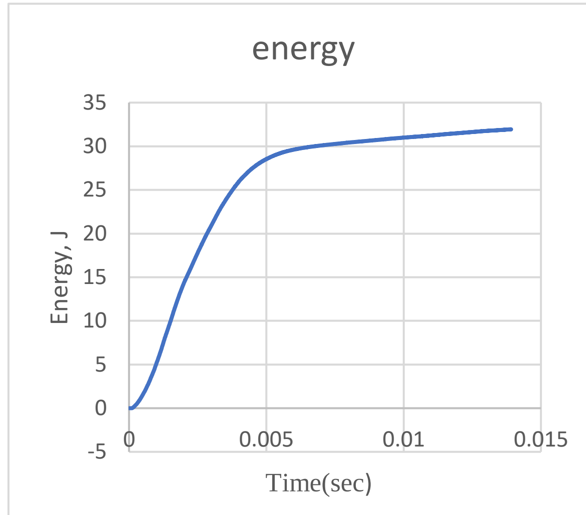

Figure 6.35 RF3 vs displacement profile of 1% nano clay Figure 6.36 Energy vs time profile for 1% at 39.2 J

2% nano clay modified

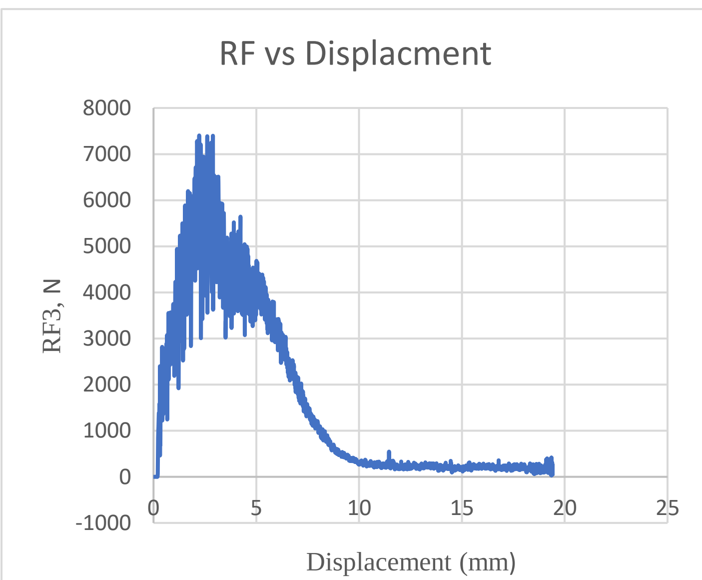

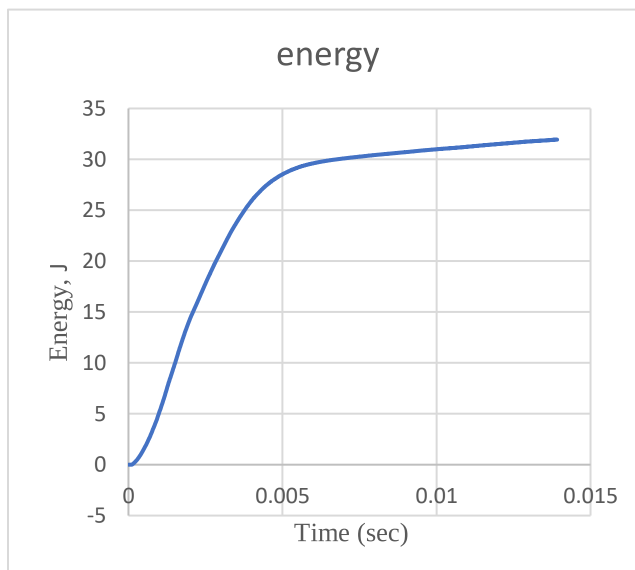

Figure 6.37 RF3 vs displacement of 2% nano clay *Figure 6.38 Energy vs time of 2% nano clay at 39.2 J*

In figure below especially in figure 6.39 shows the comparation of pristine, 1% nano clay and 2% nano clay and shows pristine is the highest in reaction force, followed by ,1% and 2% nano clay.

Comparison

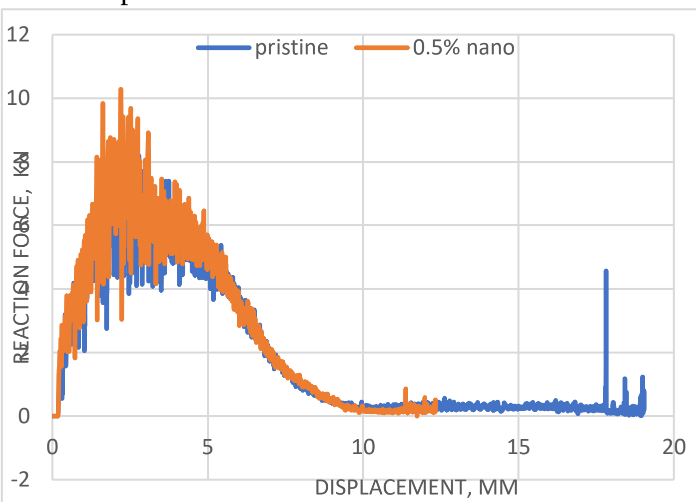

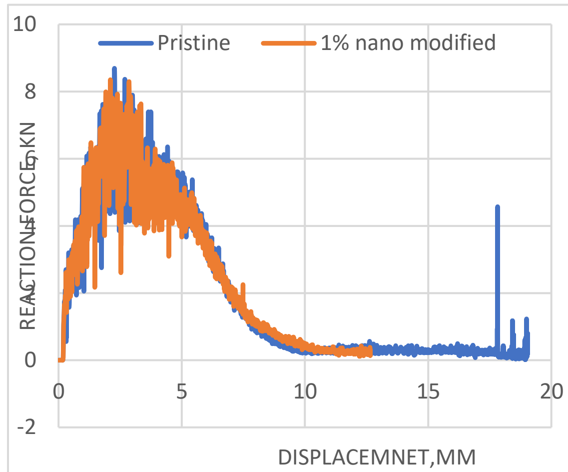

Figure 6.39 Comparation pristine and 0.5% nano clay. Figure 6.40 Comparation pristine and 1% nano clay 39.2 J

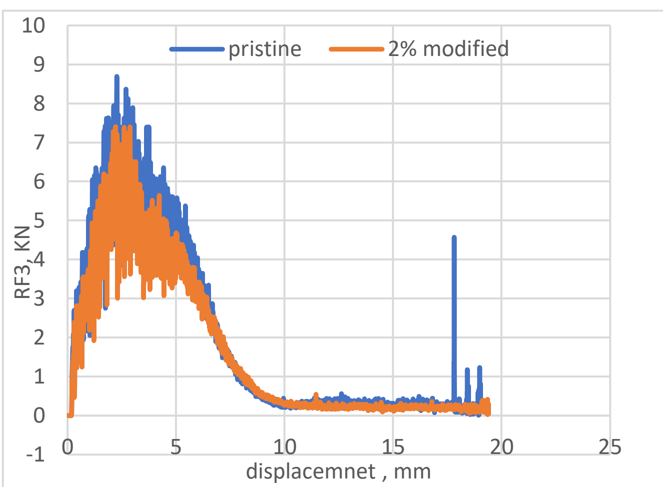

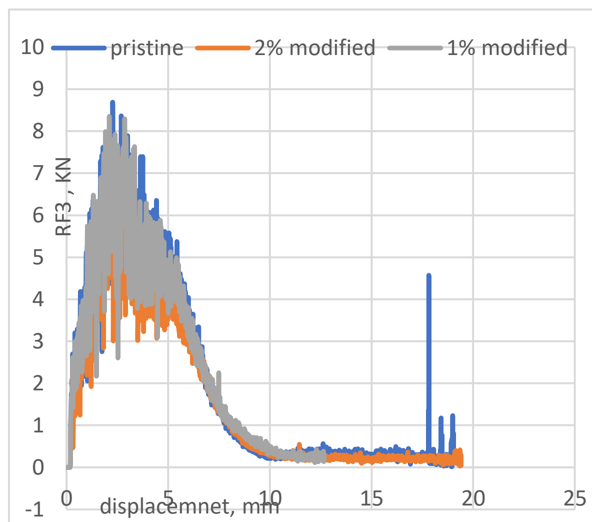

Figure 6.41 Comparison of pristine and 2% nano clay

Figure 6.42 Comparation of 0%, 1% and 2% nano clay at 39.2 J

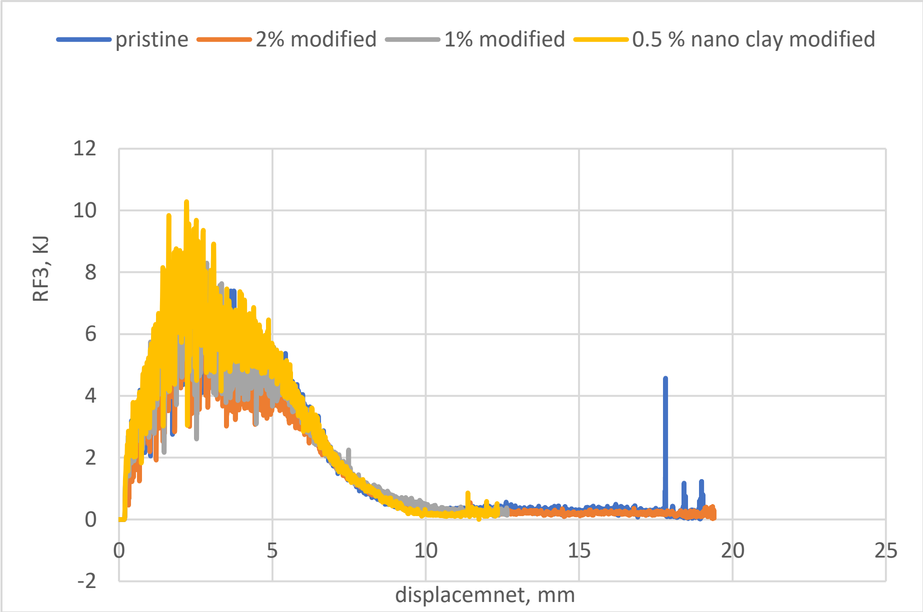

Figure 6.43 Comparison of pristine, 0.5% nano clay, 1% nano clay and 2% nano clay at 39.2 J

For 57.8 J in Figure 6.44, 6.45, 6.46 and 6.47 impact energy also show adding nano clay with 0.5% loading can with stand high load before reaching critical failure.

C) 57.8 J (m = 40 kg, v 1.7 m/sec)

Pristine

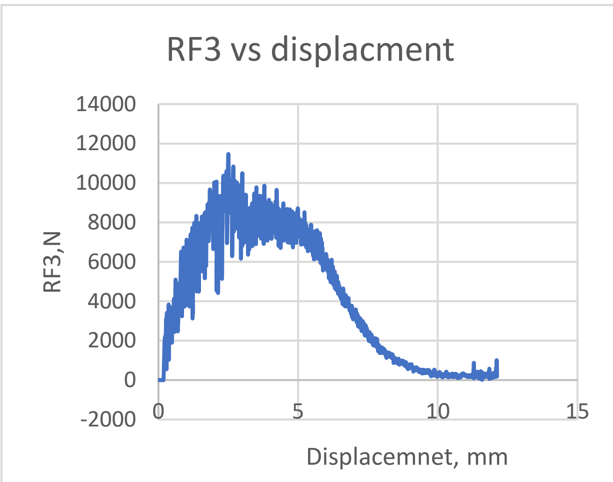

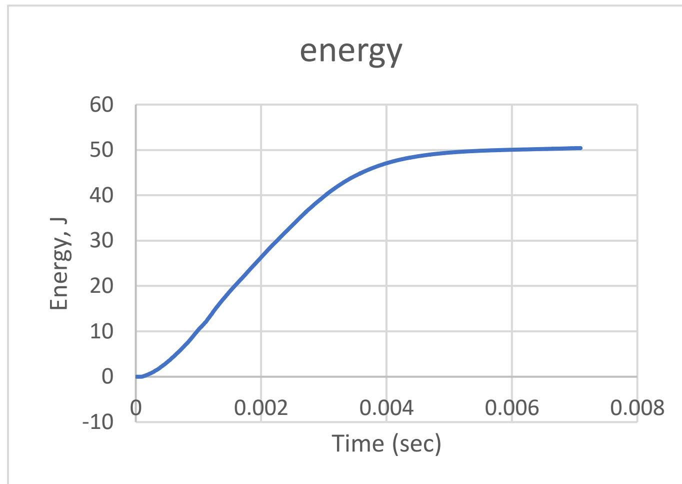

Figure 6.44 RF3 vs displacement of pristine

Figure 6.45 Energy vs time profile of pristine at 57.8 J

0.5% nano clay modified

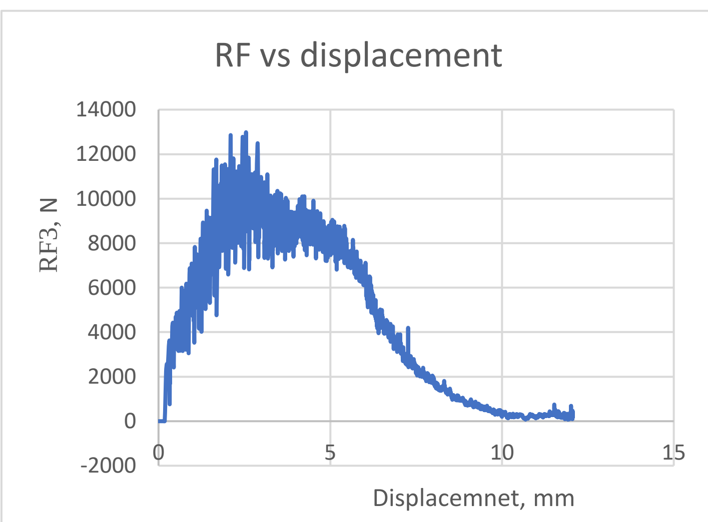

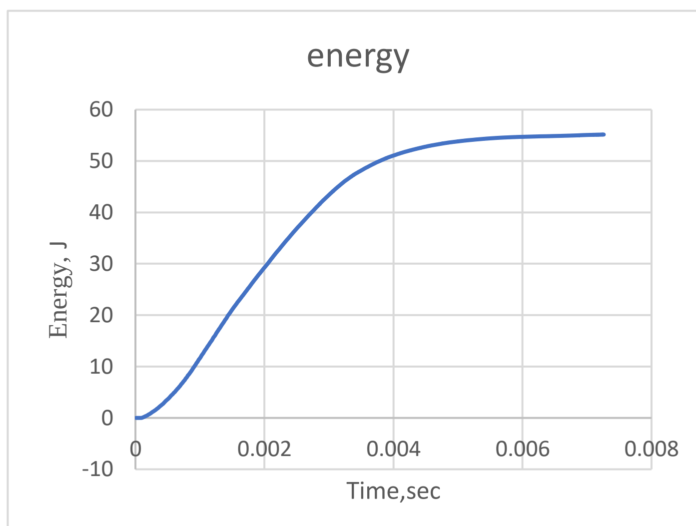

Figure 6.46 Reaction force vs displacement 0.5% nano clay at 57.8 J

Figure 6.47 Energy vs time graph, of 0.5% nano clay at 57.8 J

1% nano modified

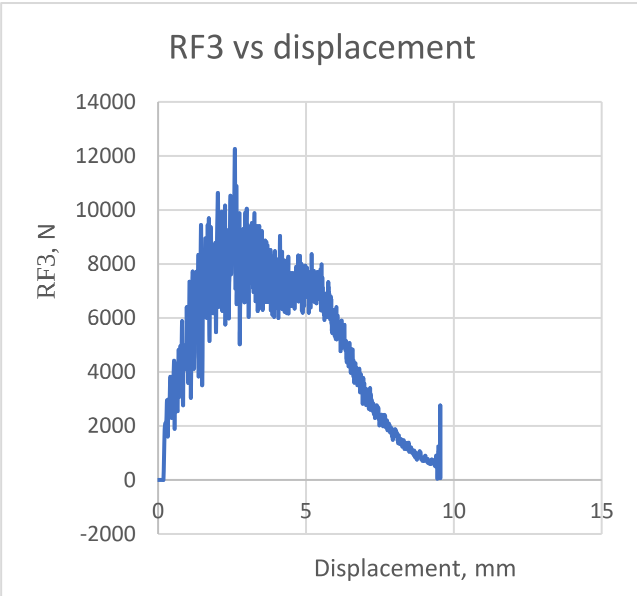

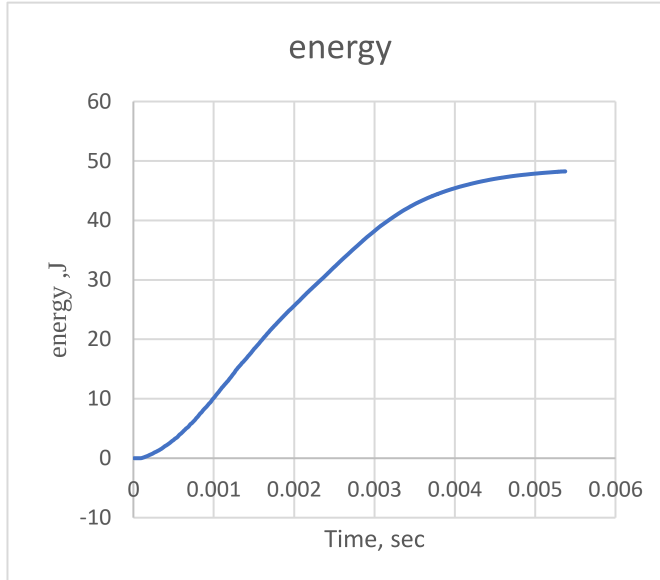

Figure 6.48 RF vs displacement of 1% nano clay at 57.8 J Figure 6.49 Energy vs time of 1% nano clay at 57.8 J

2% nano modified

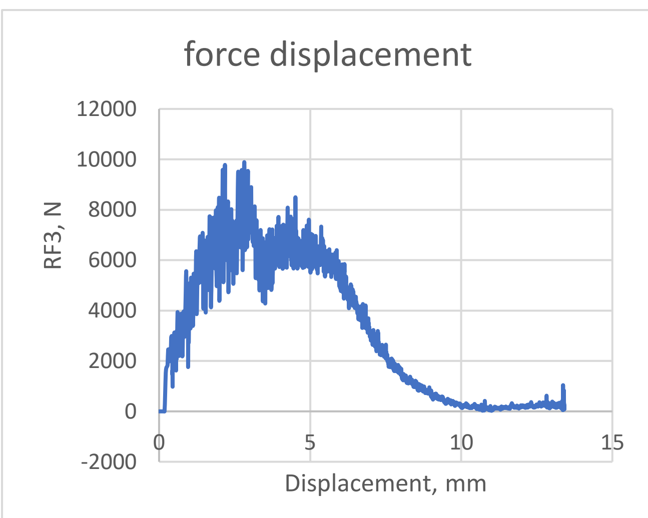

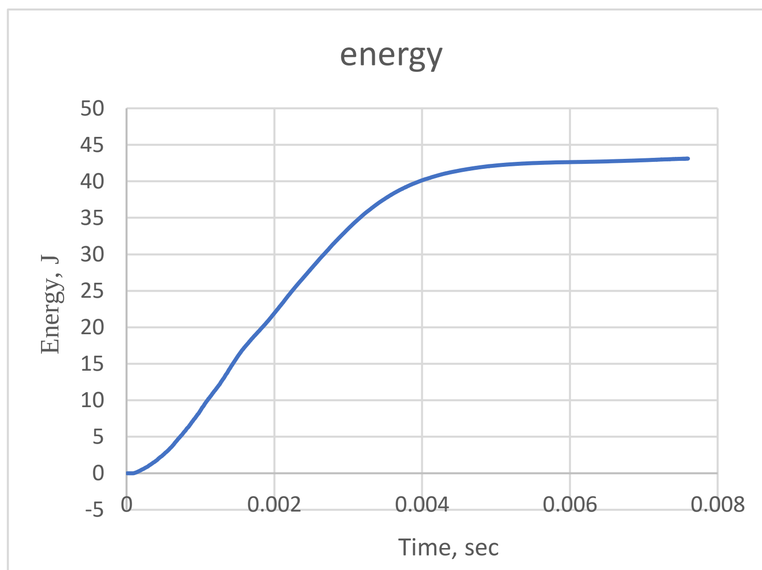

Figure 6.50 RF vs displacement of 2% nano clay at 57.8 J Figure 6.51 Energy vs time of 2% nano clay at 57.8 J

Comparison

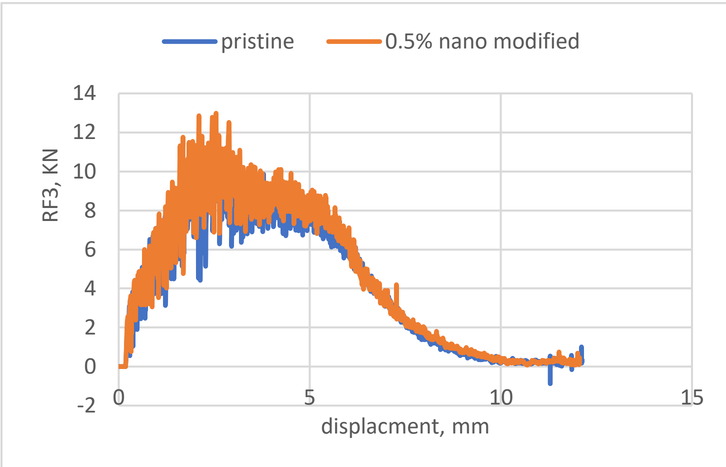

Figure 6.52 Comparation of 0% and *0.5% nano clay*

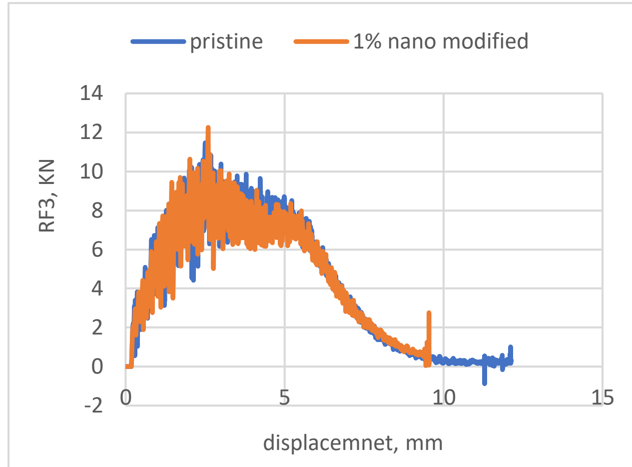

Figure 6.53 comparation of 0% and 1% nano clay at 57.8 J

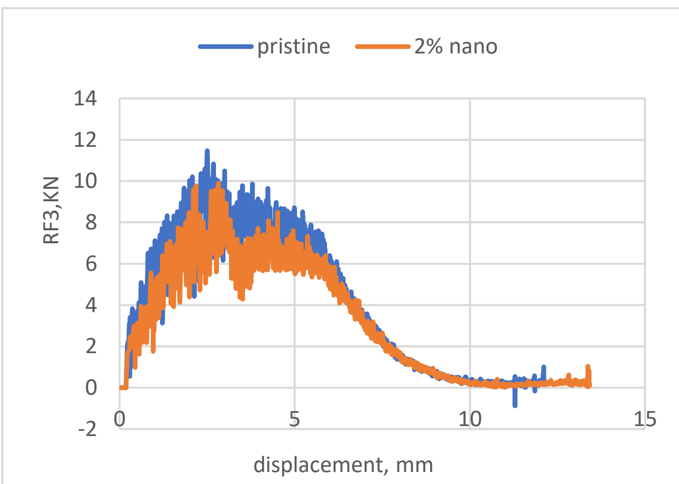

Figure 6.54 Comparison of 0% and 2% nano clay at 57.8 J

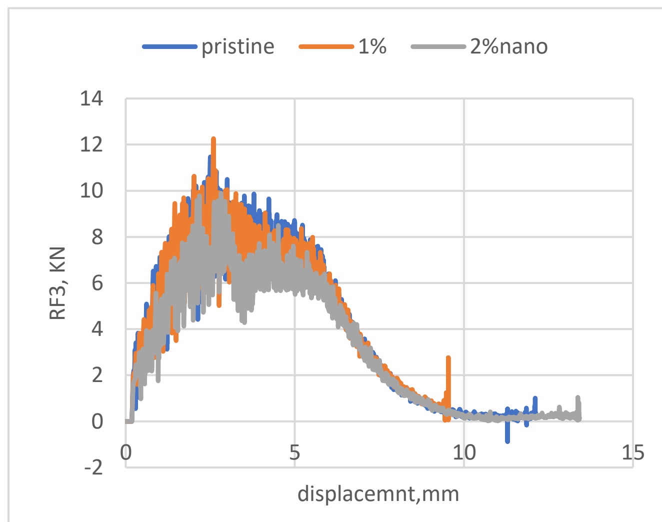

Figure 6.55 Comparation of 0%, 1%, and 2% at 57.8 J

Figure 6.56 shows the comparison of reaction force for pristine and 0.5% nano clay, and 0.5% nano clay loading shows higher reaction force than pristine material. Figure 6.61 shows the comparation of pristine, 0.5% nano clay, 1% nano clay and 2% nano clay and shows 0.5% nano clay is the highest, followed by pristine ,1% and 2% nano clay.

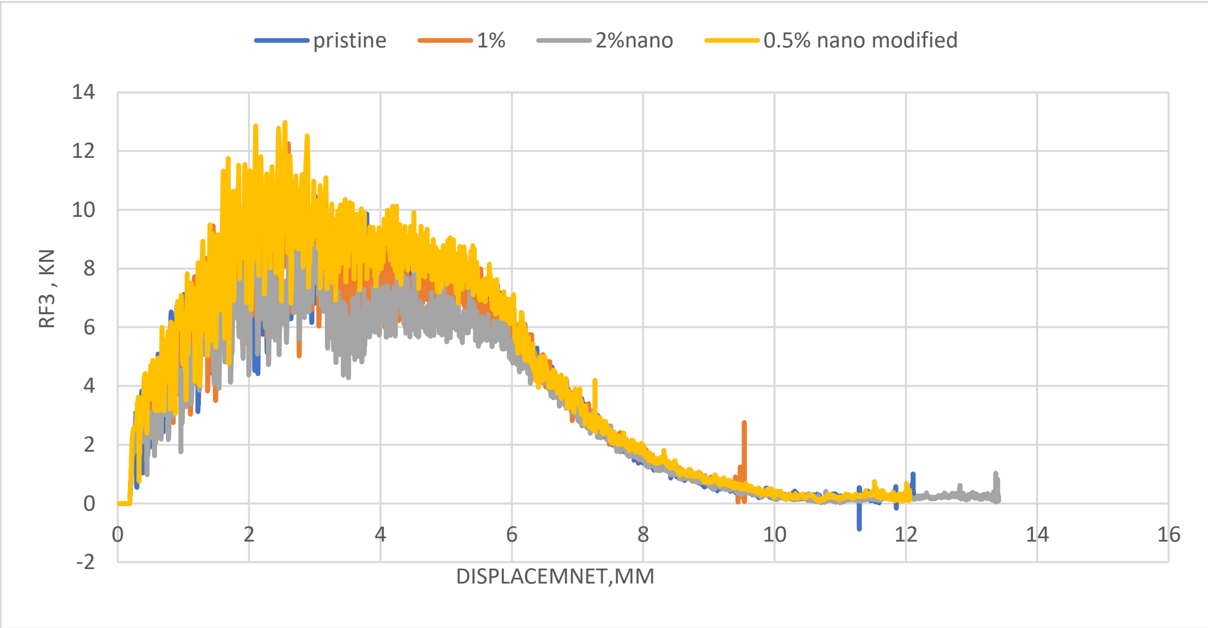

Figure 6.56 Comparation of 0%, 0.5% 1% and 2% nano clay at 57.8 J

For 72.2J in Figure 6.57, 6.58, 6.59 and 6.60 impact energy also show adding nano clay with 0.5% loading can with stand high load before reaching critical failure and loading with 2 % can with stand low load before critical load.

D) 72.2J (m = 40kg, v = 1.9 m/sec)

Pristine

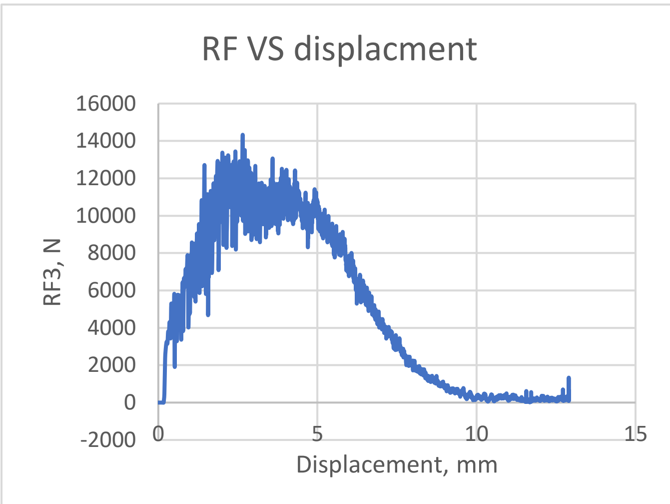

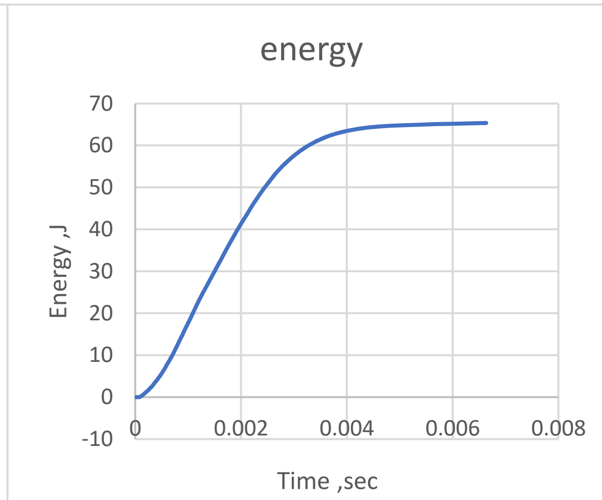

Figure 6.57 RF vs displacement of 0% nano clay at 72.2 J

Figure 6.58 Energy vs time of 0% nano clay at 72.2 J

0.5 % nano modified

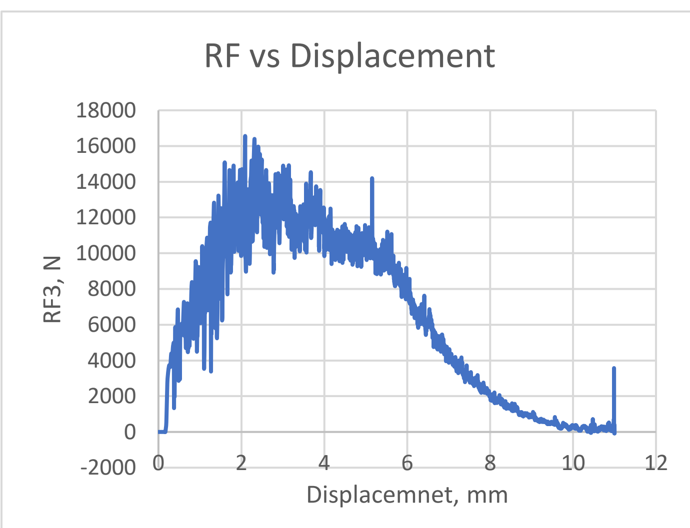

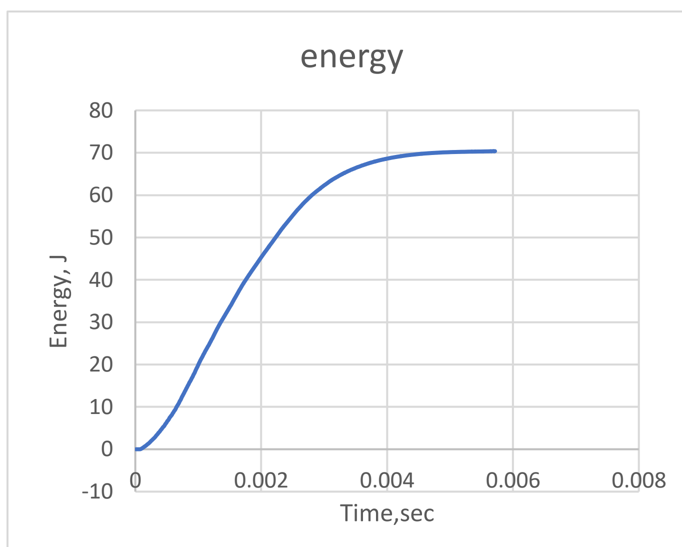

Figure 6.59 RF vs displacement of 0.5% nano clay at 72.2 J.

Figure 6.60 energy vs time of 0.5% nano clay at 72.2 J

1% nano clay modified

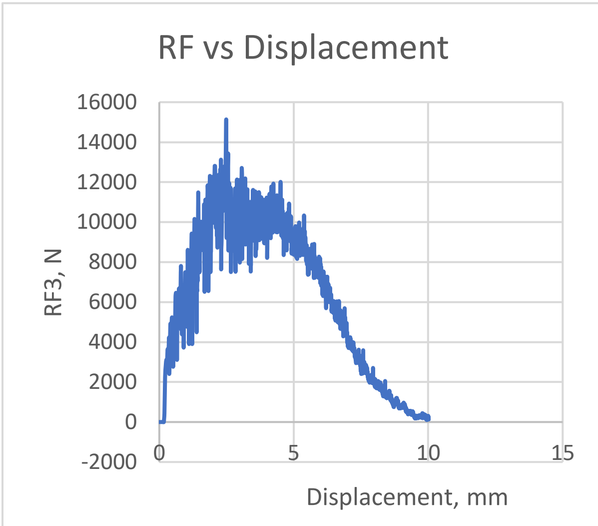

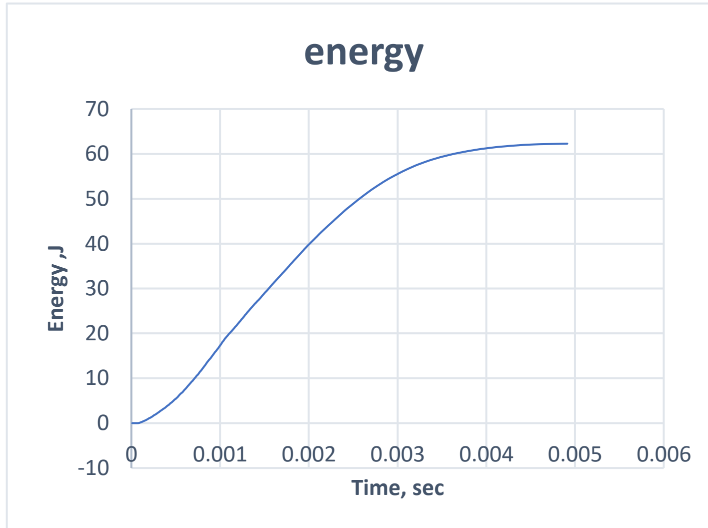

Figure 6.61 RF3 vs displacement graph of 1% nano clay

Figure 6.62 Energy vs time of 1% nano clay at 72.2 J

2 % nano clay

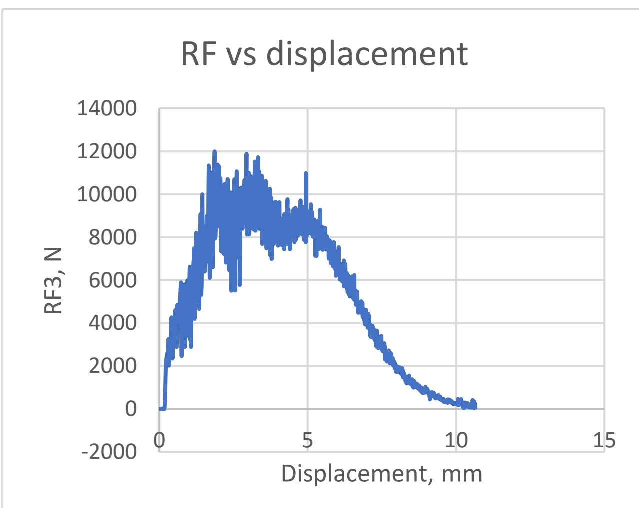

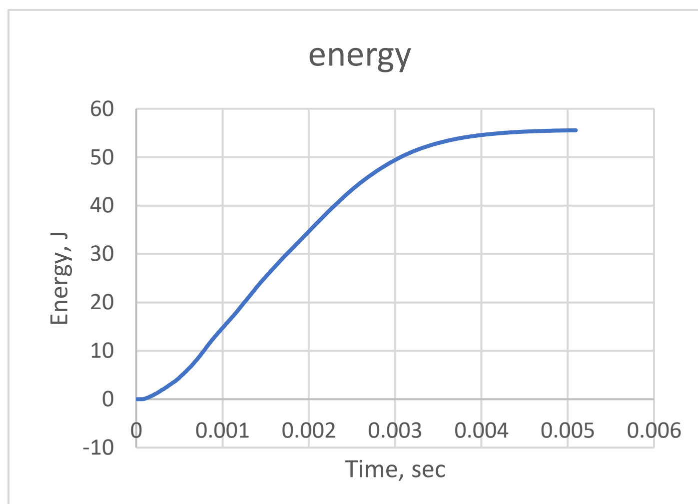

Figure 6.63 RF vs displacement of 2% nano clay at 72.2 J

Figure 6.64 Energy time of 2% nano clay, at 72.2 J

Figure 6.65 shows the comparison of reaction force for pristine and 0.5% nano clay, and 0.5% nano clay loading shows higher reaction force than pristine material. In figure 6.69 below shows the comparation of pristine, 0.5% nano clay, 1% nano clay and 2% nano clay and shows 0.5% nano clay is the highest, followed by pristine, 1% and 2% nano clay.

Comparison

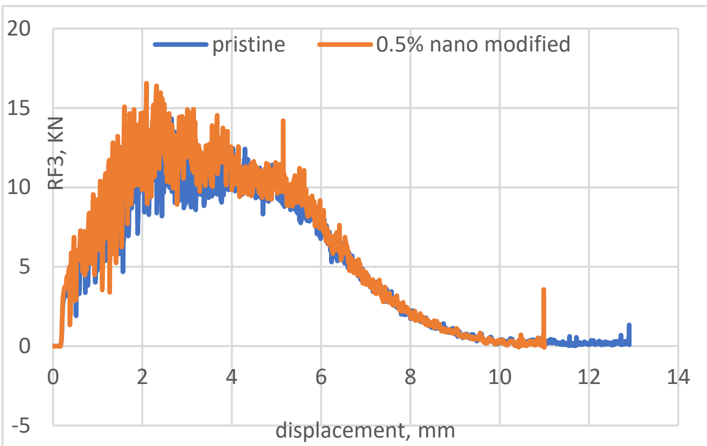

Figure 6.65 Comparation of 0% and 0.5% nano c lay at 72.2

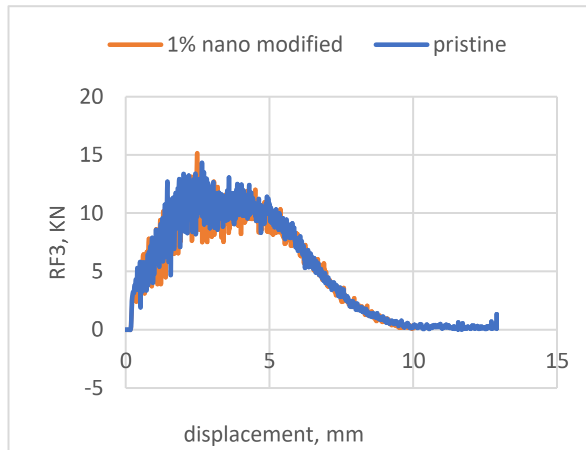

Figure 6.66 Comparation of 0% and 1% nano clay 72.2 J

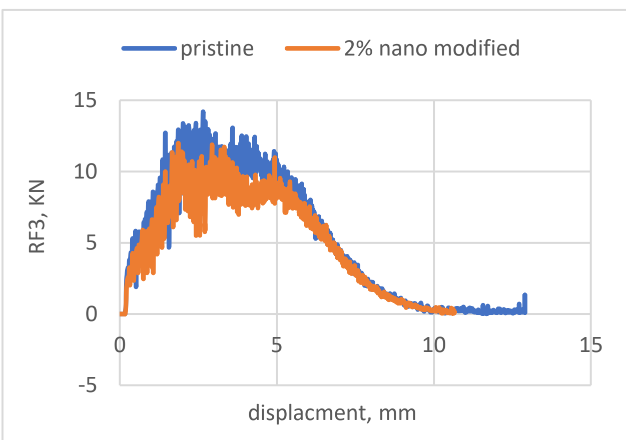

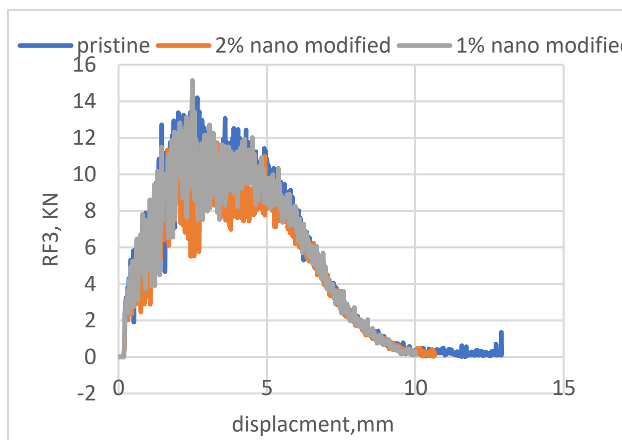

figure 6.67 Comparation of 0% and 2% nano clay at 72.2J. Figure 6.68 Comparation of 0%, 1%, and 2% nano clay

These impact damage resistance plots can be characterized by two thresholds, incipient load and peak load as marked in Figure 6.69 Incipient load is identified by the first sudden drop in the reaction-time curve which indicates the first material damage such as interface failure or matrix cracking which is present usually at/or near the back face of laminates(Rafiq et al. 2017). From exploded view of figure 6.70 incipient load of 2% nano clay is first followed by 1% and 0.5% nano clay loading and pristine is the last. This shows adding nano clay leads to first material damage.

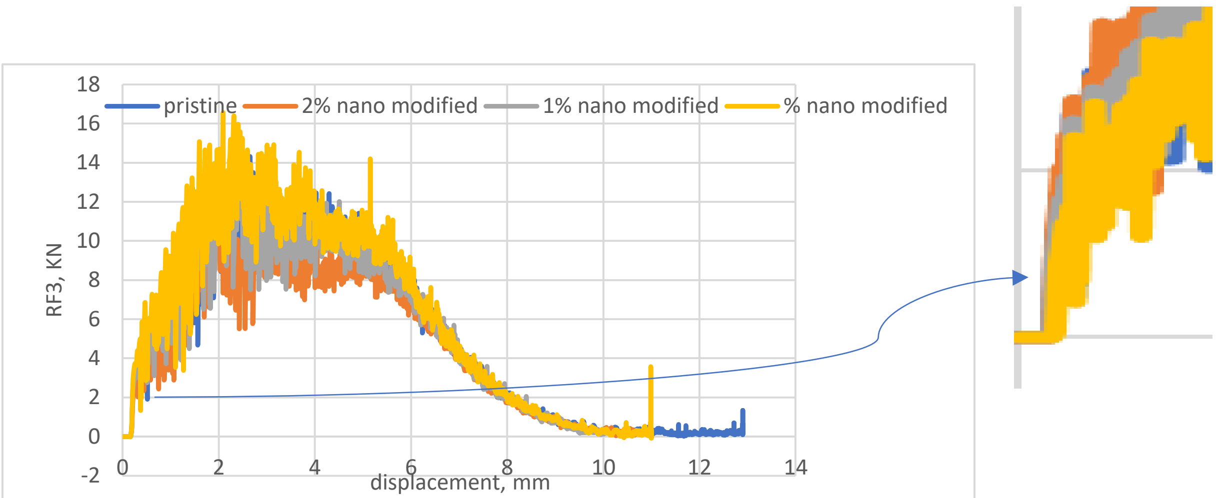

Figure 6.69 Comparation of 0%, 0.5%, 1% and 2% nano clay

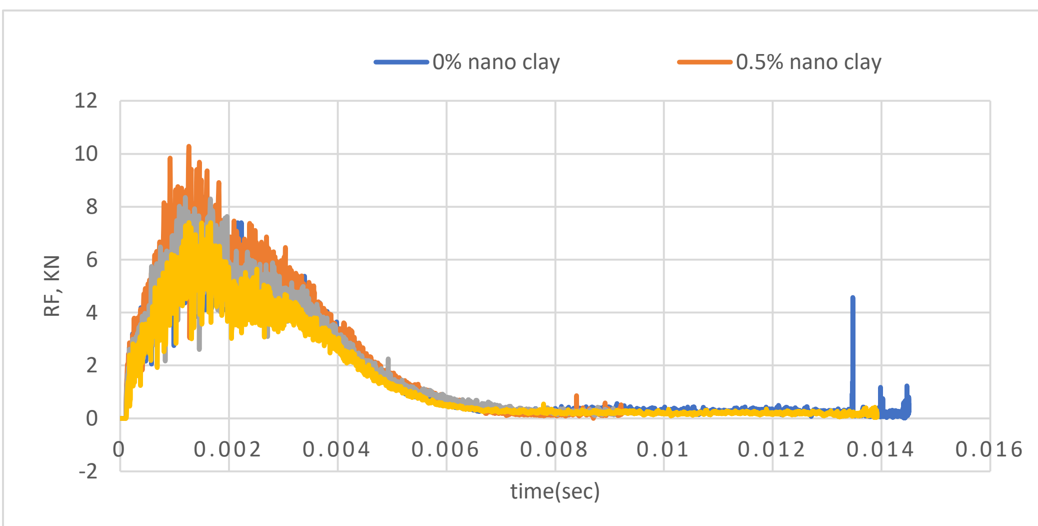

Figure 6.70 RF3 vs time of 0%, 0.5%,1% and 2% nano clay,

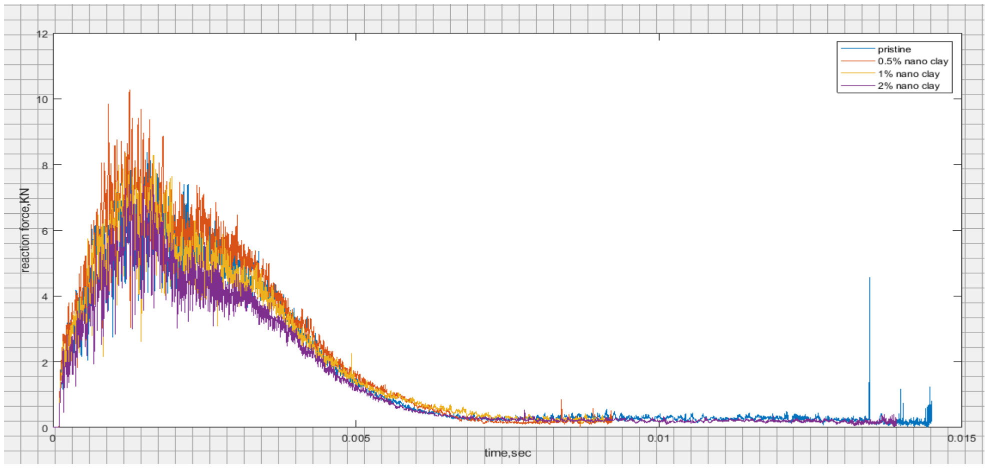

Figure 6.71 Mat lab reaction force vs time result

Based on RF, time graph figure, figure 6.70 and figure 6.71 1% nano clay reaches faster second followed by 0.5% nano clay, and 2% nano clay and pristine reaches last 57.8 J impact energy. These shows the damage initiation sequence. This shows adding nano clay to the glass fiber reinforced polymer to decrease impact initiation strength.

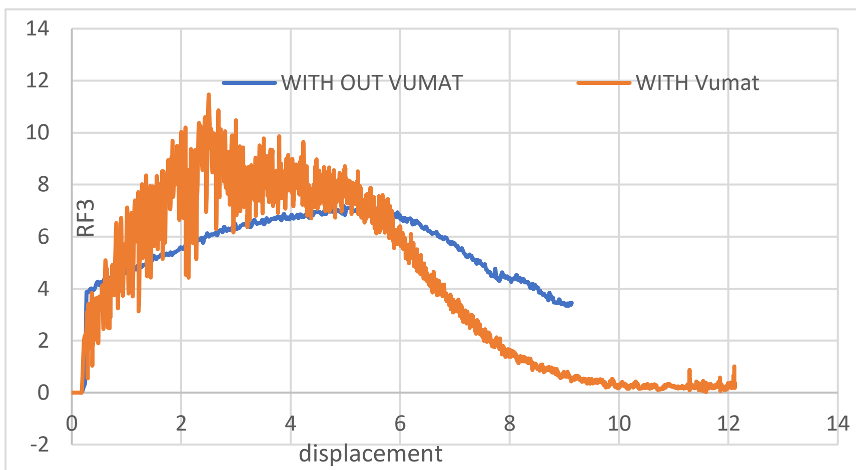

Figure 6.72 Somparation of RF3 vs displacement graph for subroutine and without subroutine

(Riccio et al. 2017) shows the relation between experimental and Vumat and shows good correlation. In figure 6.72 shows the variation of Abaqus using Vumat and without Vumat. The variation is due to failure criteria difference and the variation taken as modification or enhancing prediction of failure and analysis. These in Vumat program we are try to use two failure criteria. I.e. Hashin 3D and modified Tsi-wu or puck failure criteria. But Abaqus explicit use 2D Hashin failure criteria for composite materials.

As per (Koricho et al. 2015) adding nano clay with 1% loading increase the energy absorption capacity, while (Rafiq et al. 2017) conclude samples with 1.5 wt.% nano clay loading absorb less energy as compared to 3 wt.% and GFRE (0%) samples. But in this research, the capacity of energy absorption in comparison with pristine is depended on the amount of percent of nano-clay. Based on figure 6.73 to 6.74 the energy absorption of 0.5% nano-clay is the greater from 5 to 10 % based on impact force and energy absorption of 1% and 2% nano-clay is lower than the energy absorption capacity of pristine. In figure 6.75 which is the impact energy is 28.8 J the energy absorption of pristine and 1% nano-clay is in small variation while increasing the impact energy, Figure 6.76 shows high variation as impact energy increase. The energy-time result shows adding 2% nano clay decrease the energy absorption capacity.

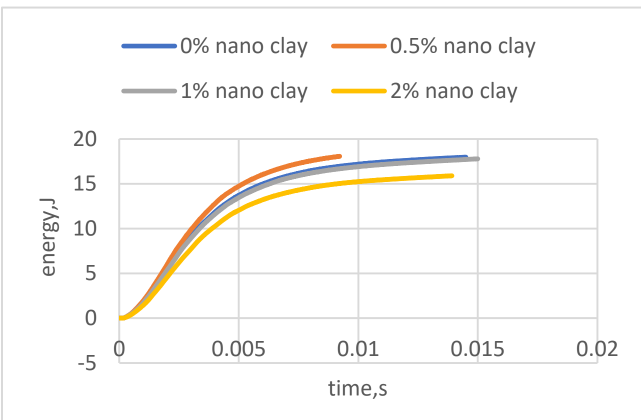

Figure 6.73 Energy vs time 28.8J

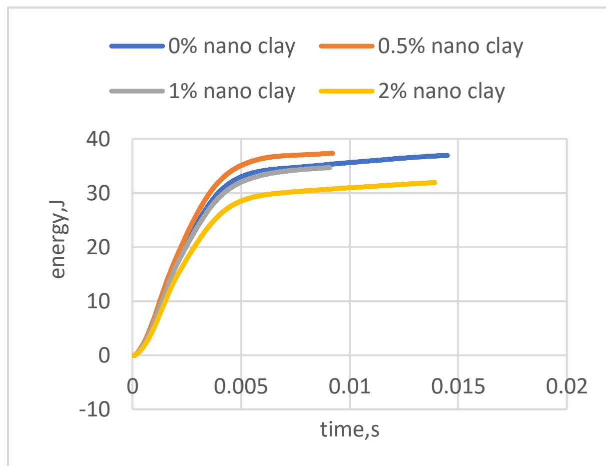

Figure 6.74 Energy vs time graph in 39.2J

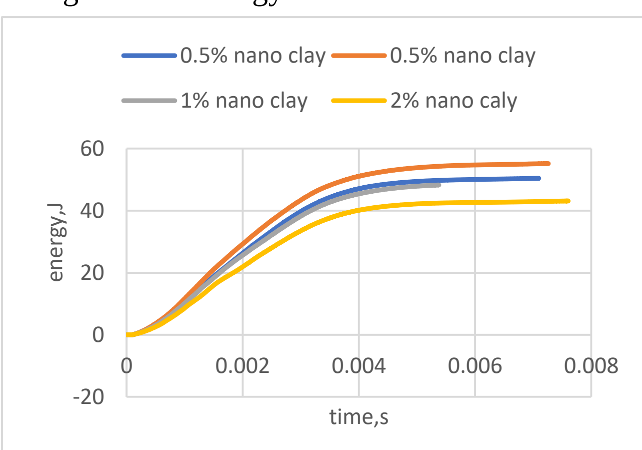

Figure 6.75 Energy vs time graph for 57.8 J

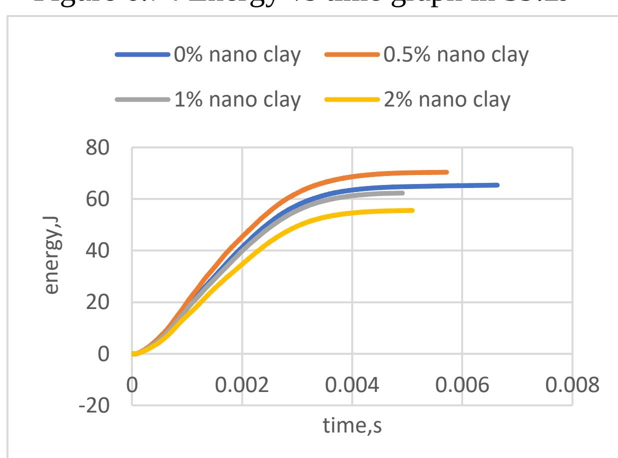

Figure 6.76 Energy vs time graph for 72.2 J

In (Hosur, Adbullah, and Jeelani 2005) Deflection or displacement at peak load is considered as an indicator of the stiffness of the material which is the higher deflection the smallest in stiffness. In figure 6.77 of this research, the addition of nano-clay with 0.5% and 1% nano clay increase the stiffness while adding of nan clay with 2% nano clay decrease the stiffness. And it has direct relation to modules of elasticity. The modulus of elasticity in transverse direction is increased for 0.5 and 1% respectively. And 2% nano clay has the list transverse modulus of elasticity and has reduced stiffness.

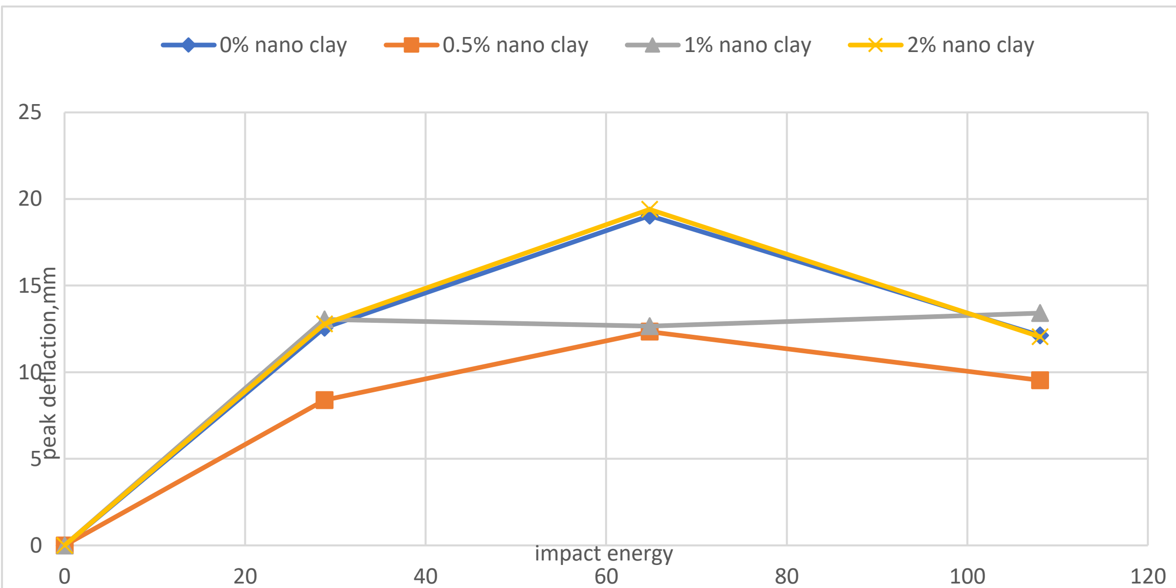

Figure 6.77 Variation of peak deflection with impact energy

The absorbed energy (Ea) less than impact energy (Ei), shown from Figure 7.3 to 7.6. Before this threshold energy, the damage is directly dependent on the impact energy, and the excessive energy (Ee)is used to rebound the impactor the impact energy is predominantly absorbed in the form of elastic and plastic deformation along with different damage modes (Rafiq et al. 2017). So, there is a probability of plastic deformation in these models and materials because in all model and material impact energy is greater than absorbed energy. Researches like (Alomari et al. 2013) shows that most energy is absorbed by delamination and addition of nano-clay increases the delamination resistance by increasing the interlaminar shear strength, and in (Rafiq et al. 2017) the addition of nano-clay reduces the absorbed energy by reducing delamination. But in this study, the energy absorption depends on the addition of Nano clay loading or percentage.

From all observations of results the best performance of material in energy absorption, obtained by loading Glass fiber reinforced polymer with 0.5% Cloisite® 20B nano clay.

Regarding damage tolerance adding nano clay with 0.5 % shows less damage tolerance while adding nano-clay with 1% and 2% shows good damage resistance this analysis is done by looking at the stress concentration area counted.

Comparation of GMT and GFRP – woven composites, based on reaction force vs time graph the GMT composites fail firstly than GFRP woven composites of all clay label.

Chapter 7

7 Conclusions, Recommendations and Future work

7.1 Conclusion

This work is mainly dealing with glass fiber reinforced plastic (GFRP) woven composites with different nano modification and Glass mat thermoplastic (GMT) composites for impact behavior study. GFRP-woven composites considered as orthotropic material and used Hashine 3D failure criteria for woven fiber and puck or modified tsi wu failure criteria for matrix through Abaqus subroutine Vumat, GMT material is assumed as isotropic material and analyze using Hashin 2D failure criteria in Abaqus. And the result shows Using two approach shows some variation in force displacement graph.

Based on numerical method used in this research loading Cloisite® 20B nano clay with 0.5 % shows good energy absorption than loading it 1%, 2% and 0% of GFRP. Regarding to damage tolerance it performs less. And loading 2% shows good capacity in resisting damage based on Abaqus explicit. Stiffness depends upon Young's Modulus Shape, size, structure (especially in composite). This research shows, the addition of nano-clay with 0.5% and 1% nano clay increase the stiffness while adding of nan clay with 2% nano clay decrease the stiffness. A stiff material has a high Young's modulus and, in this work, also as validation 0.5% nano clay has the highest modules of elasticity of all material in transverse direction followed by 1% nano clay loading. 2% nano clay loading has list in modules of elasticity and in stiffness.

.

7.2 Recommendation

From all observation of this research paper the recommendation is as follows. Using ABAQUS Vumat is good for prediction of impact behavior of GFRP composites. And nano modification for increasing properties is not the only way but also knowing the proper loading is essential. For the car manufacturers, if there is a way to use Cloisite® 20B nano clay we recommend to use GFRP - woven composites with 0.5% loading for need of energy absorption areas.

7.3 Future work

In the future work damage can analyze using CDM and different failure criterion techniques using Abaqus subroutine Vumat for failure prediction and validate using experimental techniques.

In addition, finding different nano modifier for GFRP-woven and GMT composite material is taken as future work and are dense research area.

References

Abrate. n.d. "Impact Engineering of Composite Structure."

Abrate, S. 2001. "Modeling of Impacts on Composite Structures." *Composite Structures* 51(2):129–38.

Alomari, Ammar, Saud Aldajah, Saleh Hayek, Kamal Moustafa, and Yousef Haik. 2013. "Experimental Investigation of the Low Speed Impact Characteristics of Nanocomposites." *Materials and Design* 47:836–41. Retrieved (http://dx.doi.org/10.1016/j.matdes.2012.12.079).

Cousigné, Olivier, David Moncayo, Daniel Coutellier, Pedro Camanho, and Hakim Naceur. 2014. "Numerical Modeling of Nonlinearity, Plasticity and Damage in CFRP-Woven Composites for Crash Simulations." *Composite Structures* 115(1):75–88.

Cui, W. C., M. R. Wisnom, and M. Jones. 1992. "A Comparison of Failure Criteria to Predict Delamination of Unidirectional Glass/epoxy Specimens Waisted through the Thickness." *Composites* 23(3):158–66.

Gerlach, Robert, Clive R. Siviour, Jens Wiegand, and Nik Petrinic. 2012. "In-Plane and through-Thickness Properties, Failure Modes, Damage and Delamination in 3D Woven Carbon Fibre Composites Subjected to Impact Loading." *Composites Science and Technology* 72(3):397–411. Retrieved (http://dx.doi.org/10.1016/j.compscitech.2011.11.032).

Grishanov, Sergei, Vadim Meshkov, and Alexander Omelchenko. 2009. "A Topological Study of Textile Structures. Part I: An Introduction to Topological Methods." *Textile Research Journal* 79(8):702–13.

Hashin, Z. and A. Rotem. 1973. "A Fatigue Failure Criterion for Fiber Reinforced Materials." *Journal of Composite Materials* 7(4):448–64.

Hosur, M. V., M. Adbullah, and S. Jeelani. 2005. "Studies on the Low-Velocity Impact Response of Woven Hybrid Composites." *Composite Structures* 67(3 SPEC.ISS.):253–62.

Iannucci, L. 2006. "Progressive Failure Modelling of Woven Carbon Composite under Impact." *International Journal of Impact Engineering* 32(6):1013–43.

Kaw, Autar K. and Francis Group. 2006. *Composite*.

Kim, Jang Kyo and Man Lung Sham. 2000. *Impact and Delamination Failure of Woven-Fabric Composites*. Elsevier Science Ltd. Retrieved (http://dx.doi.org/10.1016/S0266-3538(99)00166-9).

Koricho, Ermias G. et al. 2015. "Effect of Hybrid (Micro- and Nano-) Fillers on Impact Response of GFRP Composite." *Composite Structures* 134:789–98. Retrieved (http://dx.doi.org/10.1016/j.compstruct.2015.08.106).

Kuboki, T., P. Y. B. Jar, and T. W. Forest. 2003. "Influence of Interlaminar Fracture Toughness on Impact Resistance of Glass Fibre Reinforced Polymers." *Composites Science and Technology* 63(7):943–53.

Li, Yuxuan, Zhongqin Lin, Aiqin Jiang, and Guanlong Chen. 2004. “Materials & Design Experimental Study of Glass-Fiber Mat Thermoplastic Material Impact Properties and Lightweight Automobile Body Analysis.” 25:579–85.

Matzenmiller, A., J. Lubliner, and R. L. Taylor. 1995. “A Constitutive Model for Anisotropic Damage in Fiber-Composites.” 20:125–52.

Method, Standard Test. 2002. “Standard Test Method for Tensile Properties of Polymer Matrix Composite Materials 1.” 15.

Park, J. I. N. W. n.d. *THEORY OF COMPOSITES DESIGN PREFACE*.

Puck, Alfred and H.Matthias Deuschle. 2002. “Progress in the Puck Failure Theory for Fibre Reinforced Composites : Analytical Solutions for 3D-Stress.” *Composites Science and Technology* 62(3):371–78.

Rafiq, Ahmad, Nesar Merah, Rachid Boukhili, and Muneer Al-Qadhi. 2017. “Impact Resistance of Hybrid Glass Fiber Reinforced Epoxy/nanoclay Composite.” *Polymer Testing* 57:1–11.

Riccio, A., S. Saputo, A. Raimondo, and A. Sellitto. 2017. *Modeling Low Velocity Impact Phenomena on Composite Structures*. Elsevier Ltd. Retrieved (http://linkinghub.elsevier.com/retrieve/pii/B9780081008874000044).

Shinohara, Toshihiro and Jun-ya Takayama. 2005. “Analysis of Woven Fabric Structure Using X-Ray CT Images.” 17(1):9–17.

Sohn, M. S., X. Z. Hu, J. K. Kim, and L. Walker. 2000. “Impact Damage Characterisation of Carbon ® Bre / Epoxy Composites with Multi-Layer Reinforcement.” *Carbon* 31(8):681–91. Retrieved (http://dx.doi.org/10.1016/S1359-8368(00)00028-7).

Sun, X. C., M. R. Wisnom, and S. R. Hallett. 2016. “Interaction of Inter- and Intralaminar Damage in Scaled Quasi-Static Indentation Tests: Part 2 - Numerical Simulation.” *Composite Structures* 136:727–42. Retrieved (http://dx.doi.org/10.1016/j.compstruct.2015.09.061).

Tsai, Steve and Ed Wu. 2009. “The Tsai-Wu Tsai Wu Failure Criterion The Tsai Wu Failure Criterion.” (1939).

Version, Document. 2014. *Numerical Simulation of Damage Mechanisms in Composite Materials Numerical Simulation of Damage Mechanisms in Composite Materials Saman Hosseini*.

Wang, He Ran, Shu Chang Long, Xiao Qing Zhang, and Xiao Hu Yao. 2017. “Study on the Delamination Behavior of Thick Composite Laminates under Low-Energy Impact.” *Composite Structures*. Retrieved (https://doi.org/10.1016/j.compstruct.2017.09.083)

Mulugeta H/Habte Mariyam, G Belingardi, Daniel T.Reda, Ermias G Koricho, Alem T. Beyene” influence of Nano clay on modulus of elasticity and strength of glass fiber Reinforced polymer,2018 (in progress)

Iannucci L, Willows ML. An energy based damage mechanics approach to modelling impact onto woven composite materials: part II. Experimental and numerical results. Compos Part A Appl Sci Manuf 2007;38:540–54.

Pinho ST, Iannucci L, Robinson P. Physically based failure models and criteria for lam- inated fibre-reinforced composites with emphasis on fibre kinking. Part II. FE implemen- tation. Compos Part A Appl Sci Manuf 2006;37:766–77.

Puck A, Sch€ urmann H. Failure analysis of FRP laminates by means of physically based phenomenological models. Compos Sci Technol 1998;58:1045–67.

Krueger R. Virtual crack closure technique: history, approach, and applications. Appl Mech Rev 2004;57(2):109–43.

Riccio A, Raimondo A, Scaramuzzino F. A study on skin delaminations growth in stiff- ened composite panels by a novel numerical approach. Appl Compos Mater 2013;20 (4):465–88..

Aoki Y, Suemasu H, Ishikawa T. Damage propagation in CFRP laminates subjected to low velocity impact and static indentation. Adv Compos Mater 2007;16(1):45–61.

Bouvet C, Rivallant S. Damage tolerance of composite structures under low-velocity impact. In: Dynamic deformation, damage and fracture in composite materials and structures. Cambridge, UK: Woodhead Publishing; 2016. p. 1–7

Hyer, Michael W. n.d. *Stress Analysis of Fiber-Reinforced Composite Materials*.

Appendix

```
******************************************************************************************
******************************************************************************************
* Abaqus vumat used inthesis and obtaied from Abaqus software website and edited *
* uses Abaqus 2017, intel parrallel studieo 2016(visual fortan), and (Microsoft community Visual Studio 2013*
SUBROUTINE VUMAT(
C READ ONLY -1  NBLOCK, NDIR, NSHR, NSTATEV, NFIELDV, NPROPS, LANNEAL,
2  STEPTIME, TOTALTIME, DT, CMNAME, COORDMP, CHARLENGTH,
3  PROPS, DENSITY, STRAININC, RELSPININC,
4  TEMPOLD, STRETCHOLD, DEFGRADOLD, FIELDOLD,
5  STRESSOLD, STATEOLD, ENERINTERNOLD, ENERINELASOLD,
6  TEMPNEW, STRETCHNEW, DEFGRADNEW, FIELDNEW,
C WRITE ONLY -7 STRESSNEW, STATENEW, ENERINTERNNEW, ENERINELASNEW )
C
INCLUDE 'VABA_PARAM.INC'
C
C
C THE STATE VARIABLES ARE STORED AS:
C STATE(*,1) = MATERIAL POINT STATUS
C STATE(*,2:7) = DAMPING STRESSES
C
C USER DEFINED MATERIAL PROPERTIES ARE STORED AS
C * FIRST LINE:
C PROPS(1) --> YOUNG'S MODULUS IN 1-DIRECTION, E1
C PROPS(2) --> YOUNG'S MODULUS IN 2-DIRECTION, E2
C PROPS(3) --> YOUNG'S MODULUS IN 3-DIRECTION, E3
C PROPS(4) --> POISSON'S RATIO, NU12
C  PROPS(5) --> POISSON'S RATIO, NU13
C PROPS(6) --> POISSON'S RATIO, NU23
C PROPS(7) --> SHEAR MODULUS, G12
C PROPS(8) --> SHEAR MODULUS, G13
C
C * SECOND LINE:
C PROPS(9)  --> SHEAR MODULUS, G23
C PROPS(10) --> BETA DAMPING PARAMETER
C
C * THIRD LINE:
C PROPS(11) --> ULTIMATE TENS STRESS IN 1-DIRECTION, SIGU1T
C PROPS(12) --> ULTIMATE COMP STRESS IN 1-DIRECTION, SIGU1C
C PROPS(13) --> ULTIMATE TENS STRESS IN 2-DIRECTION, SIGU2T
C PROPS(14) --> ULTIMATE COMP STRESS IN 2-DIRECTION, SIGU2C
C PROPS(15) --> ULTIMATE TENS STRESS IN 3-DIRECTION, SIGU3T
C PROPS(16) --> ULTIMATE COMP STRESS IN 3-DIRECTION, SIGU3C
C
C * FOURTH LINE:
C PROPS(17) --> ULTIMATE SHEAR STRESS, SIGU12
C   PROPS(18) --> ULTIMATE SHEAR STRESS, SIGU13
C   PROPS(19) --> ULTIMATE SHEAR STRESS, SIGU23
73
DIMENSION PROPS(NPROPS), DENSITY(NBLOCK),
*  COORDMP(NBLOCK,*),
*  CHARLENGTH(*), STRAININC(NBLOCK,NDIR+NSHR),
*  RELSPININC(NBLOCK,NSHR), TEMPOLD(NBLOCK),
```

```
*  STRETCHOLD(NBLOCK,NDIR+NSHR),DEFGRADOLD(NBLOCK,NDIR+NSHR+NSHR),
*  FIELDOLD(NBLOCK,NFIELDV), STRESSOLD(NBLOCK,NDIR+NSHR),
*  STATEOLD(NBLOCK,NSTATEV), ENERINTERNOLD(NBLOCK),
*  ENERINELASOLD(NBLOCK), TEMPNEW(*),
*  STRETCHNEW(NBLOCK,NDIR+NSHR), DEFGRADNEW(NBLOCK,NDIR+NSHR+NSHR),
*  FIELDNEW(NBLOCK,NFIELDV), STRESSNEW(NBLOCK,NDIR+NSHR),
*  STATENEW(NBLOCK,NSTATEV),
*  ENERINTERNNEW(NBLOCK), ENERINELASNEW(NBLOCK)
*
CHARACTER*80 CMNAME
*
PARAMETER( ZERO = 0.D0, ONE = 1.D0, TWO = 2.D0, HALF = .5D0 )
*
PARAMETER (
* I_SVD_DMGFIBERT = 1,
* I_SVD_DMGFIBERC = 2,
* I_SVD_DMGMATRIXT = 3,
* I_SVD_DMGMATRIXC = 4,
* I_SVD_STATUSMP = 5,
* I_SVD_DAMPSTRESS = 6,
* N_SVD_REQUIRED = 6)
*
PARAMETER(
*  I_S33_XX = 1,
*  I_S33_YY = 2,
* I_S33_ZZ = 3,
*  I_S33_XY = 4,
*  I_S33_YZ = 5,
*  I_S33_ZX = 6 )
*
*  STRUCTURE OF PROPERTY ARRAY
PARAMETER (
*   I_PRO_E1 = 1,
*   I_PRO_E2 = 2,
*   I_PRO_E3 = 3,
*   I_PRO_NU12 = 4,
*   I_PRO_NU13 = 5,
*   I_PRO_NU23 = 6,
* I_PRO_G12 = 7,
*   I_PRO_G13 = 8,
*   I_PRO_G23  = 9,
*
*   I_PRO_BETA = 10,
*
*   I_PRO_SIGU1T = 11,
*   I_PRO_SIGU1C = 12,
* I_PRO_SIGU2T = 13,
*   I_PRO_SIGU2C = 14,
*   I_PRO_SIGU3T = 15,
*   I_PRO_SIGU3C = 16,
*   I_PRO_SIGU12 = 17,
*   I_PRO_SIGU13 = 18,
*   I_PRO_SIGU23 = 19 )
* TEMPORARY ARRAYS
DIMENSION EIGEN(MAXBLK*3)
*
74
*  READ MATERIAL PROPERTIES *
E1 = PROPS(I_PRO_E1)
E2 = PROPS(I_PRO_E2)
E3 = PROPS(I_PRO_E3)
```

```
XNU12 = PROPS(I_PRO_NU12)
XNU13 = PROPS(I_PRO_NU13)
XNU23 = PROPS(I_PRO_NU23)
G12 = PROPS(I_PRO_G12)
G13 = PROPS(I_PRO_G13)
G23 = PROPS(I_PRO_G23)
*
XNU21 = XNU12 * E2 / E1
XNU31 = XNU13 * E3 / E1
XNU32 = XNU23 * E3 / E2
*
*
* COMPUTE TERMS OF STIFFNESS MATRIX
GG=ONE/(ONE-XNU12*XNU21-XNU23*XNU32
*  -XNU31*XNU13-TWO*XNU21*XNU32*XNU13)
C11 = E1 * ( ONE - XNU23*XNU32 ) * GG
C22 = E2 * ( ONE - XNU13*XNU31 ) * GG
C33 = E3 * ( ONE - XNU12*XNU21 ) * GG
C12 = E1 * ( XNU21 + XNU31*XNU23 ) * GG
C13 = E1 * ( XNU31 + XNU21*XNU32 ) * GG
C23  = E2 * ( XNU32 + XNU12*XNU31 ) * GG
*
F1T = PROPS(I_PRO_SIGU1T)
F1C = PROPS(I_PRO_SIGU1C)
F2T = PROPS(I_PRO_SIGU2T)
F2C = PROPS(I_PRO_SIGU2C)
F3T = PROPS(I_PRO_SIGU3T)
F3C = PROPS(I_PRO_SIGU3C)
F12 = PROPS(I_PRO_SIGU12)
F13 = PROPS(I_PRO_SIGU13)
F23 = PROPS(I_PRO_SIGU23)
*
BETA = PROPS(I_PRO_BETA)
*
*  ASSUME PURELY ELASTIC MATERIAL AT THE BEGINNING OF THE ANALYSIS
*
IF ( TOTALTIME .EQ. ZERO ) THEN
IF (NSTATEV .LT. N_SVD_REQUIRED) THEN
CALL XPLB_ABQERR(-2,'SUBROUTINE VUMAT REQUIRES THE '//
*  'SPECIFICATION OF %I STATE VARIABLES. CHECK THE '//
*  'DEFINITION OF *DEPVAR IN THE INPUT FILE.',
*    N_SVD_REQUIRED,ZERO,' ')
CALL XPLB_EXIT
END IF
CALL ORTHOELA3DEXP ( NBLOCK,
*  STATEOLD(1,I_SVD_DMGFIBERT),
*  STATEOLD(1,I_SVD_DMGFIBERC),
*  STATEOLD(1,I_SVD_DMGMATRIXT),
*  STATEOLD(1,I_SVD_DMGMATRIXC),
*  C11, C22, C33, C12, C23, C13, G12, G23, G13,
*  STRAININC,
*  STRESSNEW )
RETURN
END IF
*
*  UPDATE TOTAL ELASTIC STRAIN
75
CALL STRAINUPDATE ( NBLOCK, STRAININC,
*  STATEOLD(1,I_SVD_STRAIN), STATENEW(1,I_SVD_STRAIN) )
*  STRESS UPDATE
CALL ORTHOELA3DEXP ( NBLOCK,
```

```
*  STATEOLD(1,I_SVD_DMGFIBERT),
*  STATEOLD(1,I_SVD_DMGFIBERC),
*  STATEOLD(1,I_SVD_DMGMATRIXT),
*  STATEOLD(1,I_SVD_DMGMATRIXC),
*  C11, C22, C33, C12, C23, C13, G12, G23, G13,
*  STATENEW(1,I_SVD_STRAIN),
*  STRESSNEW )
*
*  FAILURE EVALUATION
*
CALL COPYR ( NBLOCK,
*  STATEOLD(1,I_SVD_DMGFIBERT), STATENEW(1,I_SVD_DMGFIBERT) )
CALL COPYR ( NBLOCK,
*  STATEOLD(1,I_SVD_DMGFIBERC), STATENEW(1,I_SVD_DMGFIBERC) )
CALL COPYR(NBLOCK,
* STATEOLD(1,I_SVD_DMGMATRIXT), STATENEW(1,I_SVD_DMGMATRIXT) )
CALL COPYR(NBLOCK,
* STATEOLD(1,I_SVD_DMGMATRIXC), STATENEW(1,I_SVD_DMGMATRIXC))
NDMG = 0
CALL EIG33ANAL ( NBLOCK, STRETCHNEW, EIGEN )
CALL HASHIN3D ( NBLOCK, NDMG,
*    F1T, F2T, F3T, F1C, F2C, F3C, F12, F23, F13,
*    STATENEW(1,I_SVD_DMGFIBERT),
*    STATENEW(1,I_SVD_DMGFIBERC),
*    STATENEW(1,I_SVD_DMGMATRIXT),
*    STATENEW(1,I_SVD_DMGMATRIXC),
*    STATENEW(1,I_SVD_STATUSMP),
*    STRESSNEW, EIGEN )
*  -- RECOMPUTE STRESSES IF NEW DAMAGE IS OCCURRING
IF ( NDMG .GT. 0 ) THEN
CALL ORTHOELA3DEXP ( NBLOCK,
*    STATENEW(1,I_SVD_DMGFIBERT),
*    STATENEW(1,I_SVD_DMGFIBERC),
*    STATENEW(1,I_SVD_DMGMATRIXT),
* STATENEW(1,I_SVD_DMGMATRIXC),
*    C11, C22, C33, C12, C23, C13, G12, G23, G13,
*  STATENEW(1,I_SVD_STRAIN),
*  STRESSNEW )
END IF
*
*  BETA DAMPING
CNIE IF ( BETA .GT. ZERO ) THEN
CNIE CALL BETADAMPING3D ( NBLOCK,
CNIE * BETA, DT, STRAININC,
CNIE * STRESSOLD, STRESSNEW,
CNIE STATENEW(1,I_SVD_STATUSMP),
CNIE * STATEOLD(1,I_SVD_DAMPSTRESS),
CNIE * STATENEW(1,I_SVD_DAMPSTRESS) )
CNIE END IF
*
*  INTEGRATE THE INTERNAL SPECIFIC ENERGY (PER UNIT MASS)
*
CALL ENERGYINTERNAL3D ( NBLOCK, STRESSOLD, STRESSNEW,
* STRAININC, DENSITY, ENERINTERNOLD, ENERINTERNNEW )
*
76
RETURN
END
************************************************************
*  ORTHOELA3DEXP: ORTHOTROPIC ELASTICITY - 3D *
************************************************************
```

```
SUBROUTINE ORTHOELA3DEXP ( NBLOCK,
*    DMGFIBERT, DMGFIBERC, DMGMATRIXT, DMGMATRIXC,
*    C11, C22, C33, C12, C23, C13, G12, G23, G13,
*    STRAIN, STRESS )
*
INCLUDE 'VABA_PARAM.INC'
*  ORTHOTROPIC ELASTICITY, 3D CASE -
*
PARAMETER( ZERO = 0.D0, ONE = 1.D0, TWO = 2.D0)
PARAMETER(
*    I_S33_XX = 1,
*    I_S33_YY = 2,
* I_S33_ZZ = 3,
*    I_S33_XY = 4,
*    I_S33_YZ = 5,
*    I_S33_ZX = 6,
*    N_S33_CAR = 6 )
*
DIMENSION STRAIN(NBLOCK,N_S33_CAR),
*    DMGFIBERT(NBLOCK), DMGFIBERC(NBLOCK),
*    DMGMATRIXT(NBLOCK), DMGMATRIXC(NBLOCK),
*    STRESS(NBLOCK,N_S33_CAR)
*  -- SHEAR FRACTION IN MATRIX TENSION AND COMPRESSION MODE
PARAMETER ( SMT = 0.8D0, SMC = 0.5D0 )
*
DO K = 1, NBLOCK
*  -- COMPUTE DAMAGED STIFFNESS
DFT = DMGFIBERT(K)
DFC = DMGFIBERC(K)
DMT = DMGMATRIXT(K)
DMC = DMGMATRIXC(K)
DF = ONE - ( ONE - DFT ) * ( ONE - DFC )
*
DC11 = ( ONE - DF ) * C11
DC22 = ( ONE - DF ) * ( ONE - DMT ) * ( ONE - DMC ) * C22
DC33 = ( ONE - DF ) * ( ONE - DMT ) * ( ONE - DMC ) * C33
DC12 = ( ONE - DF ) * ( ONE - DMT ) * ( ONE - DMC ) * C12
DC23 = ( ONE - DF ) * ( ONE - DMT ) * ( ONE - DMC ) * C23
DC13 = ( ONE - DF ) * ( ONE - DMT ) * ( ONE - DMC ) * C13
DG12 = ( ONE - DF )
*    * ( ONE - SMT*DMT ) * ( ONE - SMC*DMC ) * G12
DG23 = ( ONE - DF )
*    * ( ONE - SMT*DMT ) * ( ONE - SMC*DMC ) * G23
DG13 = ( ONE - DF )
*    * ( ONE - SMT*DMT ) * ( ONE - SMC*DMC ) * G13
*  -- STRESS UPDATE
STRESS(K,I_S33_XX) = DC11 * STRAIN(K,I_S33_XX)
*    + DC12 * STRAIN(K,I_S33_YY)
*    + DC13 * STRAIN(K,I_S33_ZZ)
STRESS(K,I_S33_YY) = DC12 * STRAIN(K,I_S33_XX)
*    + DC22 * STRAIN(K,I_S33_YY)
*    + DC23 * STRAIN(K,I_S33_ZZ)
STRESS(K,I_S33_ZZ) = DC13 * STRAIN(K,I_S33_XX)
77
*    + DC23 * STRAIN(K,I_S33_YY)
*    + DC33 * STRAIN(K,I_S33_ZZ)
STRESS(K,I_S33_XY) = TWO * DG12 * STRAIN(K,I_S33_XY)
STRESS(K,I_S33_YZ) = TWO * DG23 * STRAIN(K,I_S33_YZ)
STRESS(K,I_S33_ZX) = TWO * DG13 * STRAIN(K,I_S33_ZX)
END DO
*
```

```
RETURN
END
************************************************************
*  STRAINUPDATE: UPDATE TOTAL STRAIN *
************************************************************
SUBROUTINE STRAINUPDATE ( NBLOCK,
*    STRAININC, STRAINOLD, STRAINNEW )
*
INCLUDE 'VABA_PARAM.INC'
*
PARAMETER(
*    I_S33_XX = 1,
*    I_S33_YY = 2,
* I_S33_ZZ = 3,
*    I_S33_XY = 4,
*    I_S33_YZ = 5,
*    I_S33_ZX = 6,
*    N_S33_CAR = 6 )
*
DIMENSION STRAININC(NBLOCK,N_S33_CAR),
*    STRAINOLD(NBLOCK,N_S33_CAR),
*    STRAINNEW(NBLOCK,N_S33_CAR)
*
DO K = 1, NBLOCK
STRAINNEW(K,I_S33_XX)= STRAINOLD(K,I_S33_XX)
*    + STRAININC(K,I_S33_XX)
STRAINNEW(K,I_S33_YY)= STRAINOLD(K,I_S33_YY)
*    + STRAININC(K,I_S33_YY)
STRAINNEW(K,I_S33_ZZ)= STRAINOLD(K,I_S33_ZZ)
*    + STRAININC(K,I_S33_ZZ)
STRAINNEW(K,I_S33_XY)= STRAINOLD(K,I_S33_XY)
*    + STRAININC(K,I_S33_XY)
STRAINNEW(K,I_S33_YZ)= STRAINOLD(K,I_S33_YZ)
*    + STRAININC(K,I_S33_YZ)
STRAINNEW(K,I_S33_ZX)= STRAINOLD(K,I_S33_ZX)
*      + STRAININC(K,I_S33_ZX)
END DO
*
RETURN
END
************************************************************
*  HASHIN3D W/ MODIFIED PUCK/modified Tsi wu : EVALUATE HASHIN 3D FAILURE *
*  CRITERION FOR FIBER, PUCK FOR MATRIX    *
************************************************************
             ************* SOME DATA OBMITED
INCLUDE 'VABA_PARAM.INC'
78
PARAMETER( ZERO = 0.D0, ONE = 1.D0, HALF = 0.5D0, THREE = 3.D0)
PARAMETER(
*    I_S33_XX = 1,
*    I_S33_YY = 2,
* I_S33_ZZ = 3,
*    I_S33_XY = 4,
*    I_S33_YZ = 5,
*    I_S33_ZX = 6,
*    N_S33_CAR = 6 )
*
PARAMETER(I_V3D_X=1,I_V3D_Y=2,I_V3D_Z=3 )
PARAMETER(N_V3D_CAR=3 )
*
PARAMETER ( EMAX = 1.00D0, EMIN = -0.8D0 )
```

```
*
DIMENSION DMGFIBERT(NBLOCK), DMGFIBERC(NBLOCK),
*    DMGMATRIXT(NBLOCK), DMGMATRIXC(NBLOCK),
*    STRESS(NBLOCK,N_S33_CAR),
*    EIGEN(NBLOCK,N_V3D_CAR),
*    STATUSMP(NBLOCK)
*
F1TINV = ZERO
F2TINV = ZERO
F3TINV = ZERO
F1CINV = ZERO
F2CINV = ZERO
F3CINV = ZERO
F12INV = ZERO
F23INV = ZERO
F13INV = ZERO
*
IF ( F1T .GT. ZERO ) F1TINV = ONE / F1T
IF ( F2T .GT. ZERO ) F2TINV = ONE / F2T
IF ( F3T .GT. ZERO ) F3TINV = ONE / F3T
IF ( F1C .GT. ZERO ) F1CINV = ONE / F1C
IF ( F2C .GT. ZERO ) F2CINV = ONE / F2C
IF ( F3C .GT. ZERO ) F3CINV = ONE / F3C
IF ( F12 .GT. ZERO ) F12INV = ONE / F12
IF ( F23 .GT. ZERO ) F23INV = ONE / F23
IF ( F13 .GT. ZERO ) F13INV = ONE / F13
*
DO K = 1, NBLOCK
IF ( STATUSMP(K) .EQ. ONE ) THEN
*
LFAIL = 0
*
S11 = STRESS(K,I_S33_XX)
S22 = STRESS(K,I_S33_YY)
S33 = STRESS(K,I_S33_ZZ)
S12 = STRESS(K,I_S33_XY)
S23 = STRESS(K,I_S33_YZ)
S13 = STRESS(K,I_S33_ZX)
*
* EVALUATE FIBER MODES
IF ( S11 .GT. ZERO ) THEN
*  -- TENSILE FIBER MODE
RFT = (S11*F1TINV )**2 + (S12*F12INV )**2 + (S13*F13INV)**2
IF ( RFT .GE. ONE ) THEN
LDMG = 1
79
DMGFIBERT(K) = ONE
END IF
ELSE IF ( S11 .LT. ZERO ) THEN
*  -- COMPRESSIVE FIBER MODE
RFC = ABS(S11) * F1CINV
IF ( RFC .GE. ONE ) THEN
LDMG = 1
DMGFIBERC(K) = ONE
END IF
END IF
*
*  EVALUATE MATRIX MODES
IF ( ( S22 + S33 ) .GT. ZERO ) THEN
*  -- TENSILE MATRIX MODE
RMT = ( S11 * HALF * F1TINV )**2
```

```
*    + ( S22**2 * ABS(F2TINV * F2CINV) )
*    + ( S12 * F12INV )**2
*    + ( S22 * (F2TINV + F2CINV) )
IF ( RMT .GE. ONE ) THEN
LDMG = 1
DMGMATRIXT(K) = ONE
END IF
ELSE IF ( ( S22 + S33 ) .LT. ZERO ) THEN
*  -- COMPRESSIVE MATRIX MODE
RMC = ( S11 * HALF * F1TINV )**2
*    + ( S22**2 * ABS(F2TINV * F2CINV) )
*    + ( S12 * F12INV )**2
*    + ( S22 * (F2TINV + F2CINV) )
IF ( RMC .GE. ONE ) THEN
LDMG = 1
DMGMATRIXC(K) = ONE
END IF
END IF
*
EIGMAX=MAX(EIGEN(K,I_V3D_X),EIGEN(K,I_V3D_Y),EIGEN(K,I_V3D_Z))
EIGMIN=MIN(EIGEN(K,I_V3D_X),EIGEN(K,I_V3D_Y),EIGEN(K,I_V3D_Z))
ENOMMAX = EIGMAX - ONE
ENOMMIN = EIGMIN - ONE
*
IF ( ENOMMAX .GT. EMAX .OR.
* ENOMMIN .LT. EMIN .OR.
*  DMGFIBERT(K) .EQ. ONE ) THEN
STATUSMP(K) = ZERO
END IF
*
NDMG = NDMK + LDMG
*
END IF
*
END DO
*
RETURN
END
************************************************************
*  BETADAMPING: ADD BETA DAMPING  *
************************************************************
SUBROUTINE BETADAMPING3D ( NBLOCK,
80
*    BETA, DT, STRAININC, SIGOLD, SIGNEW,
*    STATUSMP, SIGDAMPOLD, SIGDAMPNEW )
*
INCLUDE 'VABA_PARAM.INC'
*
PARAMETER(
*    I_S33_XX = 1,
*    I_S33_YY = 2,
* I_S33_ZZ = 3,
*    I_S33_XY = 4,
*    I_S33_YZ = 5,
*    I_S33_ZX = 6,
*    N_S33_CAR = 6 )
*
DIMENSION SIGOLD(NBLOCK,N_S33_CAR),
*  SIGNEW(NBLOCK,N_S33_CAR),
*  STRAININC(NBLOCK,N_S33_CAR),
*  STATUSMP(NBLOCK),
```

```
*  SIGDAMPOLD(NBLOCK,N_S33_CAR),
*  SIGDAMPNEW(NBLOCK,N_S33_CAR)
*
PARAMETER ( ZERO = 0.D0, ONE = 1.D0, TWO=2.0D0,
*    HALF = 0.5D0, THIRD = 1.D0/3.D0 )
PARAMETER ( ASMALL = 1.D-16 )
*
BETADDT = BETA / DT
*
DO K =1 , NBLOCK
SIGDAMPNEW(K,I_S33_XX) = BETADDT * STATUSMP(K) *
*    ( SIGNEW(K,I_S33_XX)
*    - ( SIGOLD(K,I_S33_XX) - SIGDAMPOLD(K,I_S33_XX) ) )
SIGDAMPNEW(K,I_S33_YY) = BETADDT * STATUSMP(K) *
*    ( SIGNEW(K,I_S33_YY)
*     - ( SIGOLD(K,I_S33_YY) - SIGDAMPOLD(K,I_S33_YY) ) )
SIGDAMPNEW(K,I_S33_ZZ) = BETADDT * STATUSMP(K) *
*    ( SIGNEW(K,I_S33_ZZ)
*    - ( SIGOLD(K,I_S33_ZZ) - SIGDAMPOLD(K,I_S33_ZZ) ) )
SIGDAMPNEW(K,I_S33_XY) = BETADDT * STATUSMP(K) *
*    ( SIGNEW(K,I_S33_XY)
*    - ( SIGOLD(K,I_S33_XY) - SIGDAMPOLD(K,I_S33_XY) ) )
SIGDAMPNEW(K,I_S33_YZ) = BETADDT * STATUSMP(K) *
*    ( SIGNEW(K,I_S33_YZ)
*    - ( SIGOLD(K,I_S33_YZ) - SIGDAMPOLD(K,I_S33_YZ) ) )
SIGDAMPNEW(K,I_S33_ZX) = BETADDT * STATUSMP(K) *
*    ( SIGNEW(K,I_S33_ZX)
*  - ( SIGOLD(K,I_S33_ZX) - SIGDAMPOLD(K,I_S33_ZX) ) )
*
SIGNEW(K,I_S33_XX) = SIGNEW(K,I_S33_XX)+SIGDAMPNEW(K,I_S33_XX)
SIGNEW(K,I_S33_YY) = SIGNEW(K,I_S33_YY)+SIGDAMPNEW(K,I_S33_YY)
SIGNEW(K,I_S33_ZZ) = SIGNEW(K,I_S33_ZZ)+SIGDAMPNEW(K,I_S33_ZZ)
SIGNEW(K,I_S33_XY) = SIGNEW(K,I_S33_XY)+SIGDAMPNEW(K,I_S33_XY)
SIGNEW(K,I_S33_YZ) = SIGNEW(K,I_S33_YZ)+SIGDAMPNEW(K,I_S33_YZ)
SIGNEW(K,I_S33_ZX) = SIGNEW(K,I_S33_ZX)+SIGDAMPNEW(K,I_S33_ZX)
*
END DO
*
RETURN
END
************************************************************
81
*  ENERGYINTERNAL3D: COMPUTE INTERNAL ENERGY FOR 3D CASE *
************************************************************
SUBROUTINE ENERGYINTERNAL3D(NBLOCK, SIGOLD, SIGNEW ,
*    STRAININC, CURDENSITY, ENERINTERNOLD, ENERINTERNNEW)
*
INCLUDE 'VABA_PARAM.INC'
*
PARAMETER(
*    I_S33_XX = 1,
*    I_S33_YY = 2,
* I_S33_ZZ = 3,
*    I_S33_XY = 4,
*    I_S33_YZ = 5,
*    I_S33_ZX = 6,
*    N_S33_CAR = 6 )
*
PARAMETER( TWO = 2.D0, HALF = .5D0 )
*
DIMENSION SIGOLD (NBLOCK,N_S33_CAR), SIGNEW (NBLOCK,N_S33_CAR),
```

```
*  STRAININC (NBLOCK,N_S33_CAR), CURDENSITY (NBLOCK),
*  ENERINTERNOLD(NBLOCK), ENERINTERNNEW(NBLOCK)
*
DO K = 1, NBLOCK
STRESSPOWER = HALF * (
*    ( SIGOLD(K,I_S33_XX) + SIGNEW(K,I_S33_XX) )
*    * ( STRAININC(K,I_S33_XX) )
*    + ( SIGOLD(K,I_S33_YY) + SIGNEW(K,I_S33_YY) )
* * ( STRAININC(K,I_S33_YY))
*    + ( SIGOLD(K,I_S33_ZZ) + SIGNEW(K,I_S33_ZZ) )
* * ( STRAININC(K,I_S33_ZZ))
*    + TWO * ( SIGOLD(K,I_S33_XY) + SIGNEW(K,I_S33_XY) )
* * STRAININC(K,I_S33_XY)
*    + TWO * ( SIGOLD(K,I_S33_YZ) + SIGNEW(K,I_S33_YZ) )
* * STRAININC(K,I_S33_YZ)
*    + TWO * ( SIGOLD(K,I_S33_ZX) + SIGNEW(K,I_S33_ZX) )
*    * STRAININC(K,I_S33_ZX) )
*
ENERINTERNNEW(K) = ENERINTERNOLD(K) + STRESSPOWER/CURDENSITY(K)
END DO
*
RETURN
END
************************************************************
* COPYR: COPY FROM ONE ARRAY TO ANOTHER   *
************************************************************
SUBROUTINE COPYR(NCOPY, FROM, TO )
*
INCLUDE 'VABA_PARAM.INC'
*
DIMENSION FROM(NCOPY), TO(NCOPY)
*
DO K = 1, NCOPY
TO(K) = FROM(K)
END DO
RETURN
END
********************************************************************
******
* EIG33ANAL: COMPUTE EIGEN VALUES OF A 3X3 SYMMETRIC MATRIX ANALYTICALLY *
82
********************************************************************
******
SUBROUTINE EIG33ANAL( NBLOCK, SMAT, EIGVAL )
*
INCLUDE 'VABA_PARAM.INC'
*
PARAMETER(I_S33_XX=1,I_S33_YY=2,I_S33_ZZ=3 )
PARAMETER(I_S33_XY=4,I_S33_YZ=5,I_S33_ZX=6 )
PARAMETER(I_S33_YX=I_S33_XY )
PARAMETER(I_S33_ZY=I_S33_YZ )
PARAMETER(I_S33_XZ=I_S33_ZX,N_S33_CAR=6 )
PARAMETER(I_V3D_X=1,I_V3D_Y=2,I_V3D_Z=3 )
PARAMETER(N_V3D_CAR=3 )
*
PARAMETER ( ZERO = 0.D0, ONE = 1.D0, TWO = 2.D0,
*    THREE = 3.D0, HALF = 0.5D0, THIRD = ONE / THREE,
*    PI23 = 2.094395102393195D0,
*    FUZZ = 1.D-8,
*    PRECIZ = FUZZ * 1.D4 )
*
```

```
DIMENSION EIGVAL(NBLOCK,N_V3D_CAR), SMAT(NBLOCK,N_S33_CAR)
*
DO K = 1, NBLOCK
SH = THIRD*(SMAT(K,I_S33_XX)+SMAT(K,I_S33_YY)+SMAT(K,I_S33_ZZ))
S11 = SMAT(K,I_S33_XX) - SH
S22 = SMAT(K,I_S33_YY) - SH
S33 = SMAT(K,I_S33_ZZ) - SH
S12 = SMAT(K,I_S33_XY)
S13 = SMAT(K,I_S33_XZ)
S23 = SMAT(K,I_S33_YZ)
*
FAC = MAX(ABS(S11), ABS(S22), ABS(S33))
FACS = MAX(ABS(S12), ABS(S13), ABS(S23))
IF( FACS .LT. (PRECIZ*FAC) ) THEN
EIGVAL(K,I_V3D_X) = SMAT(K,I_S33_XX)
EIGVAL(K,I_V3D_Y) = SMAT(K,I_S33_YY)
EIGVAL(K,I_V3D_Z) = SMAT(K,I_S33_ZZ)
ELSE
Q = THIRD*((S12**2+S13**2+S23**2)+HALF*(S11**2+S22**2+S33**2))
FAC = TWO * SQRT(Q)
IF( FAC .GT. FUZZ ) THEN OFAC = TWO/FAC
ELSE OFAC = ZERO
END IF
S11 = OFAC*S11
S22 = OFAC*S22
S33 = OFAC*S33
S12 = OFAC*S12
S13 = OFAC*S13
S23 = OFAC*S23
R=S12*S13*S23+HALF*(S11*S22*S33-S11*S23**2-S22*S13**2-S33*S12**2)
IF( R .GE. ONE-FUZZ ) THEN
COS1 = -HALF
COS2 = -HALF
COS3 = ONE
ELSE IF( R .LE. FUZZ-ONE ) THEN
COS1 = -ONE
COS2 = HALF
COS3 = HALF
ELSE ANG = THIRD * ACOS(R)
COS1 = COS(ANG)
COS2 = COS(ANG+PI23)
83
COS3 =-COS1-COS2
END IF
EIGVAL(K,I_V3D_X) = SH + FAC*COS1
EIGVAL(K,I_V3D_Y) = SH + FAC*COS2
EIGVAL(K,I_V3D_Z) = SH + FAC*COS3
END DO
*
RETURN
END
```